Hiroshima University

Graduate School of Advanced Science and Engineering

Electrical, Systems and Control Engineering Program

A Model Predictive-Based Robust Load Frequency Control Considering Renewable Energy Uncertainties

PhD Dissertation

WEICHAO WANG

March 2024

A Model Predictive-Based Robust Load Frequency Control Considering Renewable Energy Uncertainties

by

WEICHAO WANG

D214927

A Thesis
Submitted to the Graduate School of Advanced Science and Engineering
Hiroshima University
in partial fulfillment of the requirements for the degree of
Doctor of Philosophy
(Electrical, Systems, and Control Engineering Program)

Hiroshima University, Japan

March 2024

Hiroshima University
Graduate School of Advanced Science and Engineering

Kagamiyama, 1-4-1 Higashi-Hiroshima City
Hiroshima, Japan 739-8527

CERTIFICATE

To whom it may concern

We hereby certify that this is a copy of the doctoral thesis by Mr. WEICHAO WANG. This master's thesis was successfully defended and officially accepted in partial fulfillment of the requirements for the degree of Doctor of Engineering in Electrical, Systems and Control Engineering.

Advisory and Examination Committee inside of Hiroshima University:

Specially Appointed Professor Naoto YORINO

Professor Katsuhiko TAKAHASHI

Professor Ichiro NISHIZAKI

Professor Yoshifumi ZOKA

Associate Professor Yutaka SASAKI

Advisory and Examination Committee for Power Energy Professionals Waseda University Graduate Program:

Professor Tomoko KAWAKAMI (Waseda University)

Associate Professor Takao TSUJI (Yokohama National University)

Seiji KAWAUCHI (Energia Research Institute, The Chugoku Electric Power Co., Inc)

Abstract

Recently, power systems consisting of a large amount of renewable energy sources, such as photovoltaic (PV), wind turbine power (WT) and battery energy storage system (BESS) have been attracting attention toward the realization of a carbon-neutral society. In 2022, the installed renewable energy sources are increasing in worldwide, such as China, around 1161 gigawatts; US, around 352 gigawatts; Brazil, around 175 gigawatts; India, around 163 gigawatts. Among the renewable energy sources, PV is on course to account for 60% of global renewable power growth in 2022. However, the increase in renewable energy sources affects the system stability, especially the frequency stability. Meanwhile, large amount of uncertain renewable energy sources applied to power system also has reduced the output ratio of the thermal generators. The reduction in number of the thermal generators affects the inertia of the power systems. This also decreases the frequency adjustment capability of the power system. Therefore, the maintenance and improvement of the frequency stability are an important issue must be addressed. In particular, small power systems, such as microgrid (MG) system with a high percentage of renewable energy may cause significant frequency fluctuations. In small-scale power systems, the frequency problem is mainly caused by the uncertainty of renewable energy source and large disturbance. Therefore, many researchers have been studied the effective LFC methods, such as the proportional integral (PI) control etc. to address the frequency problem in power systems, highly accurate and robust load frequency control technique is required to against large disturbances for maintaining the desired frequency range.

The main objective of this work is to propose a highly accurate and robust load frequency control (LFC) method. For this purpose, a novel adaptive control method using adaptive model predictive control (AMPC) is designed to address the frequency problem. The proposed AMPC method can predict the future performance of target system based on the internal prediction model. A simplified first-order and second-order lag system as an internal prediction model is proposed for AMPC. The parameters of the internal prediction model are estimated using an unscented Kalman filter (UKF) online. In this work, we had confirmed the performance of the UKF. Meanwhile, the comparison results of the UKF with the extended Kalman filter (EKF), least square (LS), and Kalman filter show that the UKF has a better performance than other estimation methods.

To confirm the effectiveness of the proposed method, we have applied it to two types of power system.

Firstly, simulation studies have been conducted using the large-scale thermal plant, considering the large disturbance. The simulation results show that the proposed method can address the frequency problem effectively, which has the better performance compare with the PI control.

Secondly, case studies on a small-scale MG with renewable energy resources are carried out to demonstrate the effectiveness of the proposed control method. The renewable energy sources, such as PV, WT and various step change are considered to the disturbance. At the same time, a BESS as supplemental power is considered to compensate for rapid load fluctuations. The simulation results confirm that the proposed AMPC method can successfully deal with the frequency problem, and has better performance than the conventional PI control.

The thesis consists of six chapters. The research topics are mainly distributing among the chapters as follows:

Chapter 1: presents the introduction to the research objectives, scope of the research, and organization of the thesis.

Chapter 2: provides a comprehensive review of load frequency control, impact of renewable energy resources on frequency regulation, load frequency control techniques, and current world frequency technologies.

Chapter 3: presents a novel load frequency control method using adaptive model predictive control. The proposed AMPC method combine with unscented Kalman filter for capturing the optimal control operation. Meanwhile, some estimation methods are described in this chapter.

Chapter 4: presents a novel load frequency control method using adaptive model predictive control. The proposed method can cope with the frequency problem caused by disturbance. In this chapter, large-scale power systems with large disturbance are used to confirm the effectiveness of the proposed method. The numerical results show that the proposed method is effective to mitigate the frequency problem.

Chapter 5: develops a load frequency control method for small-scale microgrid (MG) using adaptive model predictive control. Large amount of renewable energy resources, such as wind turbine (WT) power, photovoltaic (PV) are installed in MG system, which can affect the MG system stability, especially the frequency stability. The developed method can address the MG system frequency problem effectively. The numerical simulation results demonstrate that the developed method is effective to mitigate the MG system frequency problem caused by the uncertain PV, WT, and types of disturbance.

Chapter 6: provides a conclusion part, where contributions of the study are discussed. In addition, some recommendations for further research in the future are presented.

Acknowledgment

I would like to express my gratitude to all those who have helped me in carrying out this research. Because their kind support and help, I have completed my research and doctoral thesis at Electric Power and Energy System Laboratory (EPESL), Graduate School of Advanced Science and Engineering, Hiroshima University. Additionally, I want to thank my parents, my uncle, my girlfriend, my friends for supporting me in Japan.

I would like to express my deepest gratitude to my supervisor, Specially Appointed Professor Naoto Yorino. This research can be completed under the guidance of my supervisor's kind help, suggestions and professional supports, who gave me his insightful teaching and thoughtful consideration.

Secondly, I would also like to express my deepest gratitude to Professor Yoshifumi Zoka and Associate Professor Yutaka Sasaki for their meaning advice and comments and professional support during the process of this research. I would also like to express my deepest gratitude to Professor Katsuhiko Takahashi and Professor Ichiro Nishizaki, for their serving as a secondary reviewer of this work.

Additionally, I would like to thank the Japanese Government Wise Program, MEXT Power Energy Professionals (PEP) Waseda University Graduate Program for the scholarship opportunity covering my study and staying in Japan. And thank Professor. Tomoko Kawakami, Associate Professor. Takao Tsuji, and Seiji Kawauchi for giving me meaning advice about this work.

I would like to thank Associate Professor Xiaodong Fei (Beijing Foreign Studies University), and Professor Norio Matsumi (Graduate School of Humanities and Social Sciences, Hiroshima University) for giving me a chance as a graduate student for beginning my Japan studying life.

Finally, I would like to express my deepest gratitude to Special Appointment Associate Professor. Ahmed Bedawy, and Mumbere Samuel Kihembo for their meaning suggestions and comments about this work. I am pleasure to meet my predecessor, Chongkai He. He gave me many meaning suggestions about research. And I want to express my most generous gratitude to Secretary. Yukiko Yamauchi, and all staff members of the EPESL for their continuous support and cooperation throughout the five years. Thanks very much.

WEICHAO WANG

2024

Significance of the research

・Significance in society

The large introduction of renewable energy sources mentioned above can affect the stability of the power system, especially the frequency stability. From the point of view of power system frequency stability, this work can provide a more effective control method for frequency problem of the power system. With its own high robustness and response speed, it can solve the frequency problem of the power system more efficiently. The proposed AMPC can achieve automatic adjustment of controller parameters with load and system characteristic changes. It does not require the operator experience and can significantly reduce labor costs.

The effective LFC method developed in this thesis can solve the frequency problem in the power system more efficiently. As a result, the amount of renewable energy introduced in the power system can be significantly increased. In other words, this is a technology that will greatly contribute to the realization of carbon neutrality. In addition to the applications of the renewable energy, MGs are expected to improve the resilience of power supply against disasters, etc., and the developed technology is expected to contribute to the development of MGs in the future. Therefore, the social significance of this research is the realization of a carbon-neutral and disaster-resistant society. As a result of the above, if MGs gain recognition and their needs increase in the future, business development can be expected.

・Significance in academics

This work proposes a novel LFC control method with high response speed and robustness. A novel autonomic control strategy using a combination of MPC and unscented Kalman filter. Simplified first-order as well as second-order models are also proposed to approximate the system dynamic response to reduce the computational time. This work gives the new possibilities for automated optimized frequency control. An effective control strategy is provided for the future frequency control field.

・Others

I am grateful that I was able to participate in the Power Energy Professionals (PEP) program. I have made many friends through this program. At the same time, I also learned

a lot about international standards and professional knowledge of my research field, which help me to accomplish this work.

For the power systems field, with this work, not only a new understanding and thinking about frequency control, but also a new understanding of power system stability studies, types of external disturbances, and the application and impact of renewable energy sources. For myself, it improves my vision and broadens my research field, which plays a vital role in my growth.

Table of Contents

List of Figures

List of Tables

Chapter 1: Introduction

1.1 Research objective・background

Recently, power systems consisting of a large amount of renewable energy sources, such as photovoltaic (PV), wind turbine power (WT) and battery energy storage system (BESS) have been attracting attention toward the realization of a carbon-neutral society. In 2022, the installed renewable energy sources are increasing in worldwide, such as China, around 1161 gigawatts; US, around 352 gigawatts; Brazil, around 175 gigawatts; India, around 163 gigawatts. Among the renewable energy sources, PV is on course to account for 60% of global renewable power growth in 2022. However, the increase in renewable energy sources affects the system stability, especially the frequency stability. Meanwhile, large amount of uncertain renewable energy sources applied to power system also has reduced the output ratio of the thermal generators. The reduction in number of the thermal generators affects the inertia of the power systems. This also decreases the frequency adjustment capability of the power system. Therefore, the maintenance and improvement of the frequency stability are an important issue must be addressed. In particular, small power systems, such as microgrid (MG) system with a high percentage of renewable energy may cause significant frequency fluctuations. In small-scale power systems, the frequency problem is mainly caused by the uncertainty of renewable energy source and large disturbance. Therefore, many researchers have been studied the effective LFC methods, such as the proportional integral (PI) control etc. to address the frequency problem in power systems, highly accurate and robust load frequency control technique is required to against large disturbances for maintaining the desired frequency range.

The main objective of this work is to propose a highly accurate and robust load frequency control (LFC) method. For this purpose, a novel adaptive control method using adaptive model predictive control (AMPC) is designed to address the frequency problem. The proposed AMPC method can predict the future performance of target system based on the internal prediction model. A simplified first-order and second-order lag system as an internal prediction model is proposed for AMPC. The parameters of the internal prediction model are estimated using an unscented Kalman filter (UKF) online. In this work, we had confirmed the performance of the UKF. Meanwhile, the

comparison results of the UKF with the extended Kalman filter (EKF), least square (LS), and Kalman filter show that the UKF has a better performance than other estimation methods.

1.2 Significance of the research

・Significance in society

The large introduction of renewable energy sources mentioned above can affect the stability of the power system, especially the frequency stability. From the point of view of power system frequency stability, this work can provide a more effective control method for frequency problem of the power system. With its own high robustness and response speed, it can solve the frequency problem of the power system more efficiently.

The proposed AMPC method considers the minimization of control cost in the objective function, which can effectively reduce the control cost. At the same time, synergizing renewable energy sources and regulating the power generation of generators can effectively protect the environment and reduce carbon emissions.

The proposed AMPC can achieve automatic adjustment of controller parameters with load and system characteristic changes. It not requires the operator experience and can significantly reduce labor costs.

・Significance in academics

This work proposes a novel LFC control method with high response speed and robustness. A novel autonomic control strategy using a combination of MPC and unscented Kalman filter. Simplified first-order as well as second-order models are also proposed to approximate the system performance to reduce the computational time. This work gives the new possibilities for automated optimized frequency control. An effective control strategy is provided for the future frequency control field.

・Others

For the power systems field, with this work, not only a new understanding and thinking about frequency control, but also a new understanding of power system stability studies, types of external disturbances, and the application and impact of

renewable energy sources. For myself, it improves my vision and broadens my research field, which plays a vital role in my growth.

1.3 Organization of the Thesis

The thesis's research objectives, methods, findings, and data analyses are meticulously detailed below across six chapters that include,

Chapter 1: presents the introduction to the research objectives, scope of the research, and organization of the thesis.

Chapter 2: provides a comprehensive review of load frequency control, impact of renewable energy resources on frequency regulation, load frequency control techniques, and current world frequency technologies.

Chapter 3: presents a novel load frequency control method using adaptive model predictive control. The proposed AMPC method combine with unscented Kalman filter for capturing the optimal control operation. Meanwhile, some estimation methods are described in this chapter.

Chapter 4: presents a novel load frequency control method using adaptive model predictive control. The proposed method can cope with the frequency problem caused by disturbance. In this chapter, large-scale power systems with large disturbance are used to confirm the effectiveness of the proposed method. The numerical results show that the proposed method is effective to mitigate the frequency problem.

Chapter 5: develops a load frequency control method for small-scale microgrid (MG) using adaptive model predictive control. Large amount of renewable energy resources, such as wind turbine (WT) power, photovoltaic (PV) are installed in MG system, which can affect the MG system stability, especially the frequency stability. The developed method can address the MG system frequency problem effectively. The numerical simulation results demonstrate that the developed method is effective to mitigate the MG system frequency problem caused by the uncertain PV, WT, and types of disturbance.

Chapter 6: provides a conclusion part, where contributions of the study are discussed. In addition, some recommendations for further research in the future are presented. The

final chapter synthesizes the contributions of the thesis, summarizing key findings and making recommendations for future research endeavors.

Chapter 2: Frequency control techniques for power systems

Frequency control is a system control technology to maintain the system frequency at 50[Hz] or 60[Hz] and it is a necessary technology to maintain normal operation of the system. Its characteristics are that the control effect is very wide-ranging regionally and the control energy is very large. They also have conflicting operating conditions, with the market demanding that power systems must be operated at low cost. The power system is obligated to provide a good quality electricity supply, where "good quality" generally means that the frequency, voltage, etc. are maintained within predetermined values, and that the power supply is sufficiently reliable to continue without power outages. System control fulfills this purpose, and includes both active power control, which targets the control of power flow and frequency, and reactive power control, which targets the rational distribution of reactive power control and the maintenance of voltage. First, let us consider why control of power system frequency and transmission line tidal current is necessary.

- From the consumer's point of view

The following advantages arise when the grid frequency is maintained at a constant level

(1) Stabilization of the frequency will stabilize the conditions for electricity use. Especially in recent years, when the use of computers and various types of automation become popular, the effect of frequency maintenance becomes very significant.

(2) In the case of electric motors, the rotational speed is almost constant, which improves the quality of the product.

(3) In the case of ordinary household electric clocks, it is desirable to keep the frequency as constant as possible.

- From the grid operator's point of view

(1) If the grid frequency is stable, speed adjustment by generators and speed regulators becomes easier, especially in large-capacity thermal power plants such as the recent ones. The vibration problem of the turbine's final-stage rotor blade can also be

reduced. This is the reason why the frequency fluctuation range is strictly defined in recent large-capacity thermal power plants.

(2) The frequency must be kept strictly constant in order to stabilize the power flow and to operate the tie line in a stable manner.

Many countries are promoting sustainable development and reducing carbon emissions. Microgrids integrate a large amount of renewable energy and distributed power generations, which are of great significance in promoting sustainable development and realizing carbon-neutral society. Many countries have set up and developed numerous projects for this purpose. For example, China: Beijing Yanqing new energy microgrid demonstration project, Zhuhai Wanshan island smart microgrid demonstration project; Japan: microgrid demonstration project in remote islands of Miyako; US: smart grid R&D program, smart grid demonstration program (SGDP) projects, and so on. With the introduction of large amounts of renewable energy into microgrids, the adjustment ability of microgrids will also be reduced. As a result, the requirement of frequency variation is stringent in power grids due to the introduction of large amounts of renewable energy. Table 2.1 summaries the frequency deviation ranges of some countries. This also demonstrates the importance of high robustness, effective controllers for frequency control.

Table 2.1 Typical frequency deviation ranges of some countries

	Frequency deviation requirements
China	50±0.2Hz
Japan	60±0.2Hz, 50±0.3Hz
US	60±0.2Hz
UK	50±0.5Hz
Spain	50±0.2Hz
German	50±0.2Hz
Ireland	50±0.5Hz

2.1 Recent frequency control techniques of the worldwide

This chapter introduces the basic concepts of frequency control and techniques of the worldwide. Power system frequency control is mainly divided into primary control, secondary control, and tertiary control. In power systems, secondary control called the

automatic generation control (AGC) plays a significant role in the control process in a power network to achieve the equilibrium between generation and load. AGC, also widely known as load frequency control (LFC), balances generation with the load consumption by commanding signals to control generators. Fig 2.1 illustrates the concept of generator control assignment and amplitude of load demand. However, there is no clear delimitation of each control in terms of periodic components.

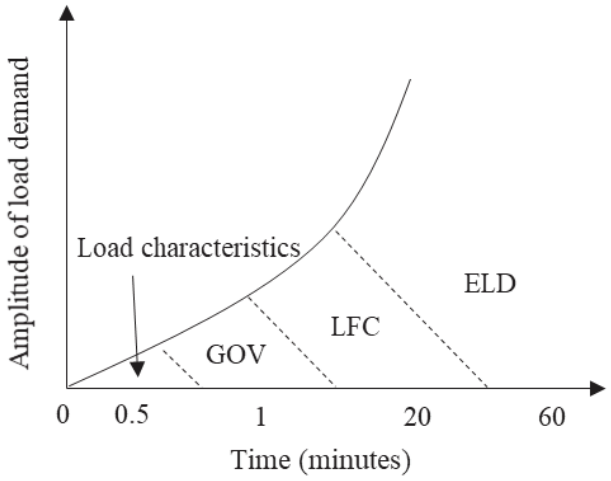

Fig 2.1 Control branch diagram.

Where, GOV means governor control, ELD means the economic load dispatch.

Fig 2.2 gives the typical frequency evolution in some countries based on different system response and period. As we know, the inertia of system depends on the installed capacity. Fig 2.2 is constructed based on data from 2019.

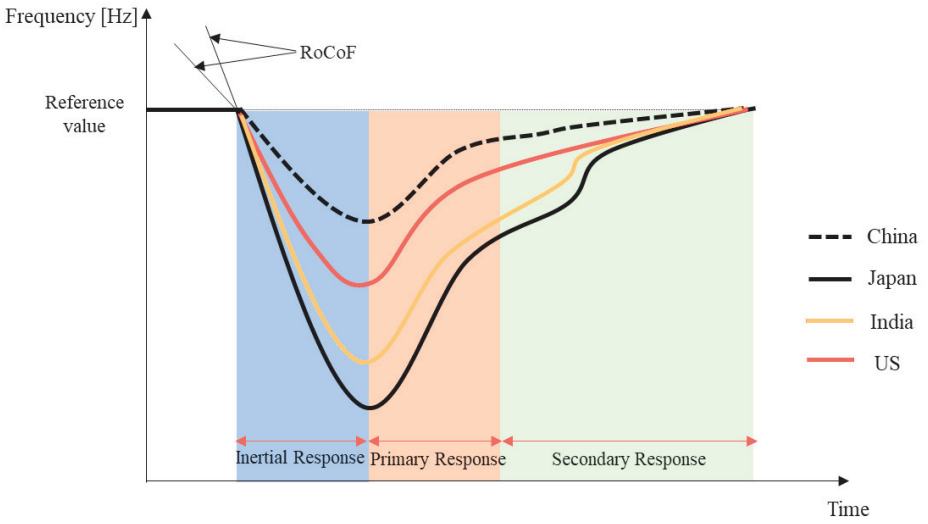

Fig 2.2 Frequency evolution.

A detailed description of this work is given in Chapter 3. Previously, the primary control1, the generator's swing equations as well as frequency control techniques are discussed in this chapter.

2.1.1 Control methods of load frequency control

Usually, flat frequency control (FFC) and tie-line load frequency bias control (TBC) are used as constant control methods for load frequency control (LFC) scheme. An overview of FFC and TBC will be explained in the following.

(a) Flat Frequency Control (FFC)

FFC detects how much the frequency deviates from the desired value. If the frequency is higher than the desired value, the output of the controlled power plant is reduced. If the frequency is lower than the desired value, the output of the controlled power plant is increased to restore the frequency.

Usually, proportional control is used, in which the change in output of the controlled power plant is proportional to the magnitude of the frequency deviation. In addition, the integral value of the frequency deviation is usually calculated and used as a control signal to the controlled power plant in order to set the integral value of the frequency deviation to zero. Therefore, the control method is called integral control.

Proportional integral (PI) control is the most popular conventional control method in most industries. It is widely used in various fields. Fig 2.3 shows the LFC with PI control in 1-area power system.

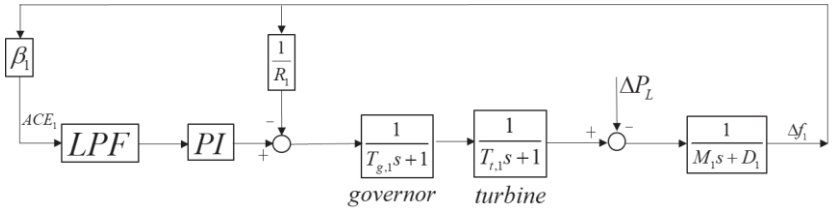

Fig 2.3 LFC with PI controller.

Here, ACE (area control error) was named as an AR (area requirement). LPF is low pass filter. the ACE is defined as follows.

$$ACE_1 = \Delta P_{tie,1} + \beta_1 \Delta f_1 \tag{2.1}$$

Where, ΔP_{tie} is power flow deviation, β is frequency response coefficient, Δf is frequency deviation.

In the system where this method is applied, the tie-line power fluctuates significantly because this control method is focused only on the system frequency. Therefore, this control method is suitable for a stand-alone system or in a main system with relatively large capacity.

(b) Tie-line load frequency bias control (TBC)

When several grids are operating in interconnection, frequency control using the FFC method causes the controlled power plants in the grid to respond not only when load changes occur in the grid, but also when load changes occur in other grids.

TBC is a control method that simultaneously detects the amount of frequency change and the interconnected power flow deviation (ΔP_T) to determine where the load change occurred, and each system has a policy to handle the load change that occurred within its own system.

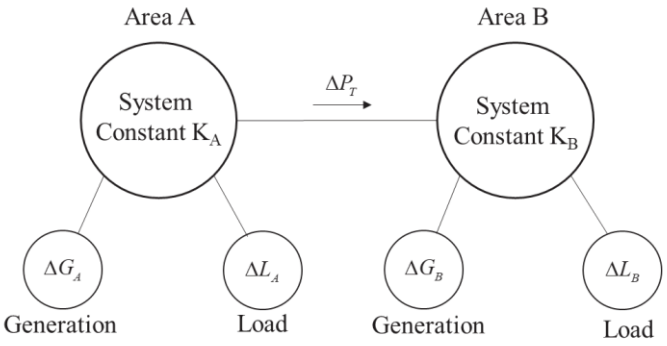

Fig 2.4 2-area power system.

Assuming the 2-area system shown in Fig 2.4, and assuming that load changes of ΔL_A, ΔL_B occur in power systems A and B, respectively. The frequency deviation is named as ΔF, the following relationship holds for the amount of load change in each system.

$$\Delta L_A = -K_A \cdot \Delta F - \Delta P_T \tag{2.2}$$

$$\Delta L_B = -K_B \cdot \Delta F + \Delta P_T \tag{2.3}$$

Furthermore, the frequency deviation can be obtained by transforming equations (2. 2) and (2.3).

$$\Delta F = -\frac{1}{K_A}\Delta L_A - \frac{1}{K_A}\Delta P_T \tag{2.4}$$

$$\Delta F = -\frac{1}{K_B}\Delta L_B + \frac{1}{K_B}\Delta P_T \tag{2.5}$$

The frequency fluctuates due to the load changes and the interconnected power flow fluctuations. In other words, knowing the frequency deviation of the system and the interconnected power flow deviation, the amount of load variation occurring in the own system can be known. Therefore, if the output of the power plant is controlled based on this amount, the plant will respond to the load changes in its own system. This value indicates the amount of control required within each interconnected system, and is called the AR or ACE.

Also, eliminating and rearranging equations (2.4) and (2.5), we can obtain

$$\Delta P_T = -\frac{K_B}{K_A + K_B}\Delta L_A + \frac{K_A}{K_A + K_B}\Delta L_B \tag{2.6}$$

This means that even if a load change occurs in system A, system B, or both systems at the same time, the interconnected power flow deviation changes, and the system frequency also changes according to equations (2.4) and (2.5).

2.1.2 Governor (GOV) control (primary control)

Primary control is mainly realized by governor control. Each generator stabilizes the frequency by having its governor respond to the frequency fluctuation. Specifically, the frequency is stabilized by looping the rotation speed of the generator to the rotational energy. The governor model of the primary delay system is shown in Fig 2.5.

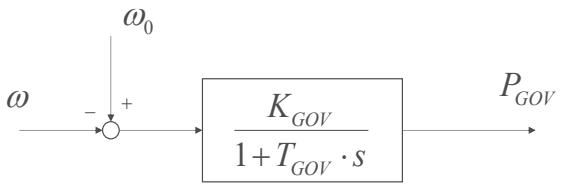

Fig 2.5 Block diagram of governor.

Where, P_{GOV} : the governor control quantity, ω_0 : center of inertia angular velocity, ω : velocity of the generator, K_{GOV} : governor gain, T_{GOV} : governor time constant.

Derive the differential equation for the governor from the block diagram.

$$P_{GOV} = \frac{K_{GOV}}{1+T_{GOV}\cdot s}\left(\omega-\omega_0\right) \tag{2.7}$$

$$\Leftrightarrow P_{GOV}\cdot s = \frac{1}{T_{GOV}}\left\{-P_{GOV}-K_{GOV}\left(\omega-\omega_0\right)\right\} \tag{2.8}$$

Inverse Laplace transform of (2.8).

$$\dot{P}_{GOV} = \frac{1}{T_{GOV}}\left\{-P_{GOV}-K_{GOV}\left(\omega-\omega_0\right)\right\} \tag{2.9}$$

The GOV control amount is determined from the difference between the system frequency and the reference frequency. This control block is shown in Fig 2.6.

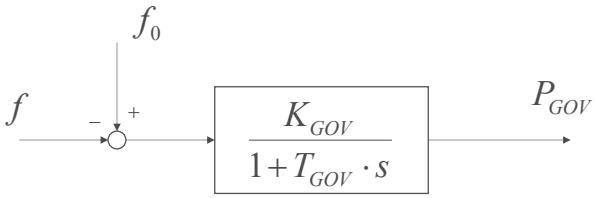

Fig 2.6 Block diagram of governor.

2.1.3 Generator's swing equations

In this study, the kinematic characteristics of the generator are simulated by an approximate model. The model is based on the linear transient reactance and the voltage behind the transient reactance, and the approximate equations of motion are used to simulate the motor's kinematic characteristics.

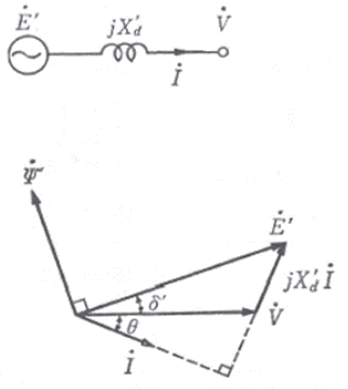

Fig 2.7 X'_d model.

In Fig 2.7, the transient internal voltage $\dot{E}'$ is obtained by the generator terminal voltage $\dot{V}$ plus the voltage drop $jX'_d\dot{I}$ at X'_d. The magnitude E' is considered constant during the oscillation. This is due to the assumption that the transient reactance X'_d of the generator and rectilinear axes X_q of the generator are equal. The transient sudden polarity is neglected and the number of chain fluxes ψ' and $\dot{E}'$ does not change during the oscillation.

The swing equation of the generator is expressed as follows.

$$\frac{M}{\omega_n}\frac{d^2\delta'}{dt^2} = P_M - P \tag{2.10}$$

Where, M : generator inertia constants, ω_n : angular velocity, δ' : $\dot{E}'$ phase angle, generator P_M, P : mechanical input, electrical output [p.u.].

The swing equation is a differential equation that expresses the state of the system. Consider a synchronous generator generating electrical torque and operating at a synchronous speed. If the mechanical torque is equal to electric torque, as follows.

$$T_m = T_e \tag{2.11}$$

Losses are ignored. The acceleration (deceleration) torque is generated by the addition of some disturbance to this torque.

$$T_a = T_m - T_e \tag{2.12}$$

$T_m > T_e$ is the acceleration, and if it is $T_m < T_e$, it is the deceleration. If this is rewritten using the inertia, the equation is as follows.

$$J\frac{d^2\delta}{dt^2} = T_a = T_m - T_e \tag{2.13}$$

Where, δ is the phase angle of the rotor, which is constant at steady state. This can be expressed using the angular velocity ω of the rotor as follows.

$$\delta = \omega t + \delta_s \tag{2.14}$$

Where, ω is the synchronous speed that maintains a constant steady state. Also, δ_s denotes the phase angle at $t = 0$, we can obtain the following equation by ω.

$$J\omega\frac{d^2\delta}{dt^2} = \omega T_m - \omega T_e \tag{2.15}$$

Since the product of angular velocity and torque equals power, equation (2.15) can be rewritten using power *P* as follows.

$$J\omega\frac{d^2\delta}{dt^2} = P_m - P_e = P_a \tag{2.16}$$

Based on the above discussion, the swing equation for generator is given and the primary control is provided by the governor. However, GOV control cannot satisfy that the frequency fluctuation range is maintained near the desired value. Therefore, the secondary control (LFC) also provides an important role in maintaining the frequency deviation and the amount of inter-area tie line power within satisfactory limits. We can also see from Fig 2.1 that when the load demand period becomes long and increases in the magnitude, it is usually necessary to combine with the ELD strategy. Therefore, in order to maintain the frequency deviation within the desired range, a large number of scholars have proposed effective control strategies. Some of the latest frequency control techniques are described below.

2.1.4 Proportional integral (PI)

Proportional integral (PI) is a simple controller with less cost, which is wildly used in industry. At the same time, PI control with integral function has an ability to minimize the steady-state error. However, in conventional PI controller, the parameters of the PI controller must be tuned to cope with various system characteristics. It requires that the system operator must have the skills to adjust it. An improperly adjusted parameter can cause delays, overshoots, and even system instability.

The block diagram of the LFC scheme using PI controller is presented in Fig 2.8. In LFC scheme, an area control error (ACE) signal is defined for evaluating the effectiveness of the frequency control. The ACE signal is also called the area requirement (AR) signal.

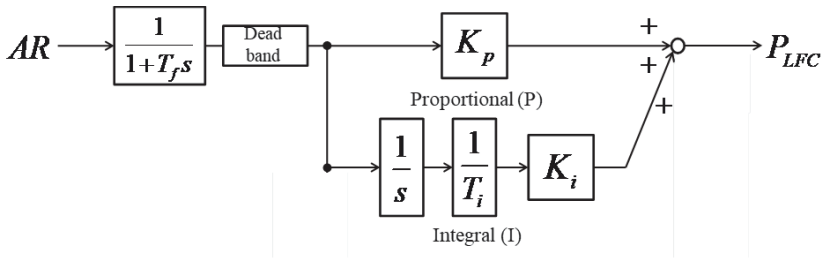

Fig 2.8 Block diagram of PI control.

Where, T_f is the time constant of the LPF. K_P, K_I are the gain of proportional and integral. P_{LFC} is the system output.

As shown in Fig 2.8, the AR is passed through a low-pass filter (LPF) to remove short-period noise. Then, PI control is performed to calculate the LFC control signal. This equation is shown in the following.

$$P_{LFC} = \frac{1}{1+T_f s}\left(K_p + \frac{K_i}{T_i s}\right) AR \tag{2.17}$$

Since the PI controller itself has the disadvantage of not able to concern with transient oscillation. Therefore, a large number of researchers have proposed various types of PI controllers, such as proportional integral derivative (PID), fractional order PID (FOPID), tilt integral derivative (TID), and so on. Compare the conventional PI control, the following control methods with optimal control algorithm can effectively address the power system frequency issue.

2.1.5 Linear quadratic regulator (LQR)

The linear quadratic regulator (LQR) control algorithm is a type of optimal control that aims to set up a quadratic objective function for the linear system. The purpose of the LQR is to satisfy the minimization of the cost of the objective function. The solution of a quadratic problem is called a linear quadratic problem, and the controller with quadratic objective function is called the LQR controller.

The optimal feedback control gain of the LQR is computed while satisfying the minimization of the objective function through state feedback process. Thus, the optimal control signal of the system is obtained by this process.

A generalized objective function without time constraints applied to LQR is written as follows.

$$J = \int_0^\infty (xQx + uRu)dt, \;\; Q \geq 0, \; R > 0 \tag{2.18}$$

Where, Q and R are the weights of the state value (x) and control signal (u)

For a linear time-invariant (LTI) system, which can be expressed by the following state-space equation, whose control block diagram is represented by Fig 2.6.

$$\begin{aligned} \dot{x}(t) &= Ax(t) + Bu(t) \\ y &= Cx(t) + Du(t) \end{aligned} \tag{2.19}$$

Where, A, B, C, D are the state-space matrices of the system. x, y are the state valuables and output of the system.

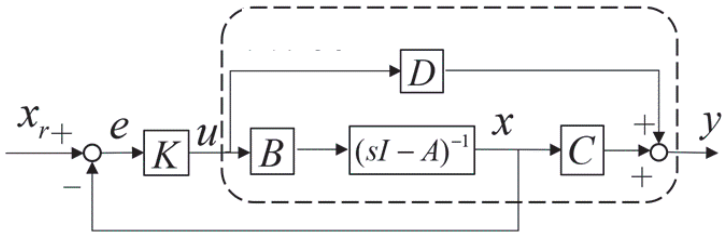

Fig 2.9 Block diagram of LGR.

From Fig 2.9, the control signal u can be computed by the feedback gain of the LQR controller, as shown in (2.20).

$$u = Ke = K(x_r - x) \tag{2.20}$$

Where, K is the LQR feedback gain, e is the error of the state value, x_r is the reference value.

Substitute (2.20) into (2.19), the following (2.21) can be obtained.

$$\begin{aligned} \dot{x}(t) &= Ax(t) + B[K(x_r - x)] \\ &= (A - BK)x(t) + Bx_rK \end{aligned} \tag{2.21}$$

When the reference value $x_r = 0$, we can obtain the following state-space equation.

$$\dot{x}(t) = (A - BK)x(t) \tag{2.22}$$

Using the Lyapunov to check the stability of the system. $V(x)$:Lyapunov function. In (2.19), consider $u = 0$, therefore, $\dot{x}(t) = Ax(t)$. We can consider the $V(x) = x^T Px$. Differentiate the $V(x) = x^T Px$. We can obtain the following equation.

$$\begin{aligned} \frac{d}{dt}V(x) &= \frac{d}{dt}x^T Px \\ &= \dot{x}^T Px + x^T P\dot{x} = 0 \end{aligned} \tag{2.23}$$

Substituting $\dot{x}(t) = Ax(t)$ into (2.23), the following (2.24) can be obtained.

$$\begin{aligned} \frac{d}{dt}V(x) &= (Ax)^T Px + x^T P(Ax) \\ &= x^T A^T Px + x^T PAx \\ &= x^T (A^T P + PA)x = 0 \end{aligned} \tag{2.24}$$

As a result, $A^T P + PA < 0$ is the Lyapunov inequality.

$\lim_{t\to\infty} V(x) = \lim_{t\to\infty} x^T Px = 0$, $\lim_{t\to\infty} x = 0$ Then, the system is asymptotically stable. At this point, the system is asymptotically stable. Adding $x^T Qx$ to (2.24), we introduce a positive definite matrix *Q*. the Lyapunov equation (2.25) is obtained.

$$A^T P + PA + Q = 0 \tag{2.25}$$

To substitute the previous equation (2.22) into equation (2.25), equation (2.25) is switched to the new coefficients as follows.

$$A_{cl}{}^T P + PA_{cl} + Q_{cl} = 0 \tag{2.26}$$

Substituting equation (1.15) and $Q_{cl} = Q + K^T RK$ into equation (2.26).

Where, *R* is the weight.

$$(A - BK)^T P + P(A - BK) + (Q + K^T RK) = 0 \tag{2.27}$$

$$PA + A^T P + \underline{(-PBK - (BK)^T P + K^T RK)} + Q = 0 \tag{2.28}$$

Due to $(XY)^T = Y^T X^T$, $P^T = P, (B^T)^T = B, (R^{-1})^T = R^{-1}, RR^{-1} = I$, we can get the following Riccati equation (2.30) for computing the feedback gain (K) of the LGR controller.

$$\begin{aligned}
&\underline{-PBK - (BK)^T P + K^T RK} \\
&= -PB(R^{-1}B^T P) - (R^{-1}B^T P)^T B^T P + (R^{-1}B^T P)^T R(R^{-1}B^T P) \\
&= -PBR^{-1}B^T P - P^T (B^T)^T (R^{-1})^T B^T P + P^T (B^T)^T (R^{-1})^T RR^{-1}B^T P
\end{aligned}$$

$$\begin{aligned}
&\underline{-PBK - (BK)^T P + K^T RK} \\
&= -PBR^{-1}B^T P \underbrace{-PBR^{-1}B^T P + PBR^{-1}B^T P}_{0} \\
&= -PBR^{-1}B^T P
\end{aligned} \tag{2.29}$$

$$PA + A^T P - PBR^{-1}B^T P + Q = 0 \tag{2.30}$$

2.1.6 Slide mode control (SMC)

Sliding mode control (SMC) as the variable structure control has been studied by an increasing number of researchers in the nonlinear control field. It is also essentially a nonlinear controller designed based on the Lyapunov principle described above section. SMC is to design a state feedback controller that introduces the so-called "sliding mode surface" concept as a new state variable. SMC reconstructs the Lyapunov function $V(x)$ so that the new Lyapunov function converges to zero over time.

The core idea of SMC is to design a sliding mode surface S that stabilizes the system when the system state is on the S. And the objective of SMC is to make the system stabilized by making how the sliding mode surface S tends to 0, which is shown in the following Fig 2.10.

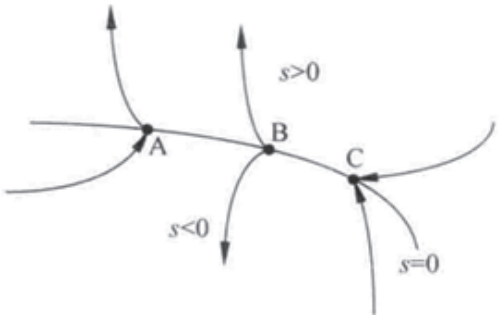

Fig 2.10 Sliding mode surface *S*.

In the LFC file, the state-space equation of power system is described by the above-mentioned equation (2.19). Therefore, the sliding mode surface *S* is usually determined by the system output *y*, which shown in the following equation.

$$\begin{aligned} s(x) &= y \\ &= Cx \end{aligned} \tag{2.31}$$

2.1.7 Conventional model predictive control (MPC)

Model predictive control (MPC) algorithm is proposed by Richalet in 1978. MPC is a method for optimal control under the constraints. MPC almost consists of three parts: (1) Prediction model, (2) Rolling optimal control, (3) Feedback correction.

MPC is one of the modern control algorithms, which determines control inputs by solving a sequential optimization problem based on a predefined system model. The MPC control method is usually described by simple models that are easily understood by engineers, such as impulse response models and step response models. Another reason is that the control cycle is relatively long in process control, allowing sufficient time for on-line calculations to determine the optimal input. Today, as computers have become more powerful, the range of applications has expanded greatly. Various theories and algorithms have been studied to date. MPC can easily handle multiple-input, multiple-output (MIMO) systems. In order to incorporate the benefits of modern control theory into the MPC framework, a state-space model with an objective function is used to predict future behaviors and solve a finite-interval optimization problem with constraints. The MPC control method is a procedure that is repeated at each sampling time to determine the input that makes the behavior as desirable as possible by solving an optimization problem in a finite interval under constrained conditions.

MPC has a prediction model (in other words, an internal model) inside the controller to predict the future performance of the controlled system over a finite interval of time from the current time. In order to perform control, it is necessary to appropriately capture the dynamic characteristics of the control target, i.e., the dynamics, and represent them as a model.

Typical examples of prediction models include step response models, impulse response models, transfer function models, and state equations. To actually perform the control behavior, the predicted results must be used to determine the control input to be given to the control target. Therefore, in MPC, the control input is uniquely determined by solving an optimization problem at each sampling time.

As shown in the Fig 2.11 below, when the output of the control target to follow a certain target value, MPC can search for a time series of control inputs that minimize the area of the tracking error in the prediction interval from the current time to the future.

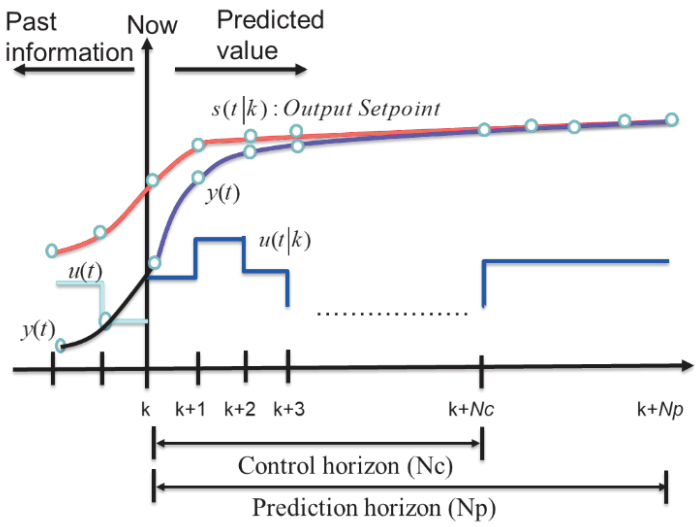

Fig 2.11 MPC.

The following technical elements are required to constitute MPC.

(1) Prediction modeling technology

Derivation of prediction models by physical or statistical modeling.

(e.g., transfer function, equation of state)

(2) Numerical optimization technology

Fast numerical optimization solver to solve optimization problems in real time

Example: Solving quadratic programming (QP) problems ... effective constraint method, interior point method, conjugate gradient method, etc.

(3) State observer design technology

State observer to estimate the state quantity of a control target that cannot be measured

Example: Kalman filter.

(4) Numerical simulation technology

Virtual experiments of closed-loop systems using computational models on a PC.

The following Table 2.2 summarizes the recent LFC techniques, along with their advantages and disadvantages.

Table 2.2 Summary of the recent frequency control techniques

Type	Advantages	Disadvantages
Proportional integral (PI)	● Easy realization ● Wide range of applications ● Easy adjustment ● Low computational burden	● Needs to be tuned ● Linear systems only ● Noise sensitivity
Linear quadratic regulator (LQR)	● Can handle MIMO system problems ● High robustness	● Large computational burden ● Without constraints
Slide mode control (SMC)	● High robustness ● High response speed ● Versatile control features ● Handles non-nonlinear	● Overshoot problem ● High frequency oscillation ● The performance of SMC depends heavily on the sliding-mode surface and the setting of the control law
Conventional model predictive control (MPC)	● Low accuracy requirements for models, easy modeling ● High robustness and stability, good dynamic	● Model accuracy has a big impact on MPC performance ● Large computational burden

	control performance, Fast response speed ● Can effectively handle multivariate, constrained problems	

2.2 Application of renewable energy sources (RESs)

Recently, power systems consisting of a large amount of renewable energy sources (RESs), such as photovoltaic (PV), and wind turbine power (WT) have been attracting attention toward the realization of a carbon-neutral society. The introduction of RESs is expected to expand as a measure to cope with global warming and energy security. On the other hand, there are concerns that the mass introduction of RESs may have various effects on the stable operation of the existing power system. In particular, WT and PV are expected to make the operation of the power system extremely difficult. Due to their large introduction because their outputs fluctuate greatly depending on the time of day and weather conditions with large uncertainties. As a result, a large amount of PV and WT etc. RESs with uncertainties are applied to current power system, which affect the frequency stability.

Table 2.3 summarizes the types of RESs that are being used worldwide and their respective characteristics.

Table 2.3 Characteristics of RESs.

Generation	Characteristics
PV	・Basically, it is not restricted by area and can be installed anywhere. ・Large area is required to ensure sufficient supply. ・High output during the daytime can be expected to reduce peak demand, but at night or when it rains or is cloudy, power is not generated and the facility utilization rate is low. ・Output varies greatly depending on weather.
WT	・Power generation is possible even at night if there is wind. ・High conversion efficiency of up to 45%.

	・Output is unstable, as it varies with wind speed, and the concentration of installations in areas with good wind conditions results in large output fluctuations in those areas. ・Installation is often far away from demand areas, resulting in long transmission distances.
Offshore WT	・Offshore WT facilities can be built in shallow water. ・Wind conditions are favorable and wind turbulence is small. ・Avoids landscape and noise problems.
Geothermal Power generation	・The unit cost of power generation is high due to the cost of exploration and development of production wells and the need to re-drill production wells when they reach the end of their useful life, although fuel is not required. ・No concern about fuel depletion or price hikes.
Biomass	・Animal resources (livestock manure) are fermented to produce methane, which is burned to recover energy, and plant resources (wood waste, straw waste) are directly burned to recover energy. ・Energy density is low, so the energy required for collection must be considered. ・CO_2 is emitted when resources are burned, but this CO_2 is only absorbed from the atmosphere during the growth of organisms and returned to the atmosphere, so atmospheric CO_2 is not increasing in the long term.

2.2.1 Overall of RESs

Recent years, PV, WT et.al RESs have been spreading rapidly around the world to cope with global warming and environmental problems. In 2022, the installed RESs are increasing in worldwide, such as China, around 1161 gigawatts; US, around 352 gigawatts; Brazil, around 175 gigawatts; India, around 163 gigawatts. Among the RESs, PV is on course to account for 60% of global renewable power growth in 2022. Fig 2.12 shows that the leading countries in installed RESs capacity worldwide in 2022. RESs have gradually become the main energy source to replace fossil fuels in worldwide due

to its cleanliness and less pollution to the environment. However, due to the RESs have large uncertainties, which bring significant challenges in power system operations, including frequency control, voltage control etc.

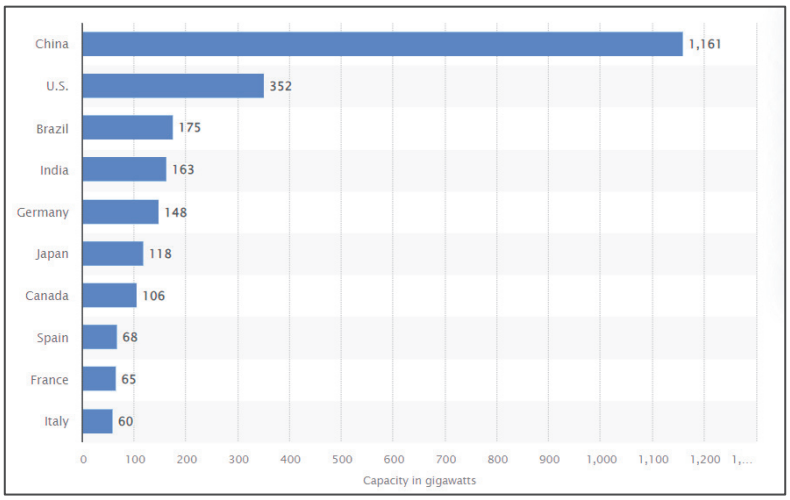

Fig 2.12 Leading countries in installed renewable energy capacity worldwide in 2022. (Source by Statista 2023)

2.3 Disturbances

In the power systems, the disturbances including lead demand, fault, system noise et.al can affect the system stability, power quality. Disturbances are usually caused by fluctuations in active power, such as changes in load, changes in generator output, or changes in the system's own parameters. Therefore, regulating the balance between generation and load disturbances to improve power quality becomes an important issue. This section discusses the types of disturbances, modeling of disturbances, white noise and step change.

2.3.1 Types of disturbances

Depending on the magnitude of the disturbances, which can usually be categorized into large and small disturbances. Small disturbances, such as noise generated by the generator itself, inter-regional power flow control, and so on. Large disturbances, such as sudden load changes, faults, disasters and other causes of system disturbances. There is also the large amount of renewable energy introduced into the power systems as mentioned in the previous section, which can be seen as the large disturbances. These disturbances potentially affect the stability of the system as well as the power quality.

As shown in Fig 2.13, disturbances are considered to have superimposed components with various periods. Although it is not a strict expression, a relatively slow component of the load fluctuation is called the sustained component, a component with a short period is called the fringe component, and a component with a shorter period is called the cyclic component. The shorter component is sometimes referred to as the cyclic component. In the current control system, the control assignment is determined for each component, and the assignment table is shown in Table 2.4.

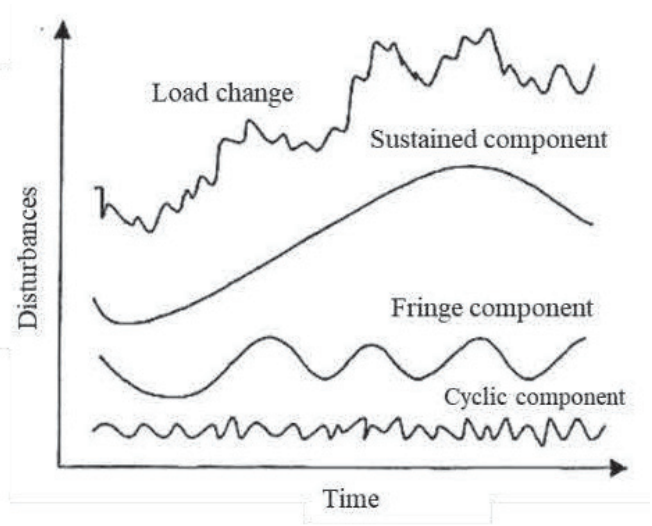

Fig 2.13 Classification of disturbance.

Table 2.4 Period of disturbance

Component name	Period	Control method
Cyclic component	Less than a few minutes	Governor
Fringe component	Several minutes	Load frequency control
Sustained component	More than 10 minutes	Economic load dispatch

To express the disturbances exactly, it is convenient to divide the disturbances into components with various frequencies and express them in terms of spectra. If the disturbance is passed through an ideal bandwidth filter that has a constant gain between the frequencies of the disturbance. Blocks out the components of the other frequencies, the output of this filter will not contain any frequencies components outside the spectrum. The mean of the squares of the output of this filter is called the spectral density.

2.3.2 Modeling of disturbances

In general, the value of the disturbance is 1% of the system capacity. For example, if the system capacity is 1pu, the value of the step disturbance is set to 0.01pu. 0.02pu and 0.1pu step disturbances are also set. A disturbance modeling calculation is given below equation (2.32)

$$\Delta P_L = 0.6\sqrt{P_{Load}} \tag{2.32}$$

Where, P_{Load} : actual load, ΔP_L : simulation load.

2.3.3 White noise disturbances

White noise is usually a random signal with a constant mean value (0). Among them, white noise obeying a Gaussian distribution has been widely studied in the power systems field. They arise from many causes, such as the generators, transformers, change in system parameters, load demand and so on. This short-period, high-frequency random white noise can have a serious impact on the stable operation of the power system, as well as affect the voltage and current. That could affect the normal operation of the power equipment. Therefore, a low-pass filter is usually used to eliminate the random white noise.

For example, a band-limit white noise based on Gaussian distribution. The equation (2.33) is determined by the following. A regular distribution chart based on variance is shown in Fig 2.14.

$$\text{Power noise (P)} = \sigma^2 \cdot T_s \tag{2.33}$$

Where, σ is variance of noise, T_s is sampling time.

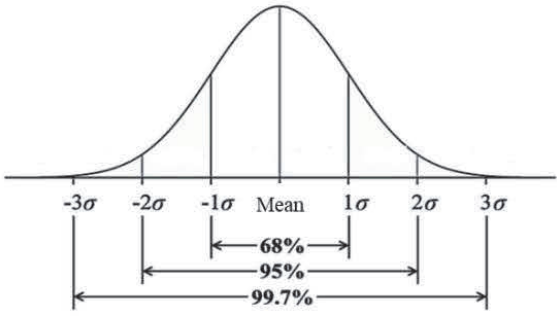

Fig 2.14 Regular distribution chart.

Fig 2.15 shows waveform when the variance σ is 0.01.

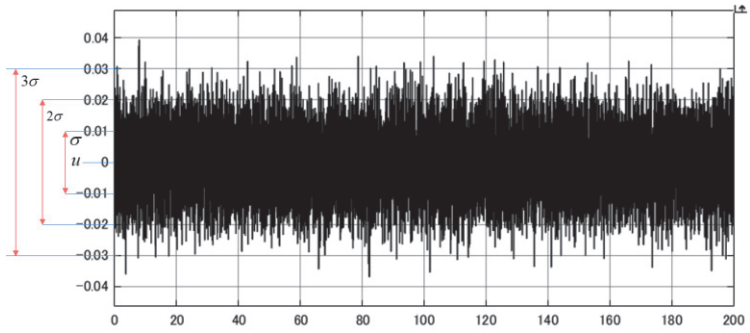

Fig 2.15 Band-limit white noise.

It has been verified that the output through such a low-pass filter follows a Gaussian distribution. The variance is determined by the following equation.

$$\sigma_{f_0} = \int_{f_0}^{\infty} G(f)\,df \tag{2.34}$$

The analysis of the disturbances in the actual system shows that for the component with a period shorter than ten minutes ($f > f_0 = \frac{1}{10}\min^{-1}$), the following $G(f)$ can be obtained.

$$G(f) = \frac{k}{f^2} \quad , \quad k = f_0\sigma_{f_0} \tag{2.35}$$

It is known from various measurements in countries of the world that the magnitude of the magnitude is 2~3% MW of the grid capacity for components shorter than a few minutes.

2.3.4 Variable step change

Load demand refers to the continuous load change in time. Generally, loads have cyclical and seasonal variations. The elimination of short-period load variations is LFC's main objective in the LFC scheme, which is given in Fig 2.1. When load demand is introduced to the power grid, the external load disturbance is considered as a continuous step change over a period of time.

For example, Fig 2.16 shows a continuous step change over a 30 minutes period.

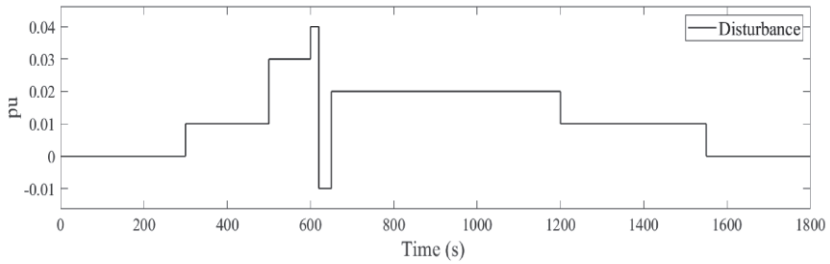

Fig 2.16 Continuous step change.

2.4 Effect of RESs and disturbances on power system frequency control

RESs and disturbances have a significant impact on the stability of the power systems, such as voltage, frequency stability. The large disturbances can lead to severe generation-demand imbalances in the power system. This is the reason for frequency fluctuation. Even that the imbalance and frequency fluctuation can lead to power outages. At the same time, because RESs with the uncertainty and unpredictability due to weather condition and other factors. Large amount of uncertain RESs applied to power system have reduced the output ratio of the conventional thermal generators. The reduction in number of the thermal generators affects the inertia of the power systems. Due to the conventional thermal generators is an important factor to provide the system inertia. This also decreases the frequency adjustment capability of the power system. Therefore, it's necessary to design a robustness LFC controller with high response speed and accuracy for addressing the frequency fluctuation issue.

To address the frequency issue caused by uncertain RESs and disturbances, more and more researchers have studied effective and robust strategies for LFC scheme due to large amount of RESs applied to power system. Some prediction methods, such as neural network, machine learning is used to estimate the generation of RESs. The published papers have reported the state of the art LFC techniques combine with the prediction methods to address the frequency problems caused by the uncertain RESs. The utilization of a large amount of uncertain RESs also bring many challenges for LFC techniques.

Chapter 3: Robust frequency control using proposed AMPC approach

3.1 A novel frequency control method using adaptive model predictive control (AMPC)

This thesis proposes a novel robust frequency control method using adaptive model predictive control (AMPC). Chapter 2 has discussed the conventional AMPC method. It is well known that the AMPC method almost consists of three components, i.e., rolling optimization, feedback correction, and internal prediction model. In this chapter, the proposed AMPC approach is introduced in detail, along with the descriptions of the three components.

3.1.1 Adaptive model predictive control (AMPC) formulation

First, the state-space equation of the power system is discretized as (3.1).

$$\begin{aligned} x(k+1) &= Ax(k) + Bu(k) \\ y &= Cx(k) \end{aligned} \tag{3.1}$$

Where, *A, B, C* are the state-space matrices of the system. *x, y* are the state valuables and output of the power system.

In order to introduce the state vector into (3.1), the state vector is increased and defined in equations (3.2), (3.3).

$$x(k) = \begin{bmatrix} \Delta x(k) & y(k) \end{bmatrix}^T \qquad y(k) = \begin{bmatrix} \Delta x(k) & y(k) \end{bmatrix}^T \tag{3.2}$$

$$\begin{aligned} \overbrace{\begin{bmatrix} \Delta x(k+1) \\ y(k+1) \end{bmatrix}}^{x(k+1)} &= \overbrace{\begin{bmatrix} A & o \\ CA & 1 \end{bmatrix}}^{A} \overbrace{\begin{bmatrix} \Delta x(k) \\ y(k) \end{bmatrix}}^{x(k)} + \overbrace{\begin{bmatrix} B \\ CB \end{bmatrix}}^{B} \Delta u(k) \\ y(k) &= \overbrace{\begin{bmatrix} o & 1 \end{bmatrix}}^{C} \begin{bmatrix} \Delta x(k) \\ y(k) \end{bmatrix} \end{aligned} \tag{3.3}$$

Where, Δx is the state valuables deviation of the system.

Based on (3.3), a new state-space model is obtained as shown in (3.4).

$$\begin{aligned} x(k+1) &= Ax(k) + B\Delta u(k) \\ y(k) &= Cx(k) \end{aligned} \tag{3.4}$$

The control and prediction horizons of AMPC are named as N_c and N_p, respectively. The predicted output at future time $k+N_p$ is obtained by the following equation.

$$\begin{aligned} y_{k+1|k} &= CAx_k + CB\Delta u_k \\ y_{k+2|k} &= CA^2 x_k + CAB\Delta u_k + CB\Delta u_{k+1} \\ &\vdots \\ y_{k+Np|k} &= CA^{Np} x_k + CA^{Np-1} B\Delta u_k + CA^{Np-2} B\Delta u_{k+1} \\ &\quad + \ldots + CA^{Np-Nc} B\Delta u_{k+Nc-1} \end{aligned} \tag{3.5}$$

AMPC can predict the future state values based on the following equation.

$$\begin{aligned} x_{k+1|k} &= Ax_k + B\Delta u_k \\ x_{k+2|k} &= Ax_{k+1|k} + B\Delta u_{k+1} \\ &= A^2 x_k + AB\Delta u_k + B\Delta u_{k+1} \\ &\vdots \\ x_{k+Np|k} &= A^{Np} x_k + A^{Np-1} B\Delta u_k + A^{Np-2} B\Delta u_{k+1} \\ &\quad + \ldots + A^{Np-Nc} B\Delta u_{k+Nc-1} \end{aligned} \tag{3.6}$$

Based on (3.6), a new state-space equation can be defined as follows.

$$Y = Fx(k) + \Phi\Delta U \tag{3.7}$$

Where,

$$Y = \begin{bmatrix} y_{k+1|k} & y_{k+2|k} & \cdots & y_{k+Np|k} \end{bmatrix}^T \tag{3.8}$$

$$\begin{aligned} F &= \begin{bmatrix} CA & CA^2 & CA^3 & \cdots & CA^{N_p} \end{bmatrix}^T \\ \Delta U &= \begin{bmatrix} \Delta u(k) & \Delta u(k+1) & \Delta u(k+2) & \cdots & \Delta u(k+N_c-1) \end{bmatrix}^T \end{aligned} \tag{3.9}$$

$$\Phi = \begin{bmatrix} CB & 0 & 0 & \cdots & 0 \\ CAB & CB & 0 & \cdots & 0 \\ CA^2B & CAB & CB & \cdots & 0 \\ \vdots & \vdots & \vdots & \vdots & \vdots \\ CA^{N_p-1}B & CA^{N_p-2}B & CA^{N_p-3}B & \cdots & CA^{N_p-N_c}B \end{bmatrix} \tag{3.10}$$

The objective function is set for AMPC by the following equation (3.11) considering the minimization of the system output and control cost.

$$J = (R_s - Y)^T (R_s - Y) + \Delta U^T \bar{R} \Delta U \tag{3.11}$$

The following Riccati equation (3.12) is used to compute the optimal feedback gain (K_{AMPC}) of AMPC based on optimal feedback control theory, which is given in Chapter 2.

$$PF + F^T P - P\Phi S^{-1}\Phi^T P + Q = 0 \tag{3.12}$$

$$K_{MPC} = (\Phi^T \Phi + S)^{-1}\Phi^T F \tag{3.13}$$

A control signal u for generator is also obtained based on the feedback gain (3.13)

$$\begin{aligned} \Delta u(k) &= -K_{MPC}\, x(k) \\ u(k) &= u(k-1) + \Delta u(k) \end{aligned} \tag{3.14}$$

3.1.2 Rolling optimization

Fig 3.1 shows the AMPC's optimal process, called rolling optimization. It is an important part of the AMPC. The K_{AMPC} of AMPC is also computed to capture the optimal input signal u based on (3.14) in this optimal process.

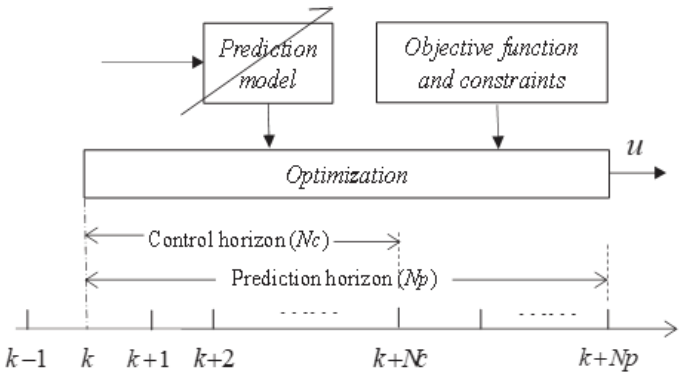

Fig 3.1 Rolling optimization.

The AMPC is an optimality approach for minimizing the objective function. The objective function in (3.15) is used in the proposed AMPC method to satisfy the frequency range and minimize the control cost.

$$\min J = \sum_{h=1}^{N_p} x(k+h\,|\,k)^T \boldsymbol{Q}\, x(k+h\,|\,k) + \sum_{h=0}^{N_c-1} \Delta u(k+h\,|\,k)^T \boldsymbol{S}\, \Delta u(k+h\,|\,k) \tag{3.15}$$

Where, $\boldsymbol{Q} \in \boldsymbol{C}^T\boldsymbol{C}$ and $\boldsymbol{S} \in 0.1 \cdot \boldsymbol{I}_{Nc\times Nc}$ are the weight matrices of the state valuables and input signal deviation; h is the sample period.

The equation (3.15) is the optimization objective function of the AMPC, which is used to design the optimal feedback gain (K_{AMPC}). AMPC is also designed using the optimal control theory (3.12) to solve (3.15). The objective function minimizes the regulated state values, and the AMPC controller cost is also considered using the weight matrices S.

In LFC scheme, to consider the safe operation and the desired frequency deviation range. The following constraints are also used in AMPC, as shown in (3.16).

$$\begin{cases} \Delta f^{\min} \le \Delta f\ (k) \le \Delta f^{\max} \\ u^{\min} \le u\ (k) \le u^{\max} \end{cases} \tag{3.16}$$

3.1.3 Feedback correction

AMPC method uses the feedback correction to form a closed-loop optimization for compensating the predicted error and stabilizing system. The following feedback correction equation is used in this thesis.

$$x_p(k+1) = x_m(k+1) + \zeta[x(k) - x_m(k)] \tag{3.17}$$

Where, ζ is the correction factor. x_p is the correction state values, x_m is the prediction state values.

With a feedback correction process, AMPC has powerful automatic adaptive capabilities to overcome system uncertainty. AMPC is not only based on the internal prediction model, but it is feedback control that also uses feedback information. Therefore, AMPC has the ability to suppress the effects of noise on control quantities

with high control accuracy. The feedback correction of AMPC is shown in Fig 3.2.

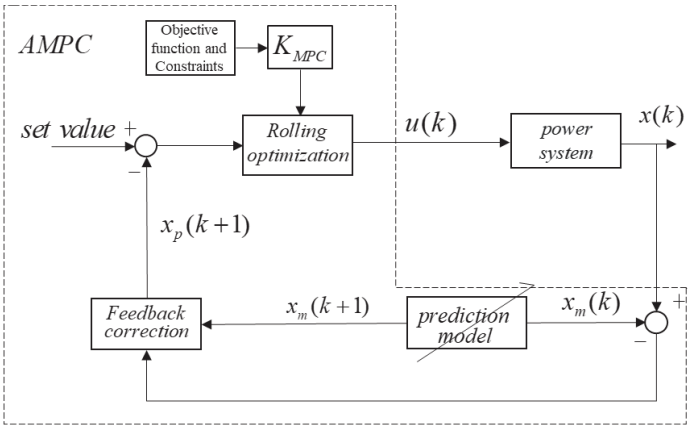

Fig 3.2 Feedback correction.

3.1.4 Prediction model

AMPC controller can predict future performance based on the internal prediction model (G_{model}). Therefore, for low computation burden, a simplified first-order and second-order lag system is applied to AMPC. The performance of the system can be approximated, as follows.

$$G_{\text{model}}(s) = \frac{K_a}{T_a s + 1} \tag{3.18}$$

$$G_{\text{model}}(s) = \frac{K_b}{T_{b1} s + 1} \cdot \frac{1}{T_{b2} s + 1} \tag{3.19}$$

Where, K_a, K_b are the adaptive gain of the proposed internal prediction model; T_a, T_{b1}, T_{b2} are the time constant of the proposed internal prediction model.

3.2 Introduction of estimation methods for the state values and parameters of the system

For complex systems, state observers are usually applied to estimate the state values and parameters of the system. Because of the physical state of the system is difficult to determine directly. It is an important measurement to know the system state using state observers. Some estimation methods, such as, least squares (LS), Kalman filter (KF), extended Kalman filter (EKF) etc. are usually applied to the system, which are presented and introduced in this section.

3.2.1 Kalman filter (KF)

Kalman filter (KF) was proposed by Kalman in 1960 and applied to the moon landing program. Nowadays, it is widely used in robotics, autopilot, and flight control. KF utilizes the state and observation equations of the system to estimate the system state value. As a result, a more accurate estimate of the state is obtained through the estimation of the system state and the correction of the observations. Due to its own limitations of modeling and estimation only for linear systems. Many scholars have proposed a nonlinear Kalman filter based on the principle of the Kalman filter, such as the extended Kalman filter (EKF), Unscented Kalman filter (UKF).

3.2.2 Extended Kalman filter (EKF)

The extended Kalman filter (EKF) is based on the idea of linearizing the nonlinear system at each time and applying a time-varying Kalman filter at each time. The basic idea of EKF was proposed by Schmidt of NASA after Kalman presented the discrete-time Kalman filter in 1960, and a practical nonlinear Kalman filter was necessary to use the Kalman filter for space development, such as satellite navigation.

Linear approximation of the nonlinear function using Taylor expansion under the assumption that prior and posterior state estimates are available at time k and $k+1$, respectively.

$$f(x(k)) = f(\hat{x}(k)) + A(k)(x(k) - \hat{x}(k)) \tag{3.20}$$

$$h(x(k)) = h(\hat{x}^{-}(k)) + c^{T}(k)(x(k) - \hat{x}(k)) \tag{3.21}$$

However,

$$A(k-1) = \left.\frac{\partial f(k)}{\partial x}\right|_{x=\hat{x}(k-1)} \tag{3.22}$$

$$C^{T}(k) = \left.\frac{\partial h(x)}{\partial x}\right|_{x=\hat{x}^{-}(k)} \tag{3.23}$$

Where, f and h are nonlinear function equation. A, C are extended matrices.

The prior state ($\hat{x}^{-}$) estimate is also expressed in the following equation.

$$\hat{x}^{-}(k) = f(\hat{x}(k-1)) \tag{3.24}$$

The prior error covariance and Kalman gain (g) can be obtained as in the following equation.

$$P^{-}(k) = A(k-1)P(k-1)A^{T}(k-1) + \sigma_{g}^{2}(k-1)bb^{T} \tag{3.25}$$

$$g(k) = \frac{P^{-}(k)c(k)}{c^{T}(k)P^{-}(k) + \sigma_{\omega}^{2}} \tag{3.26}$$

Where, P and σ_{ω} are covariance matrix of the state values and noise variance, respectively.

The state estimate ($\hat{x}$) at time k based on the above can be obtained as follows.

$$\hat{x}(k) = \hat{x}^{-}(k) + g(k)\left\{g(k) - h(\hat{x}^{-}(k))\right\} \tag{3.27}$$

The linear approximation concept of EKF is shown in Fig 3.3.

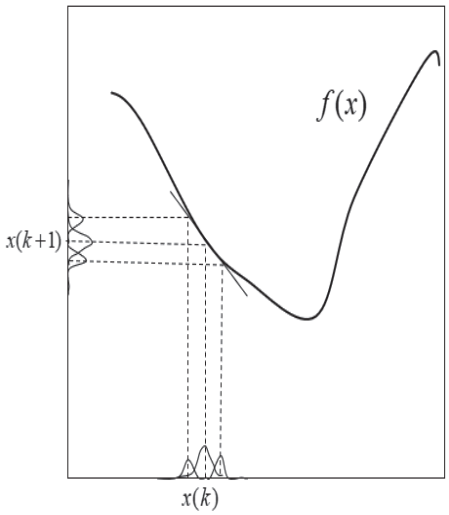

Fig 3.3 Linear approximation concept of EKF.

3.2.3 Unscented Kalman filter (UKF)

Unscented Kalman filter (UKF) is a nonlinear Kalman filter proposed by S.J. Julier and J.K. Uhlmann of Oxford University in the 1990s. When constructing a nonlinear Kalman filter, some approximation must be made, which may mean that the filter is constructed using "unmixed" operations as much as possible. The UKF is not a linear

approximation at each time of the nonlinear system, but rather a probability density. Its basic idea is a kind of statistical sampling method that approximates the probability distribution in a set-average manner by selecting a small number of sampling points. That called based on the approximation of a statistic that approximates the function (probability distribution) by a normal distribution, rather than a linear approximation at each time in a nonlinear system.

3.2.3.1 Unscented transforms (UT)

The UKF is based on the unscented transforms (UT) to select the sigma point (χ). Therefore, the UKF is also known as the sigma point Kalman filter. The following equations give the UKF how to estimate the values. Therefore, the UKF is also known as the sigma point Kalman filter. A U-transformation is the problem of transforming an n-dimensional random variable vector into an n-dimensional random variable vector *y* by nonlinear function *f* : $R^n \rightarrow R^n$

$$y = f(x) \tag{3.28}$$

In the following, we will introduce the most basic method, i.e., sampling symmetrically with respect to the mean. First, the method for selecting sigma points is given below.

$$\chi_k^{(0)} = \hat{x}_{UKF,k} \tag{3.29}$$

$$\chi_k^{(i)} = \hat{x}_{UKF,k} + \sqrt{n+\lambda}(\sqrt{P_k})_i,\ i = 1,...,n \tag{3.30}$$

$$\chi_k^{(n+i)} = \hat{x}_{UKF,k} - \sqrt{n+\lambda}(\sqrt{P_k})_i,\ i = 1,...,n \tag{3.31}$$

Where, λ is the scaling parameter, *n* denotes the dimension, $\hat{x}_{UKF}$ is estimation state values, *P* is the covariance matrix of the state values. $(\cdot)_i$ denotes the *i*-th column of the matrix square root of *P*.

The weight (*W*) for sigma point is given in the following equations.

$$W^{(0)} = \frac{\lambda}{n+\lambda} \tag{3.32}$$

$$W^{(i)} = \frac{1}{2(n+\lambda)},\ i = 1,...,2n \tag{3.33}$$

The sigma points are propagated and the priori state values are estimated using the following equations. Here, the subscript k+1 means the time step.

$$\chi_{k+1|k}^{(i)} = v(\chi_k^{(i)}, u_k),\ \ i = 1,...,2n+1 \tag{3.34}$$

$$\hat{x}_{UKF,k+1|k} = \sum_{i=0}^{2n} W^{(i)} \chi_{k+1|k}^{(i)} \tag{3.35}$$

$$P_{k+1|k} = \sum_{i=0}^{2n} W^{(i)} \left\{ \chi_{k+1|k}^{(i)} - \hat{x}_{UKF,k+1|k} \right\} \times \left\{ \chi_{k+1|k}^{(i)} - \hat{x}_{UKF,k+1|k} \right\}^T \tag{3.36}$$

The measurement output value and covariance matrix are computed based on the following equations.

$$\eta_{k+1|k}^{(i)} = z(\chi_k^{(i)}, u_k),\ \ i = 1,...,2n+1 \tag{3.37}$$

$$\hat{y}_{UKF,k+1|k} = \sum_{i=0}^{2n} W^{(i)} \eta_{k+1|k}^{(i)} \tag{3.38}$$

$$P_{xy,k+1|k} = \sum_{i=0}^{2n} W^{(i)} \left\{ \chi_{k+1|k}^{(i)} - \hat{x}_{UKF,k+1|k} \right\} \times \left\{ \eta_{k+1|k}^{(i)} - \hat{y}_{UKF,k+1|k} \right\}^T \tag{3.39}$$

$$P_{yy,k+1|k} = \sum_{i=0}^{2n} W^{(i)} \left\{ \eta_{k+1|k}^{(i)} - \hat{y}_{UKF,k+1|k} \right\} \times \left\{ \eta_{k+1|k}^{(i)} - \hat{y}_{UKF,k+1|k} \right\}^T \tag{3.40}$$

The estimation values are computed based on the gain (g) of the Kalman filter.

$$g_{k+1} = \frac{P_{xy,k+1|k}}{P_{yy,k+1|k} + \sigma} \tag{3.41}$$

$$\hat{x}_{UKF,k+1|k+1} = \hat{x}_{UKF,k+1|k} + g_{k+1} \left\{ \eta_{k+1|k}^{(i)} - \hat{y}_{k+1|k} \right\} \tag{3.42}$$

Where, σ is noise variance.

An estimation process of UKF is summarized in Fig 3.4, which including internal prediction system model, measurement model, and the state estimation.

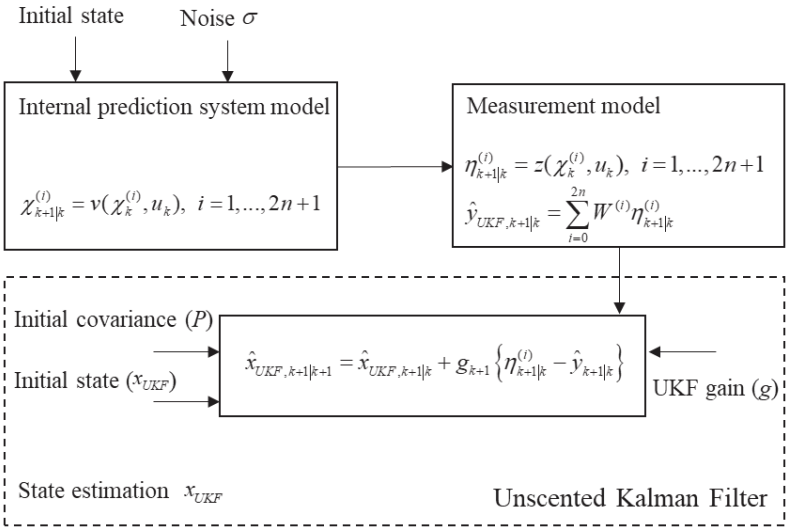

Fig 3.4 Estimation process of UKF.

The sigma point concept of UKF using sigma point is also shown in Fig 3.5.

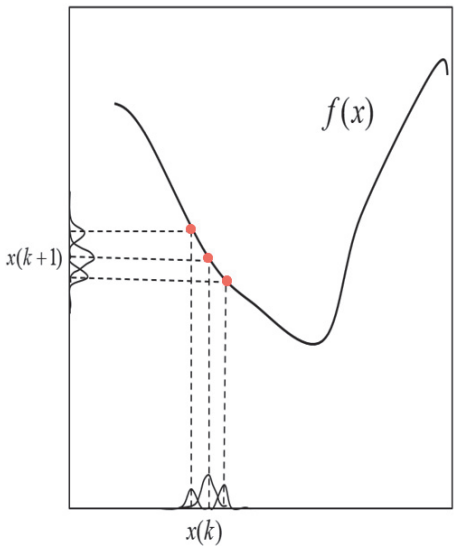

Fig 3.5 Approximation concept of UKF using sigma point.

3.3 Proposed AMPC using unscented Kalman filter (UKF)

This work proposes an AMPC approach using the MPC algorithm with a UKF, which is applied to (3.1). The UKF is applied to the AMPC for capturing the optimal system operation, whose structure is shown in Fig 3.6. The parameters of the internal prediction model of AMPC are estimated by UKF online. Therefore, optimal control is obtained in this process.

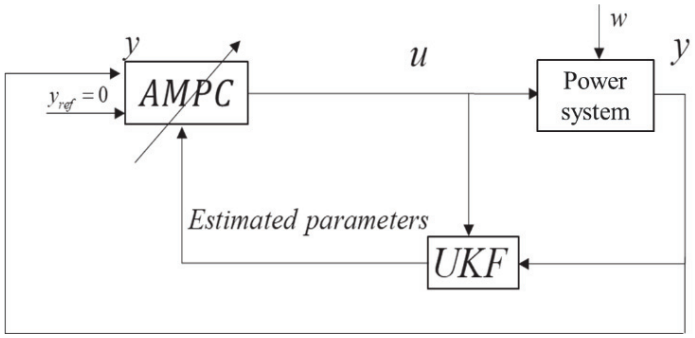

Fig 3.6 AMPC using UKF.

The control signal in (3.43), called the area control error (ACE), is determined by the system output in (3.1) for the LFC controller. A reference value (*yref*=0) is considered to minimize the ACE signal.

$$ACE = y(t) = \beta \Delta f(t) \tag{3.43}$$

Where, β is the frequency response characteristic.

Fig 3.5 shows the structure of how the UKF uses the measurements (u, y) from the target system for online estimation to obtain the optimal parameters of (3.18). In the UKF, an iterative calculation is repeated every 0.1s, and the K_{MPC} of the AMPC controller is also updated to obtain the input signal. The proposed formulation for UKF is given as follows:

$$\begin{bmatrix} x(k+1) \\ \theta(k+1) \end{bmatrix} = \begin{bmatrix} A(\theta) & 0 \\ 0 & I \end{bmatrix} \begin{bmatrix} x(k) \\ \theta(k) \end{bmatrix} + \begin{bmatrix} \boldsymbol{b} \\ 0 \end{bmatrix} u(k) \tag{3.44}$$

Where,

$$x(k) = \left[\Delta f(k)\right] \tag{3.45}$$

$$\theta(k) = [K_a(k) \;\; T_a(k)]^T \tag{3.46}$$

$$A(\theta) = \left[-\frac{1}{T_a(k)} T_s\right] \tag{3.47}$$

$$\boldsymbol{b} = \left[\frac{K_a(k)}{T_a(k)} T_s \;\; 0 \;\; 0\right]^T \tag{3.48}$$

Where, $A(\theta)$ and $\boldsymbol{b}$ are the state-space matrices of the UKF; θ is the matric of the estimated parameters; T_s is the sampling time.

As a result, the state values of UKF can be defined as follows.

$$x_{UKF}(k) = \left[\Delta f(k)\ K_a(k)\ T_a(k)\right]^T \tag{3.49}$$

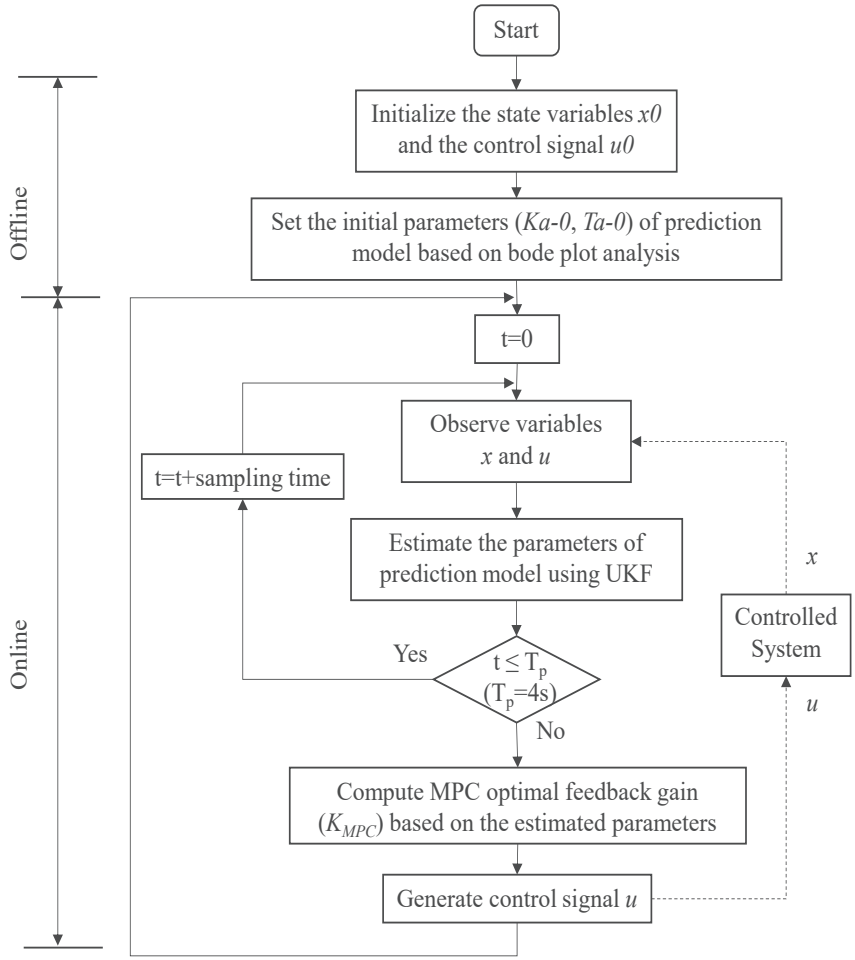

Fig 3.7 Proposed control flowchart.

The proposed control process consisting of offline and online processes is given in Fig 3.7. The parameters of the prediction model are estimated, and the optimal operation of the online process is achieved.

An optimal control algorithm is introduced in Chapter 3.1 and the detailed algorithm of the UKF is described in the aforementioned section 3.2.

Chapter 4: AMPC-based frequency regulation for power systems

4.1 Power systems modeling

A novel discrete-time AMPC controller is designed for LFC to maintain frequency stability. A standard LFC model in each area is shown in Fig 4.1, including an LFC controller, thermal power plant consisting of governor and steam turbine model, and frequency characteristic model of the power system. The thermal power plants are controlled by the LFC signal from the control center.

The area control error (ACE) signal is used for the LFC controller. The DB and LPF are usually used to eliminate the high-frequency components in the actual power plants. This is quite important in designing an LFC controller from the point of view of actual system dynamics. Then, an ACE is defined as the system output in (4.1), which is used as input signal to the AMPC controller. Output (y_i) is computed based on the measurements of the frequency (Δf_i) and the tie-line power ($\Delta P_{tie,i}$). The tie-line power reflects the contribution of the regulation characteristics of one area to another. At the same time, the tie-line power is represented by the synchronizing torque coefficient (T_{ij}). The frequency response characteristic (β_i) is generally expressed by the governor speed droop (R_i) and the power system damping constant (D_i). The system response to load change is also determined by the inertia constant (M_i) and the damping constant, as seen in the power system block in Fig 4.1.

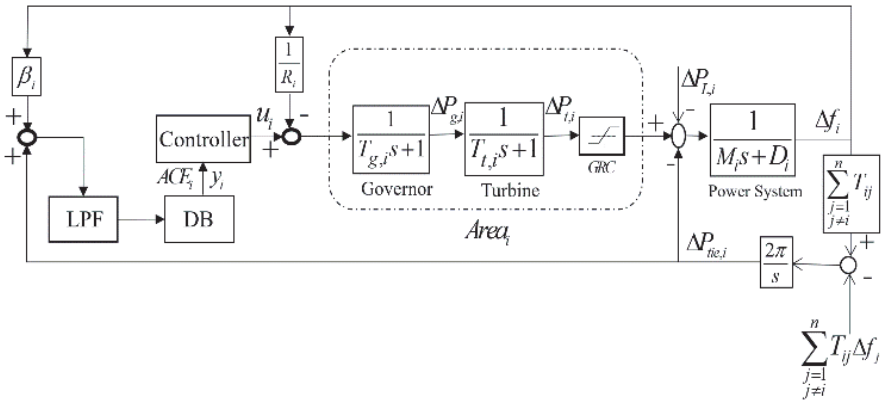

Fig 4.1 Standard LFC Model for Area *i*.

The following equations describe the LFC model.

$$y_i(t) = ACE_i(t) = \Delta P_{tie,i}(t) + \beta_i \Delta f_i(t) \tag{4.1}$$

$$\Delta P_{tie,i}(t) = \frac{2\pi}{s}\left[\sum_{\substack{j=1 \\ j\neq i}}^{n} T_{ij}\,\Delta f_i(t) - \sum_{\substack{j=1 \\ j\neq i}}^{n} T_{ij}\,\Delta f_j(t)\right] \tag{4.2}$$

The following state-space equation defines the dynamic model of a multi-area power system.

$$\begin{aligned} x_i(k+1) &= A_i\,x_i(k) + B_i\,u_i(k) + E_i\,w_i(k) \\ y_i(k) &= C_i x_i(k) \end{aligned} \tag{4.3}$$

$$y_i(k) = C_i\,x_i(k) \tag{4.4}$$

Where subscript i implies area number. State variable x_i(k) consists of state vector for area i $x_{sys,i}$, the power system output frequency deviation (Δf_i), the tie-line power ($\Delta P_{tie,i}$).

$$x_i(k) = \left[\ \Delta f_i(k)\ \ \Delta P_{tie,i}(k)\ \ x_{sys,i}(k)^T\ \right]^T \tag{4.5}$$

4.2 Internal prediction model for AMPC

Referring to Fig 4.1, “Controller” is designed based on the proposed AMPC. The transfer function is represented by the system matrices (A, B, C) from AMPC measurement (u) to AMPC input (y) as follows:

$$G(s) = \frac{y_i(k)}{u_i(k)} = C_i(sI - A_i)^{-1}B_i \tag{4.6}$$

The prediction model for area i (A_i, B_i, C_i) approximates the actual system, corresponding to area i in the following Fig 4.2 and Fig 4.3, respectively. Fig 4.2 for connected two-area system and Fig 4.3 for connected three-area system.

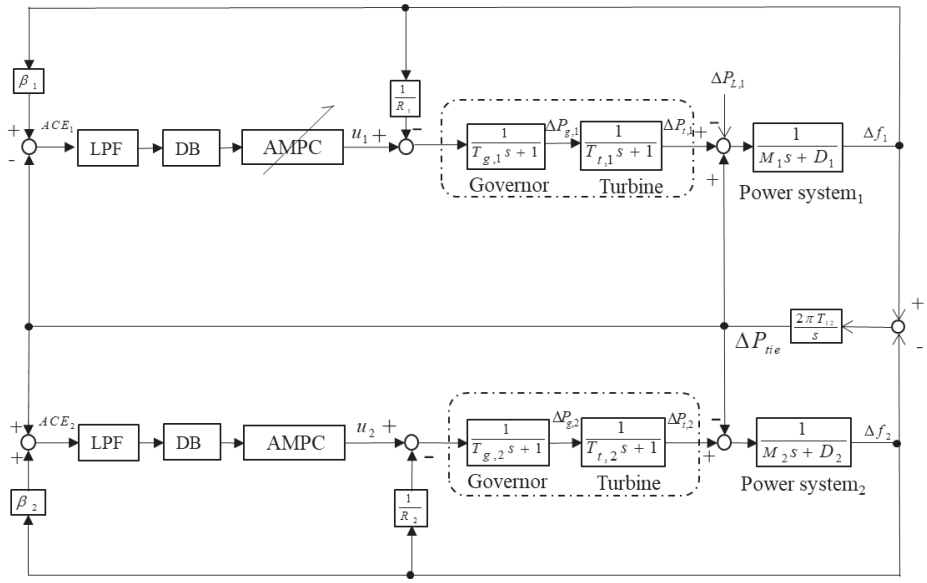

Fig 4.2 The connected two-area system model for AMPC.

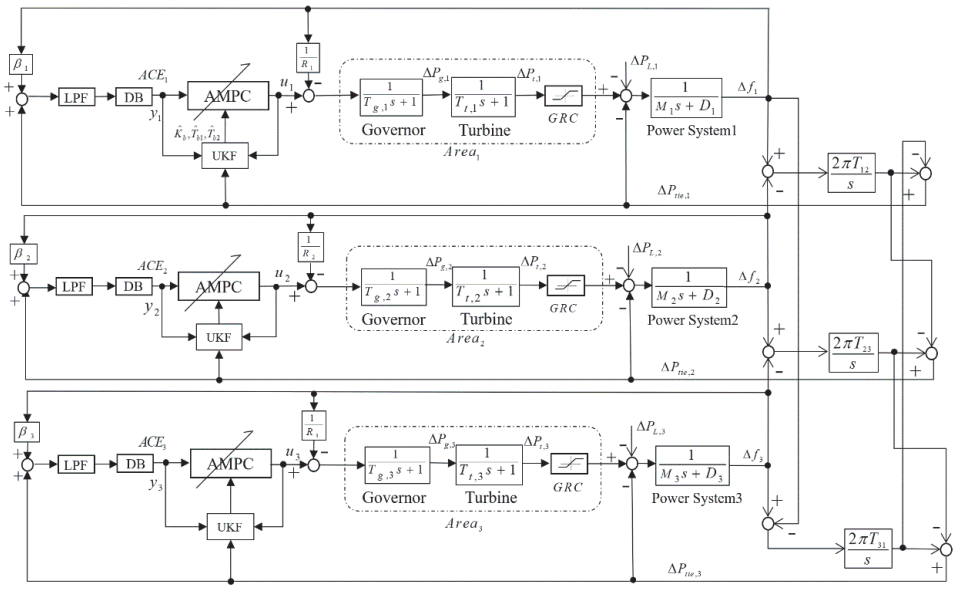

Fig 4.3 The connected three-area system model for AMPC.

This thesis uses the detailed plant model in Fig 4.1 and 4.2 as examples of actual systems whose dynamics are usually changeable, and the load characteristics are unknown in general. However, the detailed model used here is an authorized typical model that has been used in various conventional studies of this kind. Various investigations have been performed to identify a suitable prediction model, which corresponds to the approximation of $G(s)$. Therefore, after trial-and-error examinations, the following simplified models (4.7) and (4.8) are proposed as internal prediction models (PM) for the AMPC.

$$G_{PMa}(s) = \frac{K_a}{T_a s + 1} \tag{4.7}$$

$$G_{PMb}(s) = \frac{K_b}{T_{b1} s + 1} \cdot \frac{1}{T_{b2} s + 1} \tag{4.8}$$

Where, the following simplified first-order lag system PM is proposed for the AMPC of an interconnected two-area system.

$$G_{PM}(s) = \frac{K}{T_1 s + 1} \tag{4.9}$$

4.2.1 Bode plot of interconnected two-area power systems

Fig 4.4 shows the bode plots of the detailed model and the internal prediction model with proper parameters. It is observed that the proposed internal prediction model suitably approximates the detailed model within a frequency range less than 0.1Hz (T_1=10 sec). This covers all ranges of effective LFC signals from the control center to thermal power plants as will be discussed later. Now that the internal prediction model (4.9) can be a useful model that suitably approximates the target power system response, an adaptive control structure in the chapter 3 Fig 3.5 is adopted to estimate parameters of (4.9), where UKF is used for real-time estimation. We suggest that parameters (K, T_1) in (4.9) will be estimated using real on-line measurements (u, y). In UKF, a convergence calculation is repeated every 0.05 second, and the optimal feedback gain of the AMPC controller is also updated to get an optimal input value u. Note that the control ability of the AMPC is much faster than the real system response and that the accuracy of the internal model in the range less than 0.1Hz is enough to realize maximum performance.

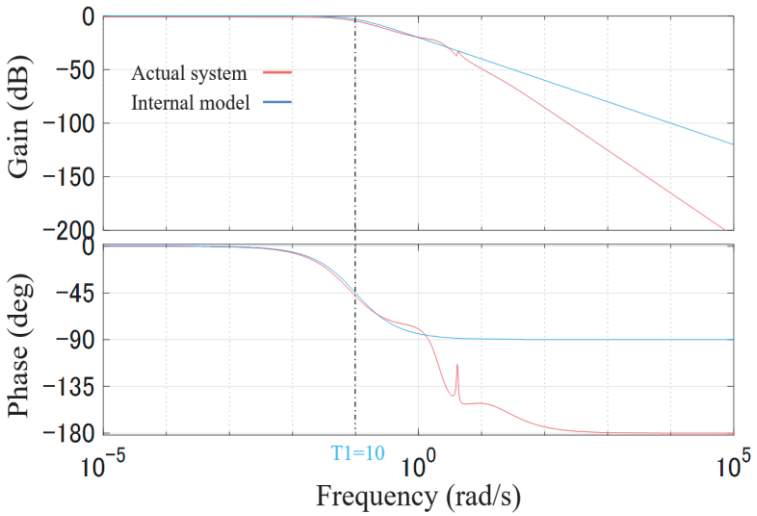

Fig 4.4 Bode plot for connected two-area system.

4.2.2 Bode plot of interconnected three-area power systems

Fig 4.5 shows the bode plots of the detailed target system model in Fig 4.1, and the internal prediction models (4.7) and (4.8) with proper parameters. As will be discussed later, internal prediction model (4.8) more suitably represents the target system than internal prediction model (4.7). It is observed that, compared with internal prediction model (4.7), model (4.8) can be used as an equivalent frequency response model within a frequency range less than 2Hz, corresponding to a slow response time greater than 0.5sec.

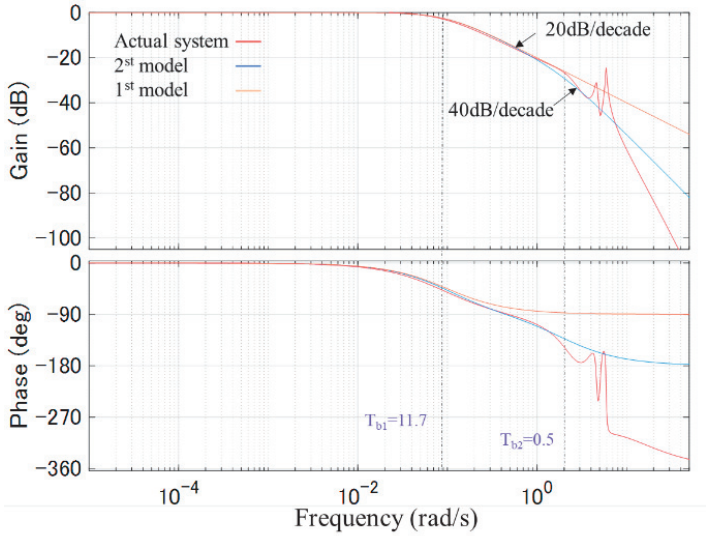

Fig 4.5 Bode plot for connected three-area system.

This covers all ranges of effective LFC signals from the control center to thermal power plants. Now that the internal prediction model (4.8) can be a useful model that suitably approximates the target power system response.

4.3 Case study Simulation settings

This section carries out the simulation studies to demonstrate the effectiveness of the proposed AMPC method. The system model in Fig 4.1 is adopted to represent the actual system of each area, which is interconnected to each other through the tie line. The simplified models (4.7, 4.8, and 4.9) are used as the internal prediction model for the AMPC controller. The MPC Toolbox in MATLAB/Simulink (R2020a) is used to tune the robustness and aggressiveness of the proposed AMPC controller. In this work, the total capacity of each area is assumed 1GW (1pu). The LFC reserve capacity is assumed 2% of the total generation capacity.

4.4 Simulation cases

4.4.1 Interconnected two-area power systems

Simulation cases for interconnected two-area power systems are given in Table 4.1. It is assumed that the detailed model given by Fig 4.2 is used to represent a real system, which is Case 1 is for the comparison, where the PI control with optimal parameter setting is adopted. In those cases, random disturbances from t=0s and 0.1pu step change at t=60s and -0.1pu step change at t=120s are added to load consumption, as shown in Fig 4.6. The simulation time is set to 200 seconds.

Table 4.1 Case settings for connected two-area system

	Purpose	**System Model**	**Input to System**	**Load Disturbance**	
				Random	**Step**
Case 1	PI Control	Fig 4.2	PI Control Input	0.01pu	0.1pu at t=60s and -0.1pu at t=120s
Case 2	Performance of Proposed Method		UKF & AMPC control Input		

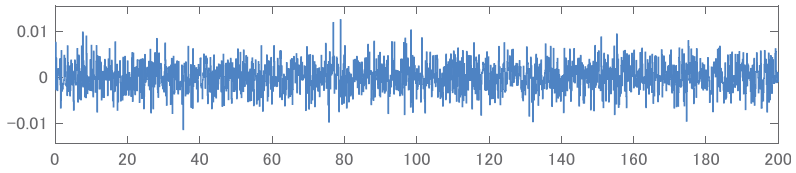

(a) Maximum 0.01pu random disturbance.

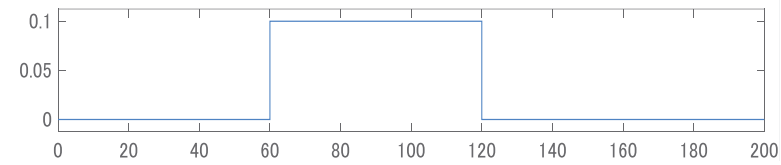

(b) 0.1pu Step disturbance.

Fig 4.6 Disturbance settings.

The parameters of two-area power system are given in Table 4.2.

Table 4.2 Parameters of two-area power system

Area	D (pu/Hz)	M (pu s)	R (Hz/pu)	T_g (s)	T_t (s)	β (pu/Hz)	T_{ij} (pu/Hz)
1	0.015	0.1667	3.00	0.08	0.40	0.3483	T_{12}=0.20
2	0.016	0.2017	2.73	0.06	0.44	0.3827	T_{21}=0.20

4.4.2 Interconnected three-area power systems

Simulation cases for interconnected three-area power systems are given in Table 4.3. Cases A1 and A2 evaluate UKF performance for the parameter estimation of the prediction model of (4.8). Case A1 stands for an ideal fictitious situation where the target system for parameter estimation is exactly the same as the prediction model. Case A2 represents actual circumstances where complex real system dynamics are identified using the prediction model of (4.8). Cases B1 and B2 are for comparison, where the PI control with the optimal parameter is adopted. It is assumed that the detailed model given by Fig 4.3 represents an actual system in this case as well as in cases C1 and C2, which demonstrates the performance of the proposed AMPC method. The input signal is used with the observation of ACE to identify the prediction model, which is used to compute the AMPC optimal feedback gain on-line. Case D is to examine the performance of the proposed method when the simplified prediction model is used.

In those cases, random and step disturbances are added to the load consumption. Different sizes of random disturbances are applied to the individual cases during the whole simulation period. Step changes of 0.1pu are applied upward at t=60s and downward at t=120s, same as in Fig 4.6. The simulation time is set to 200s.

A simulation study is performed in the following examinations, where a time step of 0.05s is adopted for numerical integration. The parameters of three-area power systems are given in Table 4.4.

Table 4.3 Case settings for connected three-area system

<table>
<tr><th rowspan="2"></th><th rowspan="2">Purpose</th><th rowspan="2">System Model</th><th rowspan="2">Input to System</th><th colspan="2">Load Disturbance</th></tr>
<tr><th>Random</th><th>Step</th></tr>
<tr><td>Case A1</td><td rowspan="2">UKF Performance Examination</td><td>Eqn. (4.8)</td><td rowspan="2">0.1pu Step Change at t=0s</td><td>-</td><td>-</td></tr>
<tr><td>Case A2</td><td>Fig 4.3</td><td>-</td><td>-</td></tr>
<tr><td>Case B1</td><td rowspan="2">Comparison to PI Control</td><td rowspan="4">Fig 4.3</td><td rowspan="2">Conventional PI Control Input</td><td>0.01pu</td><td rowspan="5">0.1pu at t=60s and -0.1pu at t=120s</td></tr>
<tr><td>Case B2</td><td>0.001pu</td></tr>
<tr><td>Case C1</td><td rowspan="2">Performance Examination of Proposed Method</td><td rowspan="2">UKF & MPC Control Input</td><td>0.01pu</td></tr>
<tr><td>Case C2</td><td>0.001pu</td></tr>
<tr><td>Case D</td><td>Examination of prediction model (9)</td><td>Fig 4.3</td><td>UKF & MPC Control Input</td><td>0.001pu</td></tr>
</table>

Prediction model (4.8) is used for all cases except case D.

Table 4.4 Parameters of 3-area Power System

Area	D (pu/Hz)	M (pu s)	R (Hz/pu)	T_g (s)	T_t (s)	β (pu/Hz)	T_{ij} (pu/Hz)
1	0.015	0.1667	3.00	0.08	0.40	0.3483	T_{12}=0.20 T_{13}=0.25
2	0.016	0.2017	2.73	0.06	0.44	0.3827	T_{21}=0.20 T_{23}=0.12
3	0.015	0.1247	2.82	0.07	0.30	0.3692	T_{31}=0.25 T_{32}=0.12

4.5 Simulation results and discussions

4.5.1 Interconnected two-area power systems

4.5.1.1 Performance of proposed AMPC method

This section lists the simulation results to verify the effectiveness of the AMPC method. Fig 4.7 shows the comparative results of PI control for Table 4.1 case 1, and Fig 4.8 shows the proposed AMPC for Table 4.1 case 2. Frequency deviation, tie-line power, and the ACE indices are the main evaluation measurements in interconnected power system, which are used to confirm the effectiveness of the proposed method. From the results, the convergence time of the PI controller is 23.3s and the proposed AMPC controller is 13.2s. Furthermore, we can observe that the proposed AMPC method converges to the desired value faster than the PI controller, almost 10s. As a result, the performance of the proposed MPC controller is superior to the PI controller at a glance in both cases.

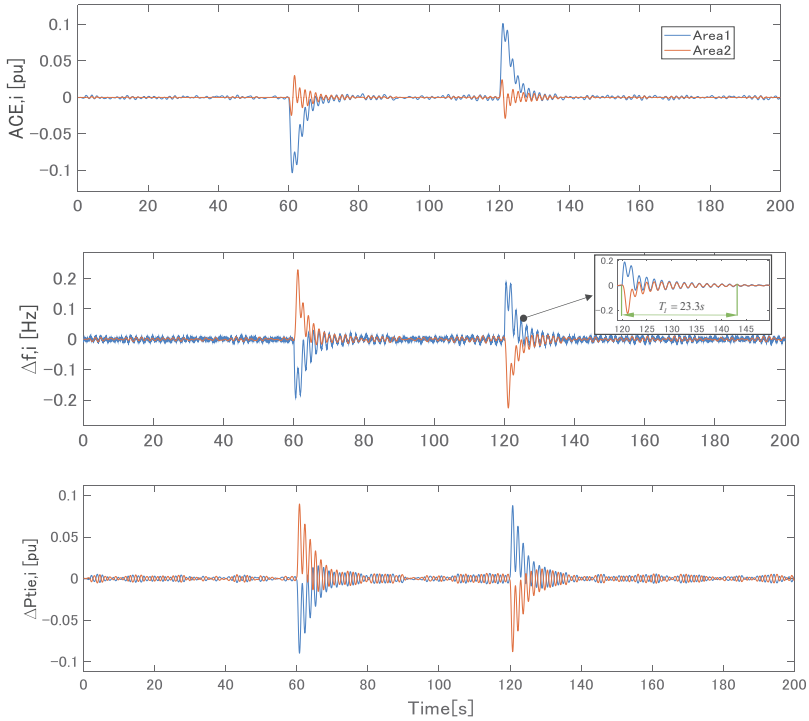

Fig 4.7 PI controller in case 1.

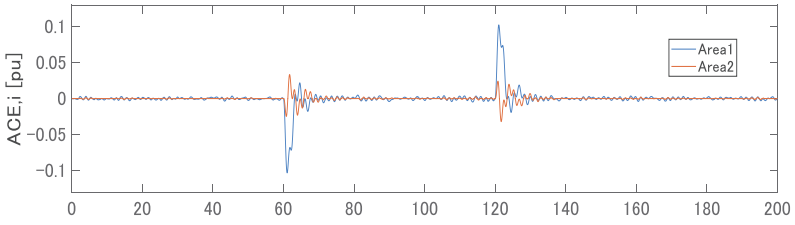

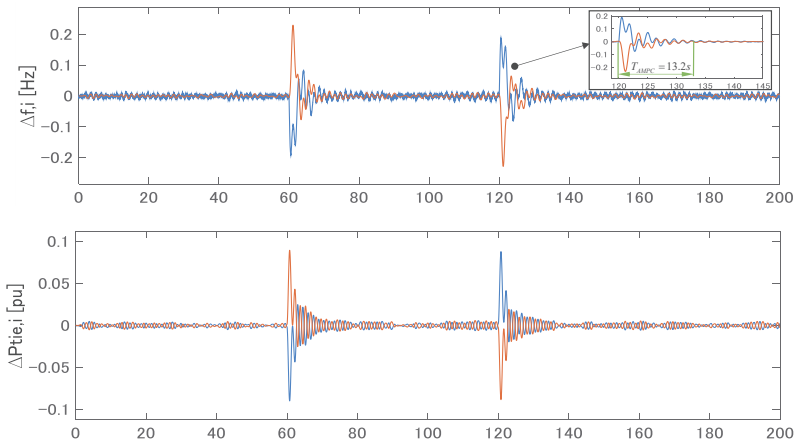

Fig 4.8 Proposed AMPC controller using UKF in case 2.

The UKF can estimate the internal model parameters and update AMPC on-line, which are used to compute the feedback gain. Fig 4.9 shows the internal prediction model estimation parameters variation using UKF, and the initial parameters are confirmed by bode plots (Fig 4.4). We can see the estimation parameters change a lot to choose the correct value when the load addition is at t=60s and converge to a constant value at 80s. The parameters approximately converge to the original set value when the -0.1pu step change is added to the test system at t=120s. The results also verify that the UKF has a better estimation performance.

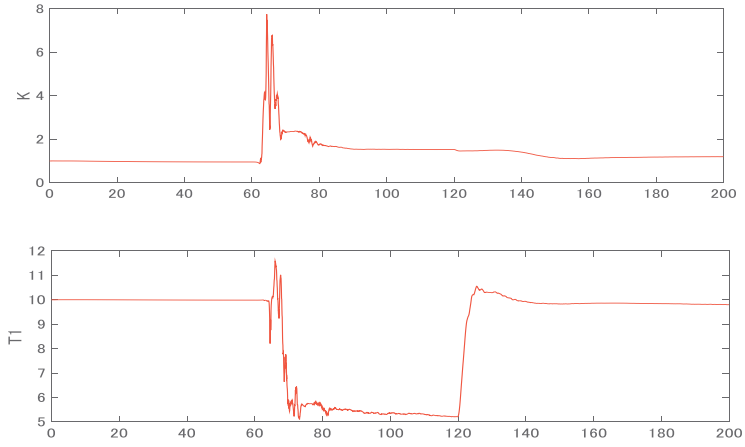

Fig 4.9 Estimation internal model parameters using UKF.

4.5.1.2 Performance indexes

Table 4.5 lists the comparative data based on Fig 4.7 and 4.8, which includes the standard deviation (STD) of the frequency deviation and the integral errors of the ACE.

We can also notice that the proposed AMPC method has better performance than the PI control.

Table 4.5 Comparative data analysis

		PI	AMPC
STD (Δf_i, Hz)	Area 1	0.0220	0.0192
	Area 2	0.0216	0.0181
IAE		1.3880	0.7806
ITAE		13.8374	10.0145
ISE		0.0492	0.0316
ITSE		3.9728	2.4452

Where, performance indexes using the integral absolute error (IAE), integral time absolute error (ITAE), integral squared error (ISE), and integral time squared error (ITSE) , whose details are given in Appendix.

4.5.2 Interconnected three-area power systems

4.5.2.1 Examination of UKF

The performance of UKF for the parameter estimation is studied in this section. The initial parameters of (4.8) are set to K_b=0.5, T_{b1}=6, T_{b2}=0.1 in this case based on bode plot (Fig 4.5). The simulation results are shown in Fig 4.10. It is noticed that, for the step-change 0.1pu in the plant control signal, the parameter estimation for (K_b, T_{b1}, T_{b2}) successfully converged to 1, 11.7, 0.5 respectively at around 30s as shown in Fig 4.10 in Table 4.3 case A1, where the prediction model and the target model are identical. It is also understood from Fig 4.11 in Table 4.3 case A2 that the parameter values (K_b, T_{b1}, T_{b2}) are successfully converged to their right values (K_b≈1, T_{b1}≈11.77, T_{b2}≈2.1) whose validity is studied in the previous section. Those examinations confirm that UKF can successfully estimate the parameters of the prediction model to be used in the AMPC controller.

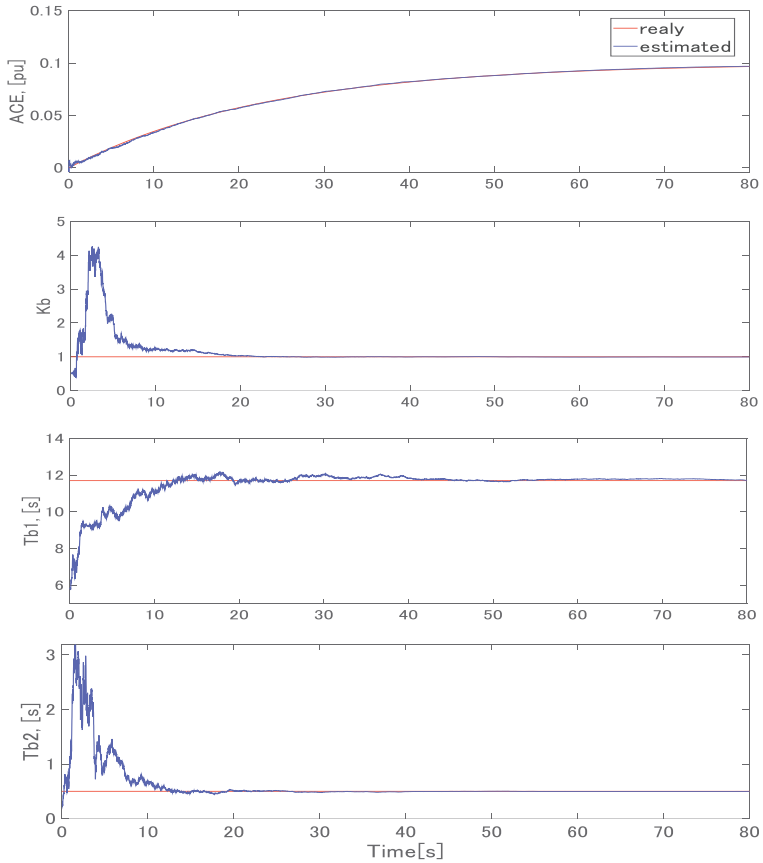

Fig 4.10 UKF Performance for Parameter Estimation in Case A1.

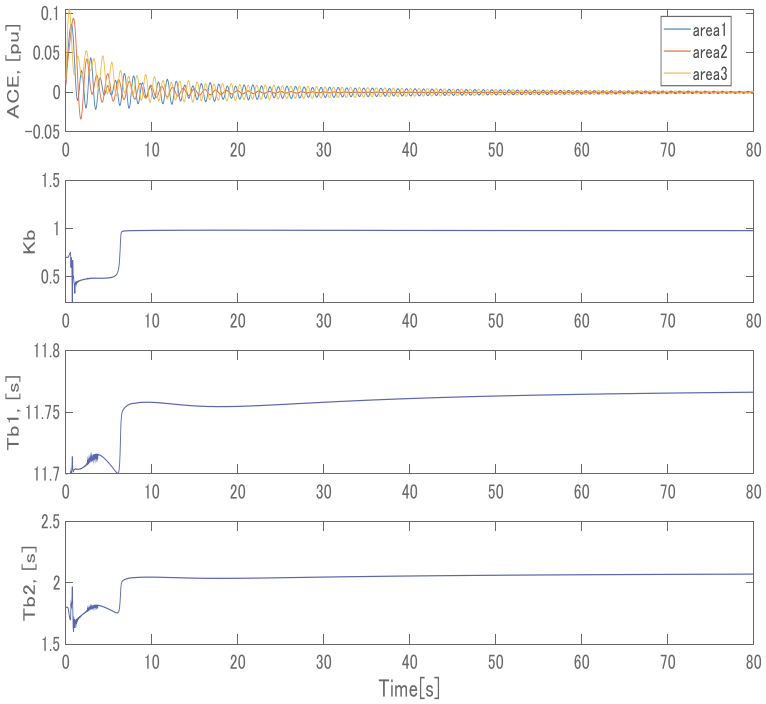

Fig 4.11 UKF Performance for Parameter Estimation in Case A2.

4.5.2.2 Performance of proposed AMPC method

In this section, simulation studies are performed to demonstrate the performance of the proposed AMPC method, that is, the combination of UKF and AMPC with the prediction model of (4.8). Figs 4.12 and 4.13 for cases B1 and B2 in Table 4.3, respectively, show the simulation results for the PI control method.

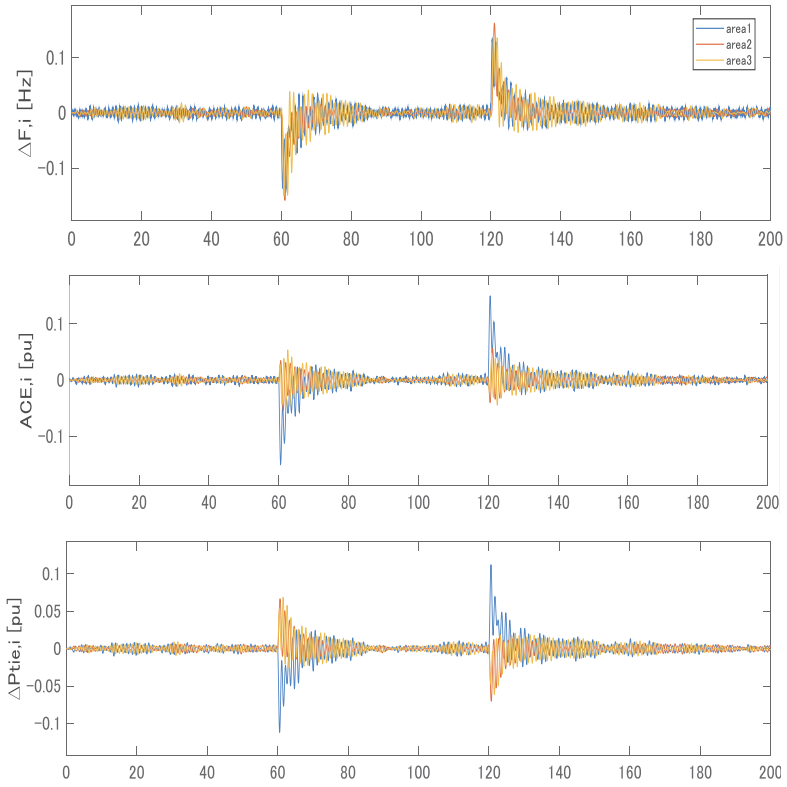

Fig 4.12 PI Controller in Case B1 in Table 4.3.

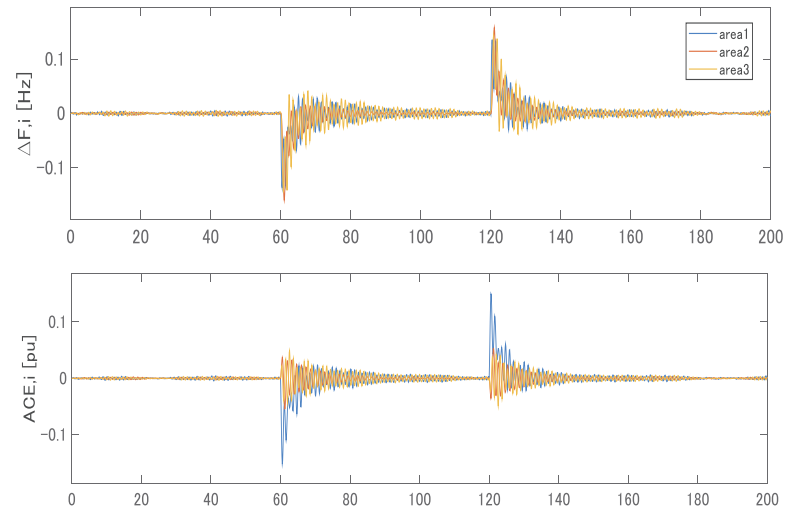

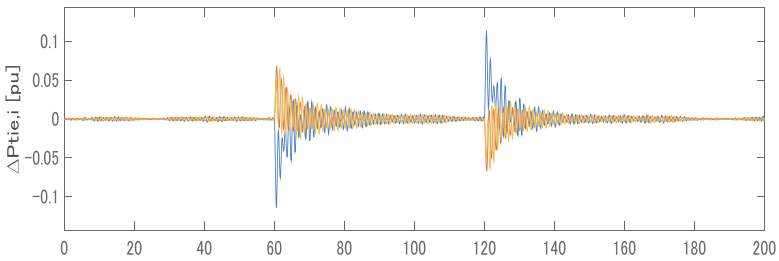

Fig 4.13 PI Controller in Case B2 in Table 4.3.

In this circumstance, UKF works on-line to identify the AMPC prediction model, which is used to compute the optimal gain of the AMPC controller. The simulation results are given in Fig 4.14 for Table 4.3 case C1 and Fig 4.15 for Table 4.3 case C2. We can see that the performance of the proposed AMPC controller is superior to the PI controller in both cases.

It is also observed from Fig 4.14 for cases C1 and Fig 4.15 for case C2 in Table 4.3, respectively that the proposed AMPC can effectively handle the disturbance. The initial parameters of the prediction model in case C of Table 4.3 are set to the same value (K_b=1, T_{b1}=11.7, T_{b2}=1.1).

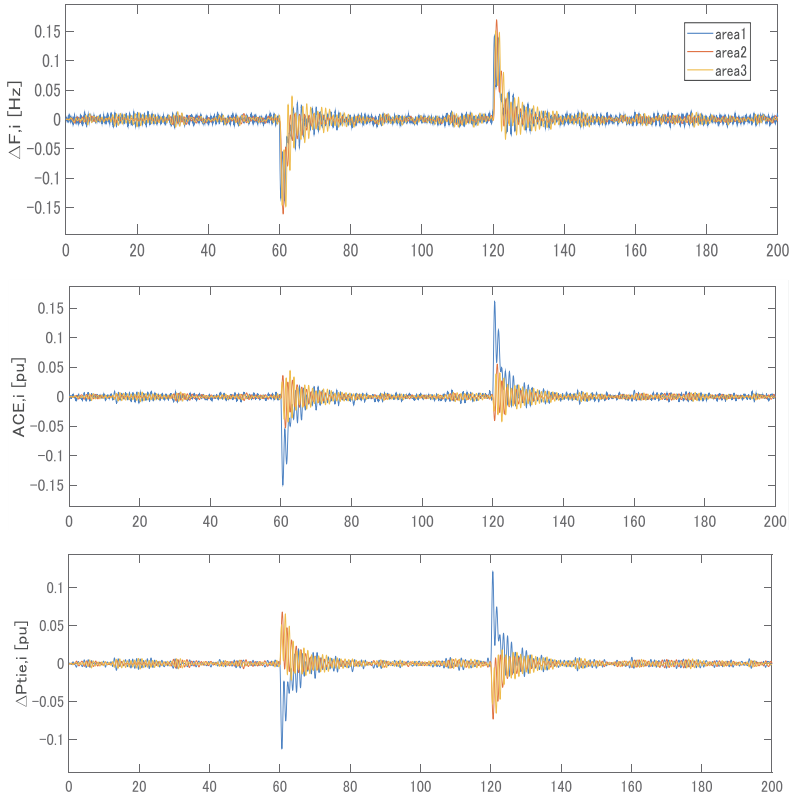

Fig 4.14 Proposed MPC Controller using UKF in Case C1 of Table 4.3.

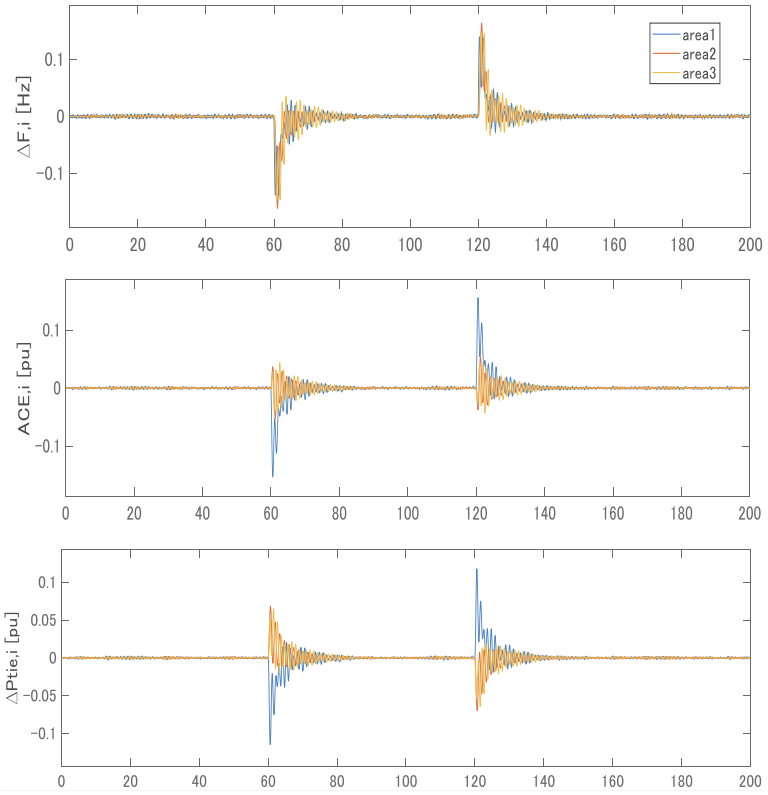

Fig 4.15 Proposed MPC Controller using UKF in Case C2 of Table 4.3.

Concerning the performance of UKF, we can notice that parameters of prediction model (4.8) almost converge to their correct values before around 60s from Fig 4.16.

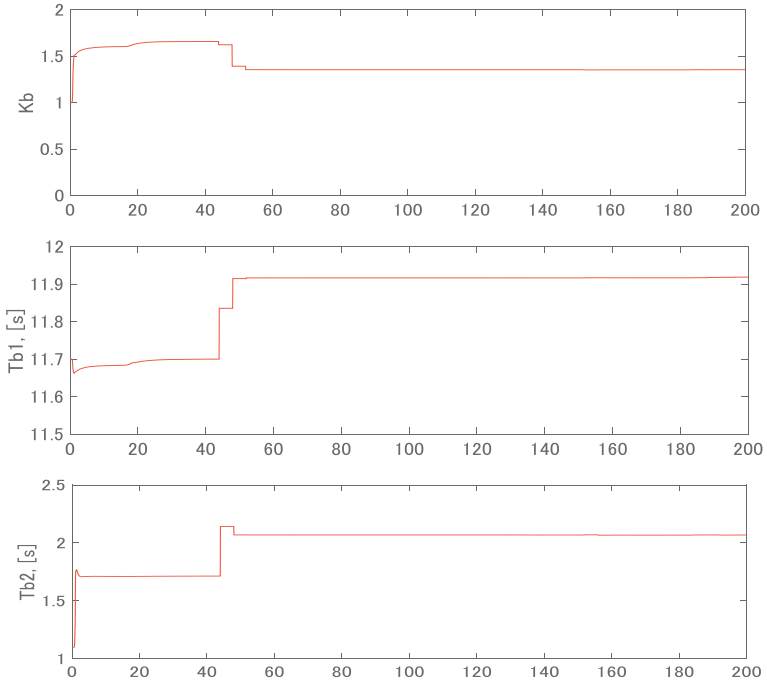

(a) prediction parameters for Case C1.

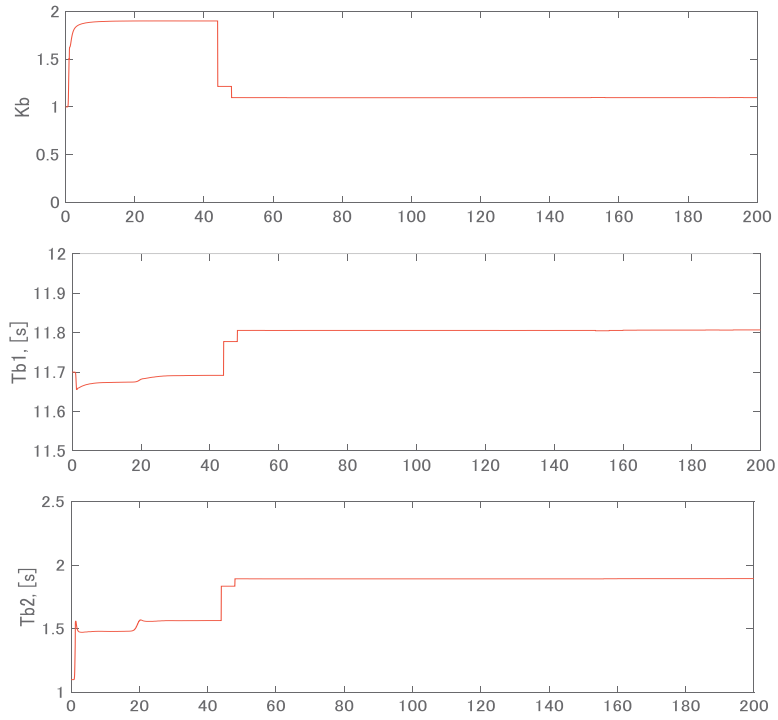

(b) prediction parameters for Case C2.

Fig 4.16 Prediction Parameters using UKF.

The dynamic frequency characteristics are compared in Fig 4.17, which is the enlarged waveforms of Δf in area 1 for case C1 of Table 4.3 in Fig 4.14. The proposed AMPC shows a better performance compared to the PI controller, where the improved frequency nadirs and zeniths are observed.

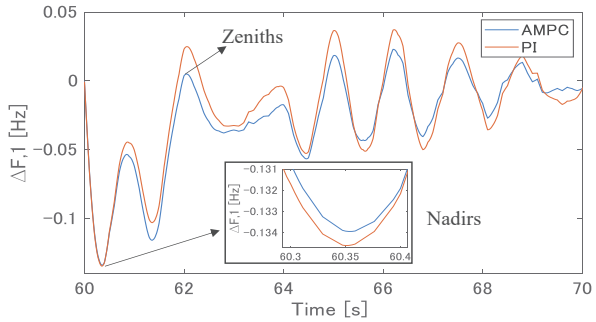

Fig 4.17 Comparison of frequency nadirs/zeniths for the proposed AMPC and PI control (area 1 in case C1).

4.5.2.3 Performance indexes

The performance of the proposed AMPC method compared with the PI control method based on the simulation results is summarized in Table 4.6, which shows the standard deviation (STD) of the frequency deviation and the errors of the frequency and the tie-line power. They are evaluated by integral absolute error (IAE), integral time

absolute error (ITAE), integral squared error (ISE), and integral time squared error (ITSE), which are defined in the Appendix. All those error show that the proposed AMPC controller performs better than the PI controller

Table 4.6 Comparative Data Analysis

		PI	**AMPC**
STD (Δf_i)	Area1	0.0159 Hz	0.0011 Hz
	Area2	0.0155 Hz	0.0037 Hz
	Area3	0.0188 Hz	0.0053 Hz
IAE		0.1567	0.1437
ITAE		11.4553	7.8321
ISE		0.0035	0.0020
ITSE		0.5138	0.4004

We discuss the performance of the proposed AMPC including the effect of the prediction model. The performance is evaluated by IAE, ITAE, ISE, and ITSE.

Fig 4.18 shows the comparison between Cases C2 and D in Table 4.3, where different prediction models (4.8) and (4.7) are used, respectively. We can observe that Case C2 in Table 4.3 shows better control performance than Case D, especially in ISE and ITSE. This implies that the preliminary examination of the prediction model as given in Fig 4.5 is quite important for the total performance of the control system. On the other hand, the proposed control scheme is reliable since the controller successfully identifies the internal model to compute the optimal control for the given prediction model.

CPU time of the proposed AMPC method is listed in Table 4.7, where the maximum CPU times for the computations for UKF and MPC in every 4 second are given, corresponding to the tasks in the boxes of “UKF” and “MPC gains”. The result indicates that the computation performance is enough for generating a control signal every 4 seconds. The comparison of Case C2 and D in Table 4.3 shows that there is no significant difference in the computation time. This implies that the proposed AMPC is useful for real-time control from the point of view of computational burden.

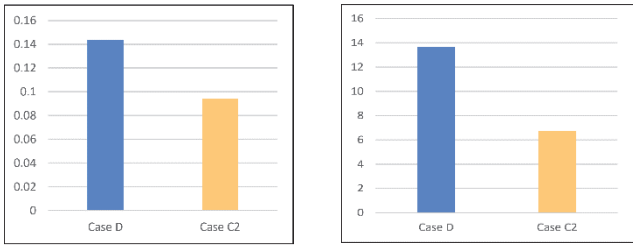

(a) IAE (b) ITAE

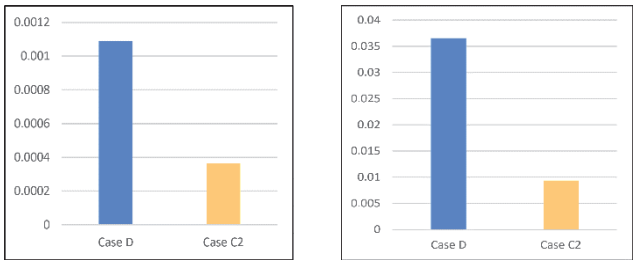

(c) ISE (d) ITSE

Fig 4.18 Evaluation of prediction model.

Table 4.7 Max. CPU time for UKF and MPC in every 4 (s)

	UKF for single iteration (s)	**MPC gain computation (s)**
Case C2	0.006	0.0151
Case D	0.005	0.0147

4.6 Conclusions

This work proposes a new AMPC control scheme for thermal plants for the LFC problem. A novel prediction model is suggested for an adaptive MPC using UKF. Connected two-area and three-area power system model are used to confirm the effectiveness of the proposed method. The advantages of the proposed method for LFC controller design lie in that the optimal feedback is realized for the thermal plants, which only respond to the slow input signals. In addition, the control scheme has robust characteristics in its performance with flexible and adaptive nature. The simulation results show that the proposed method has those superior performances to the PI control.

In the LFC problem in general, although there exist the interconnections among the individual areas through the tie-lines, the proposed control scheme works successfully. Harmful interactions among controllers with UKFs are not observed in the individual areas. This is because the dead band and LPF used for the protection of the thermal

power plants in the practical LFC system are effectively modeled in the proposed equivalent system, which successfully works to avoid the interactions of the individual LFC input and output signals. In other words, it is stated that the proposed method effectively identifies the prediction model consisting of only observable and controllable major dynamics in the restricted control circumstance of actual LFC systems.

In our future work, the internal prediction model will be upgraded to identify the frequency characteristics to consider the renewable source with high uncertainty such as solar generations.

Chapter 5: AMPC-based frequency regulation for microgrid systems

5.1 Microgrid systems modelling

In this chapter, the proposed robust AMPC method in chapter 3 is applied to microgrid (MG) system considering the uncertain renewable energy sources (RESs), such as wind turbine (WT) power, photovoltaic (PV). Meanwhile, a large disturbance is also considered in this circumstance.

This work assumes an islanded MG system model and connected two-area MG equivalent frequency response model represents the actual system. The systems include the governor model, the diesel engine generators (DEGs) model, the battery energy storage system (BESS) model, and the frequency characteristic model of the MG, as shown in Fig 5.1 for islanded MG and Fig 5.2 for connected two-area MG, respectively.

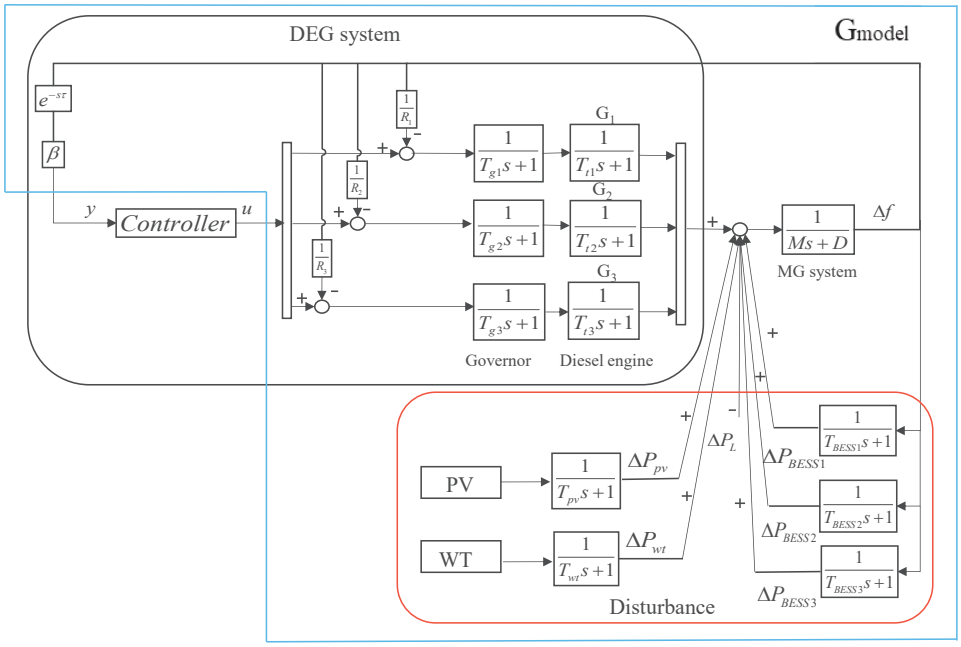

Fig 5.1 Islanded MG system.

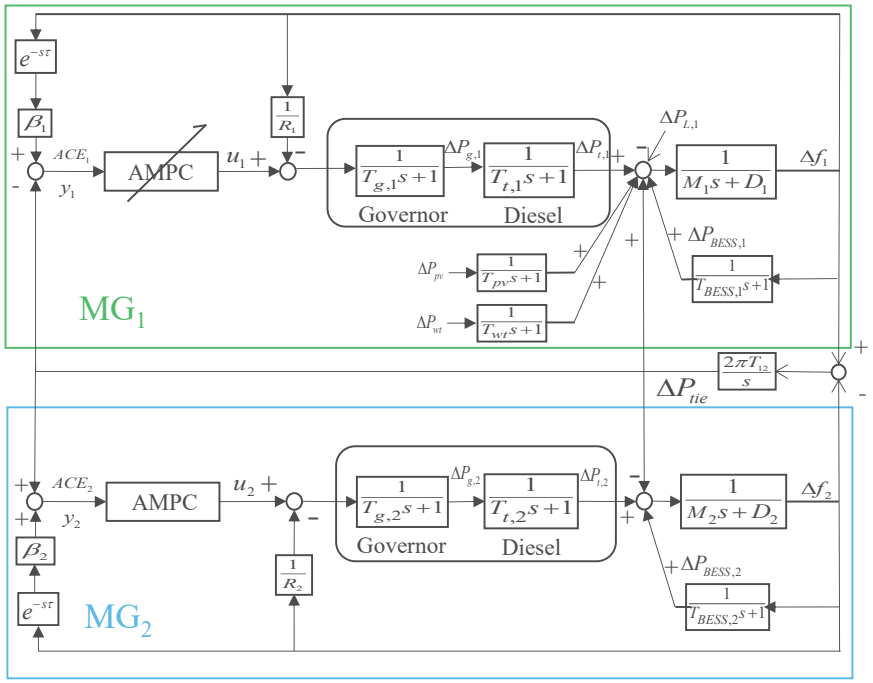

Fig 5.2 Connected two-area MG system.

A dynamic state-space equation is presented for the MG system, which is used to design the AMPC controller, as shown in (5.1), (5.2).

$$\begin{aligned} x_i(k+1) &= \boldsymbol{A}_i x_i(k) + \boldsymbol{B}_i u_i(k) + \boldsymbol{E}_i w_i(k) \\ y_i(k) &= \boldsymbol{C}_i\, x_i(k) \end{aligned} \tag{5.1}$$

$$x_i(k) = \begin{bmatrix} \Delta P_{g,i}(k) & \Delta P_{t,i}(k) & \Delta f_i(k) \end{bmatrix}^T \tag{5.2}$$

Where, $\boldsymbol{A} \in \mathbb{R}^{N\times N}$, $\boldsymbol{B} \in \mathbb{R}^{N\times N_B}$, $\boldsymbol{C}^T \in \mathbb{R}^{N\times 1}$, and $\boldsymbol{E} \in \mathbb{R}^{N\times 1}$ are the state-space matrices, N is the number of the state valuables, N_B is the number of the input signal; $x \in \mathbb{R}^{N\times 1}$ is the state valuables of the system; w is the disturbance and load; y and u are the system output and input signal; ΔP_g, ΔP_t, and Δf are the governor output deviation, diesel engine output deviation and frequency deviation; k is the sample moment; i is the number of MG; $e^{-s\tau}$ is equivalent to a communication time delay for the actual control system ($\tau = 0.1s$).

The behavior of WT power, PV generation, and BESS is approximated by the first-order lag system model, shown in (5.3).

$$Output: \Delta P_m = \frac{1}{T_m s + 1} \times input,\ m = PV, WT, BESSs \tag{5.3}$$

Where, T_{pv}, T_{wt}, and T_{BESS} are the time constant of the PV, WT, and BESSs,

respectively.

In the LFC scheme, the generation balance with the load consumption is required. Therefore, the generation and load consumption balance in (5.4) can be obtained based on this point.

$$\Delta P_t + (\Delta P_{BESS}^{+} - \Delta P_{BESS}^{-}) = \Delta P_L - \Delta P_{pv} - \Delta P_{wt} \tag{5.4}$$

Where, ΔP_{BESS}^{+} and ΔP_{BESS}^{-} are the power discharge and charge of BESS; ΔP_L is the load consumption; ΔP_{pv} is the PV output; ΔP_{wt} is the WT output.

A large amount of WT, PV generations, and load consumption affects the frequency stability. Therefore, a fast response BESS is used as a supplementary power to maintain the balance, which is charged and discharged to mitigate the rapid fluctuation.

Fig 5.3 show the system stability based on the eigenvalue characteristics. The results show that the MG systems used in this thesis are stability.

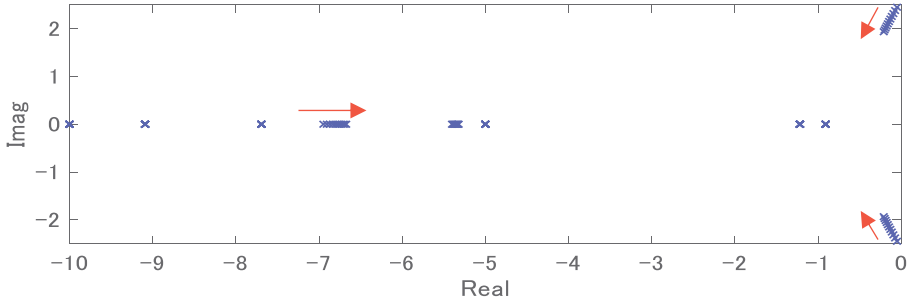

(a) Islanded MG system.

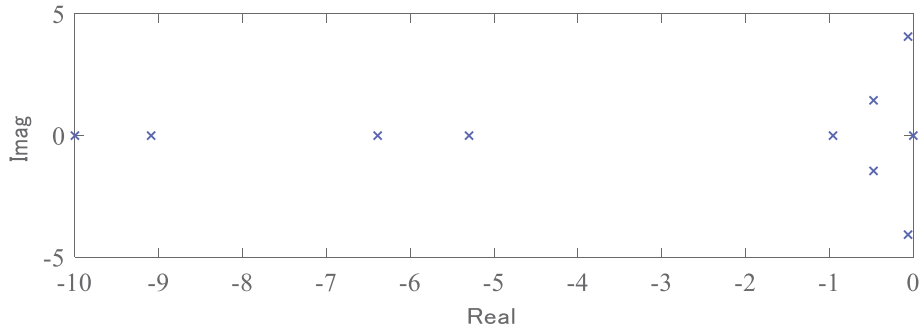

(b) Connected two-area MG system.

Fig 5.3 System stability (eigenvalue characteristics).

5.2 Internal prediction model for AMPC

AMPC controller can predict future performance based on the internal prediction

model (G_{model}). In addition, a simplified first-order lag system is applied to AMPC. The performance of the system can be approximated, as shown in (5.5).

$$G_{\text{model}}(s) = \frac{K_{a,i}}{T_{a,i}s + 1} \tag{5.5}$$

Where, K_a is the adaptive gain of the proposed internal prediction model; T_a is the time constant of the proposed internal prediction model.

Fig 5.4 shows the bode plot of the proposed internal prediction model and the MG system, which is used to decide the initial values of the proposed first-order lag system. We can observe that the proposed first-order lag system has a fast response speed and suitably approximate the performance of the MG system in the frequency range of less than 0.33Hz ($1/T_{a-0}$).

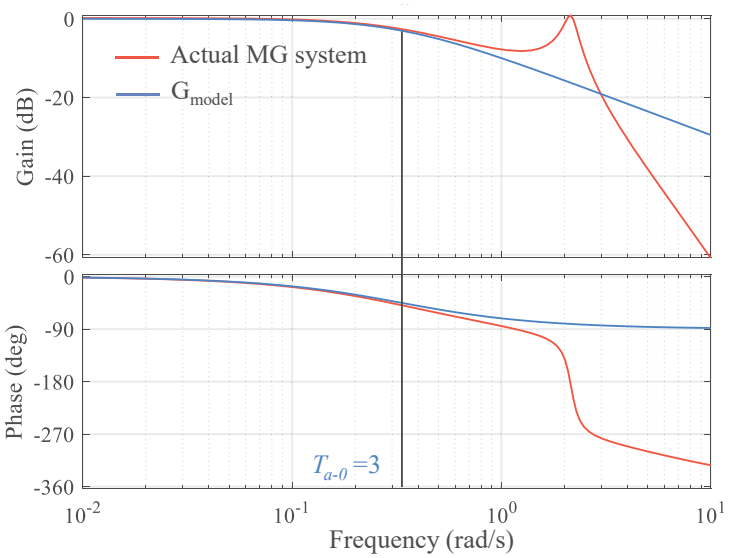

Fig 5.4 Bode plot.

5.3 Simulation settings

The proposed AMPC method and the simulation environment are built using MATLAB/Simulink R2021b software. The initial parameters of (5.5) are set to $K_{a\text{-}0}$=1 and $T_{a\text{-}0}$=3 through the bode plot of Fig 5.4.

A PI controller with optimal parameters is compared with the proposed AMPC method. The parameters of proportional (K_P) and integral (K_I) are chosen by checking

the frequency response of the system. The total capacity of the MG is assumed to be 5MW (1pu).

5.4 Simulation cases

5.4.1 Simulation cases for islanded MG systems

An islanded MG system model described in Fig 5.1 is used to determine the effectiveness of the proposed method, whose parameters are described in Table 5.1. The PV and the WT outputs are shown in Fig 5.5. The parameters of PV, WT, and BESS are listed in Table 5.2.

Simulation cases are provided in Table 5.3 where the simulation time is set to 1800s. Cases 1 and 2 are used to evaluate the performance of the AMPC in complicated disturbance conditions. The continuously varying step change is used in case 1. In case 2, we assume that a rapid step change disturbance is used from 600s to 650s. The prediction horizon (N_P=20), and the control horizon (N_C=2) are set to the AMPC in case 3, which is used to verify the proposed AMPC performance with the disturbance of case 2. The PV and WT outputs used in case 1 are also applied to cases 2 and 3. Meanwhile, the disturbance period is divided into four terms (I, II, III, IV) with 450s intervals to compare with the PI controller, as shown in Fig 5.5 (a). Parameters of the PI controller are set to K_P=0.02, and K_I=-0.1 for comparison.

Table 5.1 Parameters of islanded MG system

Symbol	Quantity	Value
D	Damping constant	0.012 (pu/Hz)
M	Inertia	0.200 (pu s)
β	Frequency response characteristic	0.345 (pu/Hz)
R_1, R_2, R_3	Governor speed droop characteristic	3.0, 3.0, 3.0 (Hz/pu)
T_{g1}, T_{g2}, T_{g3}	Time constant of governor	0.200, 0.200, 0.160 (s)
T_{t1}, T_{t2}, T_{t3}	Time constant of diesel engine	1.100, 1.100, 0.700 (s)

Table 5.2 Parameters of BESSs, PV, WT

T_{BESS1} (s)	T_{BESS2} (s)	T_{BESS3} (s)	T_{PV} (s)	T_{WT} (s)
0.100	0.110	0.130	1.8	1.5

Table 5.3 Case settings

	System Model	AMPC Controller	Input to System	Load Disturbance	WT PV
Case1	Fig.1	N_P=10, N_C=2	UKF & MPC Control Input	Fig.6 (a)	Fig.6 (a)
Case2				Fig.6 (b)	
Case3		N_P=20, N_C=2			

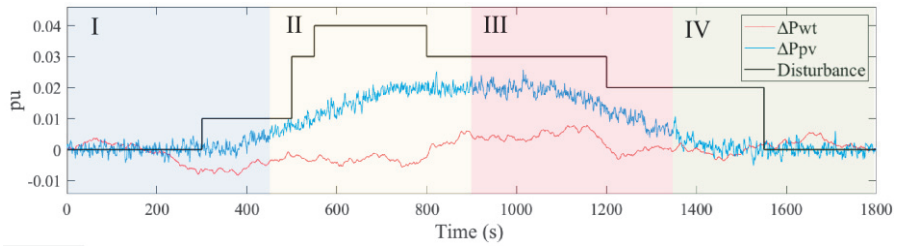

(a) PV, WT output and Disturbance in case 1.

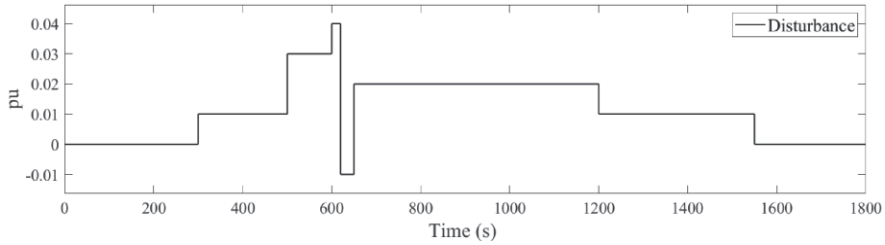

(b) Disturbance in case 2.

Fig 5.5 PV, WT Output and Disturbance.

5.4.2 Simulation cases for low inertia islanded microgrids

The proposed AMPC method is confirmed in an isolated MG system, whose parameters are summarized in Table 5.4 and 5.5. Case setting is given in Table 5.6. In case A, we assume that the MG system with high penetration of the renewable energy source and large step disturbance during cloudy weather. In case B, when a large amount of PV, and WT is imported into the MG system, and diesel engine G_2 and G_3 in Fig 5.1 have stopped generating power during sunny weather, because of the PV generation is increasing in this circumstance. However, it can decrease the system inertia and potentially lead to system instability. Therefore, it is necessary to consider the influence of a large amount of PV and WT imported in MG system. meanwhile the effectiveness

of proposed method must be determined in this case. In those case, 0.02pu step change at 600s and -0.02pu step change at 1200s are also shown in Fig 5.6 (a). Figs 5.6 (a), (b) also show the PV and WT output to consider the different periods frequency and amplitude. This is an important point due to the PV and WT output can be affected by the weather. Finally, the simulation time is set to 1800s.

Table 5.4 Parameters of low inertia MG system

D (pu/Hz)	**M (pu s)**	**β (pu/Hz)**	**R_1 R_2 R_3 (Hz/pu)**	**T_{g1} T_{g2} T_{g3} (s)**	**T_{t1} T_{t2} T_{t3} (s)**
0.012	0.200	0.345	3.0 3.0 3.0	0.20 0.20 0.16	1.1 1.1 0.7

Table 5.5 Parameters of BESSs, PV, WT

$T_{BESS,1}$ (s)	**$T_{BESS,2}$ (s)**	**$T_{BESS,3}$ (s)**	**T_{PV} (s)**	**T_{WT} (s)**
0.100	0.110	0.130	1.8	1.5

Table 5.6 Case setting

	System model	**Variable renewable**
Case A	Fig 5.1 (M=0.200, D=0.012 with G_1, G_2, G_3 diesel engine generators)	$\Delta PV_1 + \Delta PV_2$ $\Delta WT_1 + \Delta WT_2$
Case B	Fig 5.1 (M=0.150, D=0.010 with G_1 diesel engine generator)	$\Delta PV_1 + 2\times\Delta PV_2$ $\Delta WT_1 + 2\times\Delta WT_2$

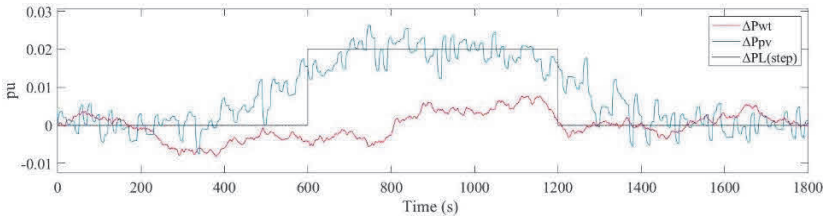

(a) WT_1, PV_1 output and step change.

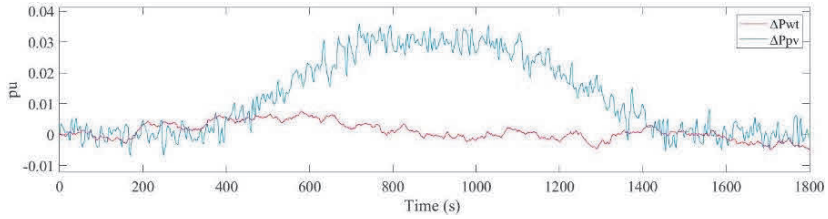

(b) WT_2, PV_2 output.

Fig 5.6 WT, PV output and step change.

5.4.3 Simulation cases for interconnected two-area MG systems

The proposed AMPC method is the same as in Table 5.3 case 3, which is confirmed in an interconnected two MGs systems considering the tie line power. The WT output, the PV output, and the disturbance are applied to MG_1. High penetration of renewable energy is imported into the MG_1 system, and diesel engine G_2 and G_3 in Fig 5.1 have stopped generating power. In this circumstance, it can decrease the system inertia and potentially lead to system instability. In order to address this issue, the MG_2 system communicates with MG_1 through the tie line, which can provide power support to MG_1 to improve the stability of the entire system. The structure of interconnected two-area MG systems is shown in Fig 5.2.

Internal prediction model (5.5) with fixed values K_a=1 and T_a=5 is applied to the AMPC of the MG_2 for getting a fast response and small computational burden to minimize the cost when the MG_1 experiences instability or emergence. In the normal support (small WT, PV, and disturbance), the parameters of the internal model are also estimated and updated by UKF to obtain small estimation errors and high control accuracy.

An interconnected two low-inertia MGs system with high penetration renewable energy is shown in Fig 5.2, whose parameters are summarized in Table 5.7. The parameters of BESSs, PV, WT are same as Table 5.2. The simulation conditions with 0.01pu step change at 60s are shown in Fig 5.7.

Table 5.7 Parameters of two-area MG system

MG	D (pu/Hz)	M (pu s)	β (pu/Hz)	R (Hz/pu)	T_g (s)	T_t (s)	T_{12} (s)
1	0.011	0.180	0.344	3.0	0.2	1.1	0.2
2	0.009	0.160	0.342	3.0	0.17	0.7	0.2

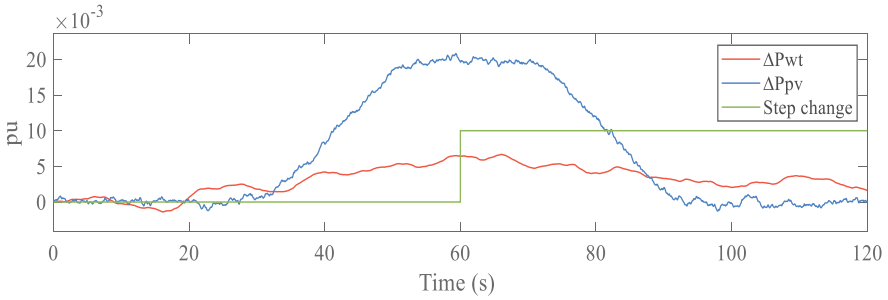

Fig 5.7 WT, PV output and step change.

5.5 Simulation results and discussions

5.5.1 Simulation results for islanded MG system

Fig 5.8 and Fig 5.9 show the performance of the AMPC method for cases 1 and 2 of Table 5.3. From Fig 5.8, we notice that the AMPC can cope with the system frequency fluctuations caused by the continuous step change and the WT, and PV outputs. Fig 5.8 (a) also exhibits a small prediction error between the real value and the estimation value by the UKF. It also shows that the UKF has a high estimation accuracy.

The simulation results of the estimation parameters are shown in Fig 5.8 (b). The estimation process is almost from 0s to 100s to capture the optimal parameters of the current system. The results show that the parameters estimation is mainly affected by the continuously varying step change. Finally, the parameters of K_a and T_a converge to an almost constant value at K_a≈0.987, T_a≈2.530.

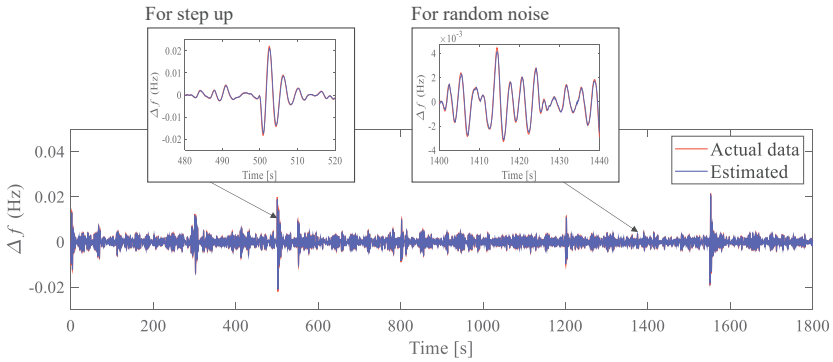

(a) Frequency Deviation in Case 1 of Table 5.3.

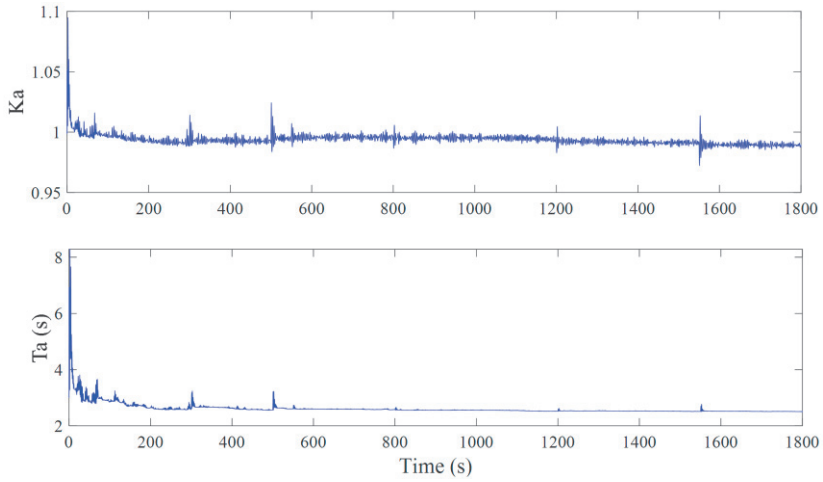

(b) Estimation Parameter Using UKF.

Fig 5.8 AMPC in Case 1 of Table 5.3.

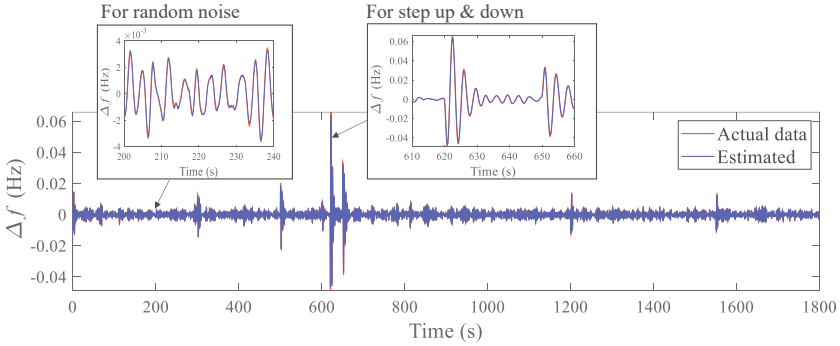

(a) Frequency Deviation in Case 2 of Table 5.3.

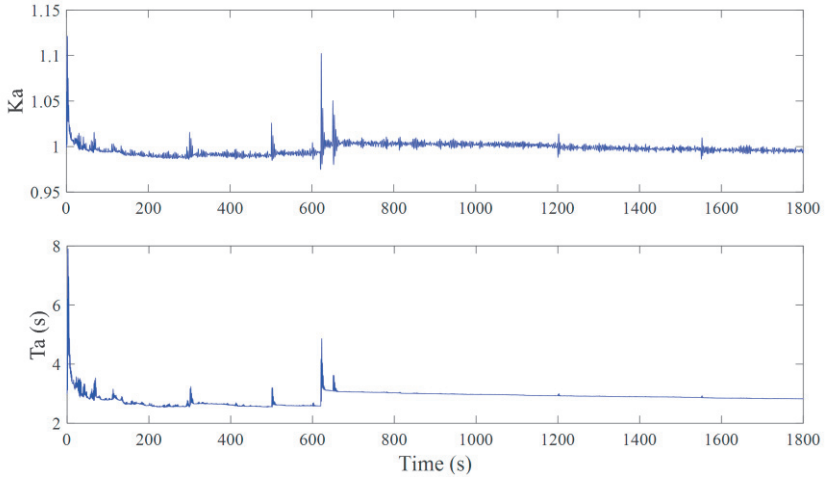

(b) Estimation Parameter Using UKF.

Fig 5.9 AMPC in Case 2 of Table 5.3.

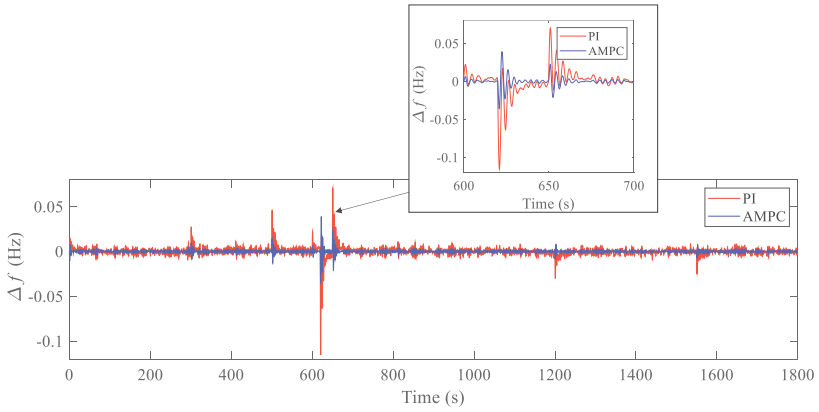

Fig 5.10 Comparative Results Based on Case 1 of Table 5.3.

In Fig 5.9 (a), we can also see that the AMPC in Table 5.3 cases 1 and 2 exhibits a fast control speed to cope with the rapid step change. Furthermore, the simulation results also show that the AMPC in Table 5.3 cases 1 and 2 can converge quickly when the rapid step change is introduced at 600s to 650s. At the same time, the parameters estimation results in Fig 5.9 (b) also show that the UKF can predict the optimal parameters when the system conditions change sharply.

Fig 5.10 shows the comparison results between the AMPC in Table 5.3 cases 1 and 2 and the PI controller. The results verify that the AMPC in Table 5.3 cases 1 and 2 performs better than the PI control.

Fig 5.11 shows the simulation results of the proposed AMPC. From Fig 5.11 (a) results, compared to case 2, the proposed AMPC performs better with a smaller frequency deviation amplitude and faster convergence ability. The parameters estimation results in Fig 5.11 (b) are almost identical to case 2. The parameter K_a converges to 1.001 and T_a converges to 2.862.

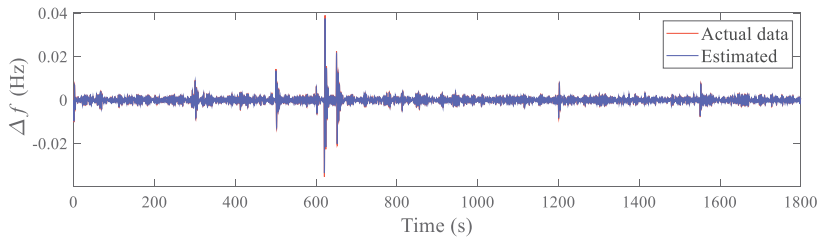

(a) Frequency Deviation in case 3.

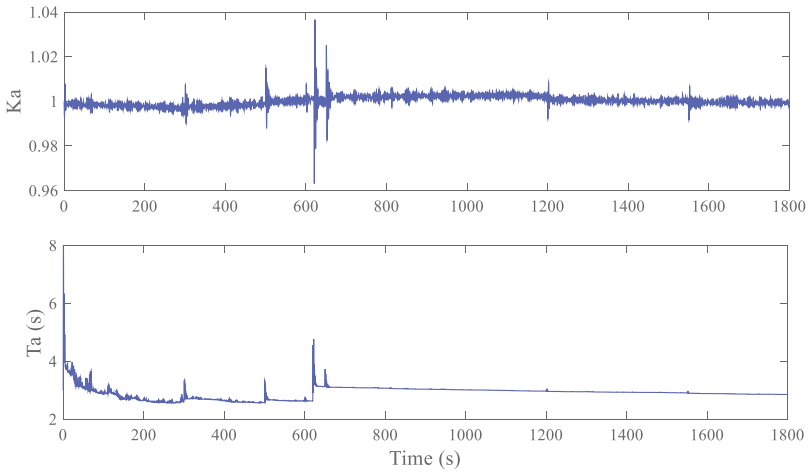

(b) Estimation Parameter Using UKF.

Fig 5.11 AMPC in Case 3.

Fig 5.12 shows the comparison result of the frequency deviation, which also shows that the AMPC method has better performance than the PI control.

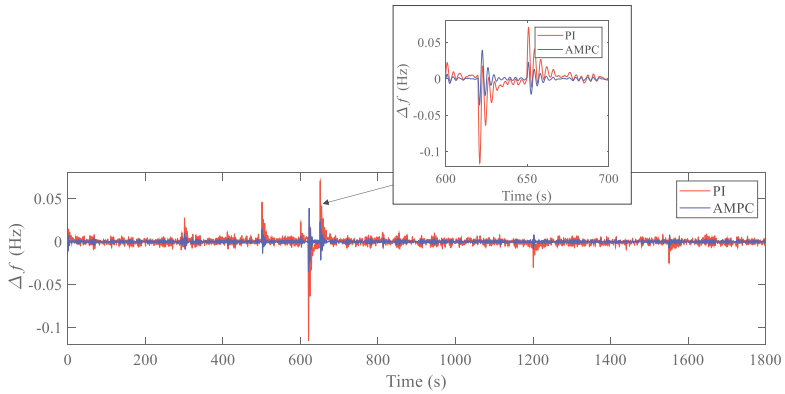

Fig 5.12 Comparative Results Based on Case 3.

Table 5.8 shows a comparison data of the frequency deviation. The minimization (Min), and the maximization (Max) indices are used to evaluate the performance based on the results of cases 2 and 3 during the four terms (I, II, III, IV).

Table 5.8 Comparative data analysis

Term	Indices (Hz)	PI	Table 5.3 case 1 and 2	Proposed AMPC
I	Min.	-0.0090	-0.0144	-0.0079
	Max.	0.0274	0.0126	0.0088
II	Min.	-0.1163	-0.0471	-0.0353
	Max.	0.0692	0.0645	0.0381
III	Min.	-0.0293	-0.0118	-0.0080
	Max.	0.0019	0.0136	0.0077
IV	Min.	-0.0249	-0.0104	-0.0066
	Max.	0.0082	0.0124	0.0076

Table 5.9 Comparative data analysis using STD

PI	Table 5.3 case 1 and 2	Proposed AMPC
0.0056Hz	0.0034Hz	0.0021Hz

From the isolated MG results, the proposed AMPC method represents a better stability performance than the others during the simulation time. A comparative analysis data with standard deviation (STD) of frequency deviation is listed in Table 5.9. Although the performance of some local points is not as good as PI control, but the proposed AMPC approach is superior to PI control in entire terms of staying probability, which is very close to reference value. These results show the proposed AMPC performs better than the PI control.

5.5.2 Simulation results for low inertia islanded MG system

Fig 5.13 gives the simulation results of frequency deviation for case A in Table 5.6. We can observe that the frequency deviation occurs a fluctuation at 0s due to the initial estimation parameters, but it converges quickly. The proposed AMPC method perform a fast response when the step disturbance is imported at 600s and 1200s and rapidly convergence to the desired range. There is a small estimation error between actual data

and estimated state variables by UKF. The simulation results show that the proposed AMPC method can effectively cope with the frequency problem.

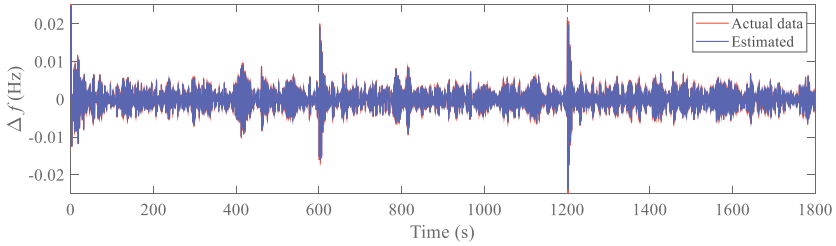

Fig 5.13 Frequency deviation in case A of Table 5.6.

Fig 5.14 shows the results of estimation parameter by UKF. We can observe that the estimation parameter occurs a fluctuation from 0s to almost 40s to obtain the optimal parameter for MG system, and stables at a constant value T_a≈2.21. The enlarged plot in Fig 5.14 also shows that the UKF can estimate the optimal parameters to address the system dynamic fluctuation. UKF performs a high estimation accuracy and fast speed when the step change is imported.

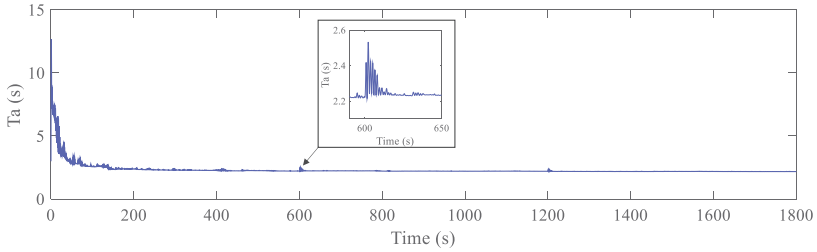

Fig 5.14 Estimation parameter by UKF in case A of Table 5.6.

Fig 5.15 shows the comparative results based on case A of Table 5.6, whose comparative data of frequency deviation using minimization (Min.), maximization (Max.), and standard deviation (STD) indices is given in Table 5.10. Form the results, the proposed AMPC method has better performance than the PI controller to address the frequency problem. At the same time, the proposed method has faster convergence speed and smaller overshoot from the enlarged plot in Fig 5.15.

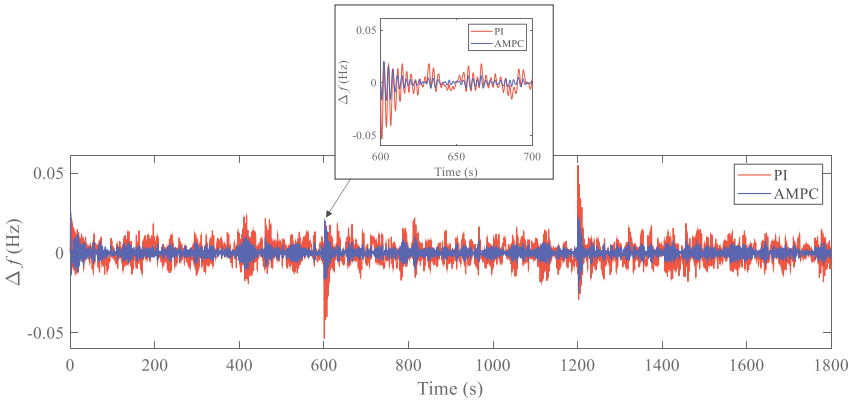

Fig 5.15 Comparative results based on case A of Table 5.6.

Table 5.10 Comparative analysis based on Case A of Table 5.6

(Hz)	PI	AMPC
Min.	-0.0534	-0.0250
Max.	0.0550	0.0253
STD	0.0066	0.0028

Figs 5.16, 5.17, and 5.18 show the simulation results for case B in Table 5.6. From the results, we can observe that the propose AMPC can address the frequency problem effectively when the large amount of renewable energy is imported in low-inertia circumstance from Fig 5.16. The estimation parameters result in Fig 5.17 shows that the UKF can estimate parameter with high accuracy. The estimation parameter Ta stables at almost 1.8s. The proposed AMPC has the faster response speed than that in Table 5.6 case A to against the large fluctuation caused by large amount of PV and WT. However, the PI controller exhibits an instability performance from Fig 5.18 due to the parameters of PI controller must be tuned when the system chrematistics are change.

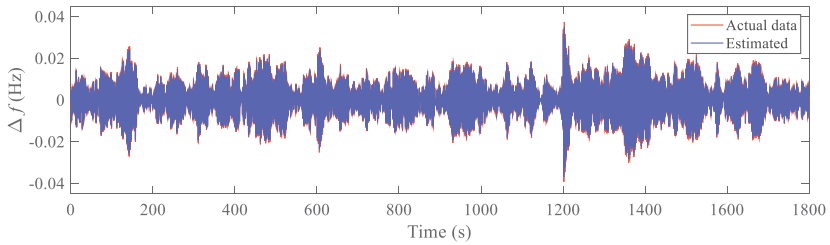

Fig 5.16 Frequency deviation in Table 5.6 case B.

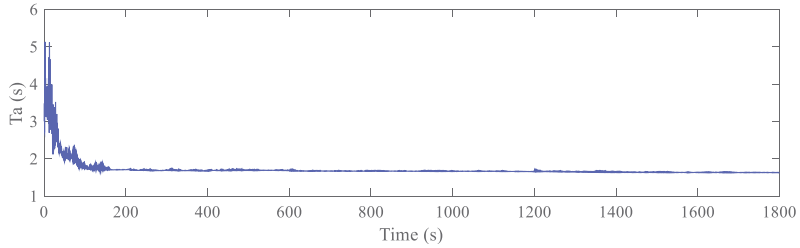

Fig 5.17 Estimation parameter by UKF in case B.

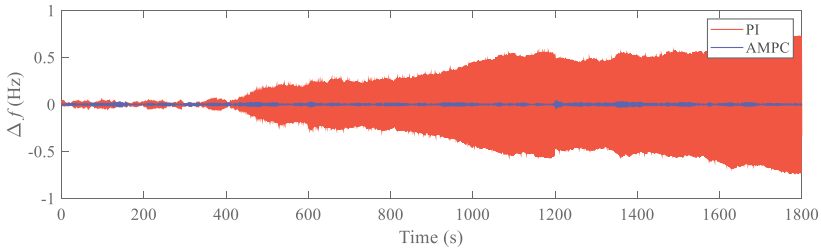

Fig 5.18 Comparative results based on Table 5.6 case B.

Fig 5.19 gives the total capital of PV, WT in case B. we can notice that the PI controller appears instability when the event occurs almost from 200s.

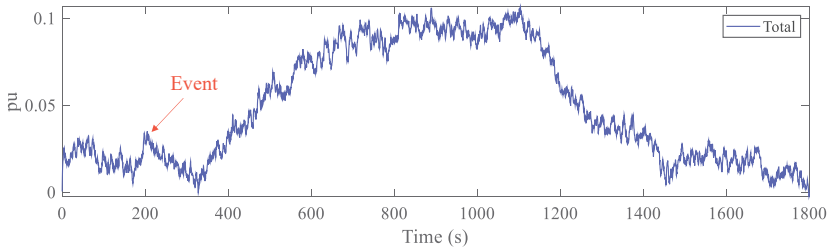

Fig 5.19 Total capital of PV and WT in Table 5.6 case B.

5.5.3 Simulation results for interconnected two-area MG system

The effectiveness of the proposed method and the conventional PI control is examined in a low-inertia isolated MG_1 system before connecting with MG_2, whose simulation results are shown in Fig 5.20 and 5.21. From the results, the PI controller must tune the parameters to obtain satisfied control performance when the system characteristics change. However, the proposed AMPC approach exhibits better control effectiveness than the PI control because it can realize the automated optimal control to address the variation of system characteristics.

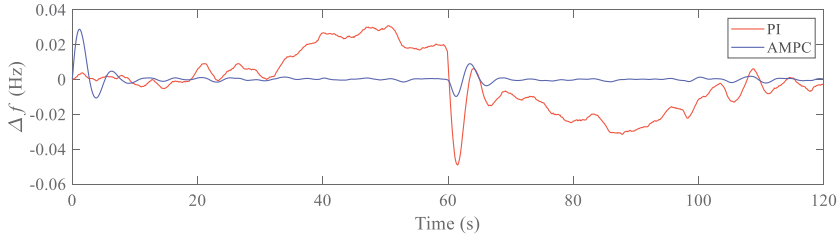

Fig 5.20 PI with original parameters.

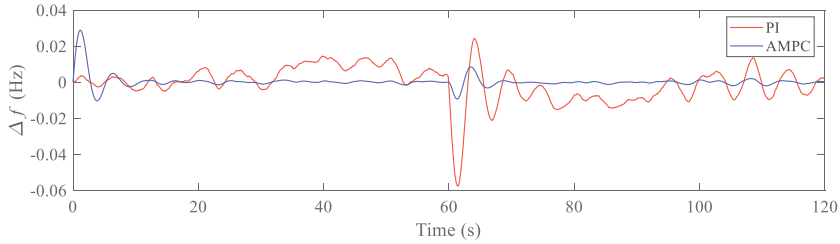

Fig 5.21 PI with tuned parameters.

Fig 5.22 gives the simulation results of frequency deviation ACE, and tie-line power of interconnected two MGs system. We can observe that the frequency deviation, ACE, and tie-line power fluctuate at 0s due to the initial estimation parameters, but they are stable at almost 10s. The proposed AMPC method response quickly when the step disturbance is imported. The simulation results show that the proposed AMPC method can effectively cope with the frequency problem.

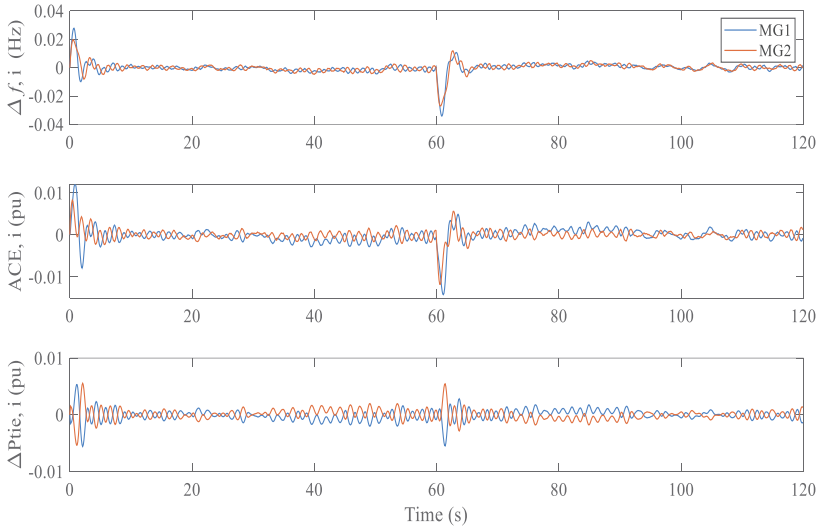

Fig 5.22 Frequency deviation, ACE, and tie line power.

Fig 5.23 shows the estimation results of UKF. The results show an estimation process from 0s to 22s to predict the optimal values into the proposed AMPC and stable values are continued after 20s. Although the estimation time is longer than the

isolated MG, the proposed AMPC method still has a fast response speed.

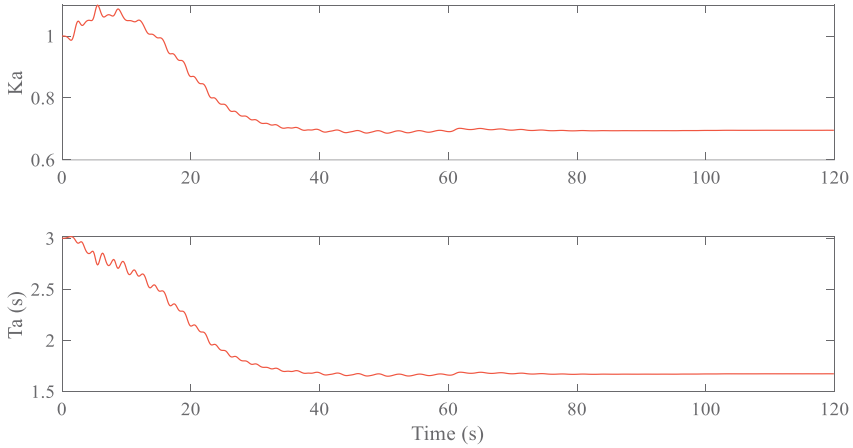

Fig 5.23 Estimation parameters by UKF.

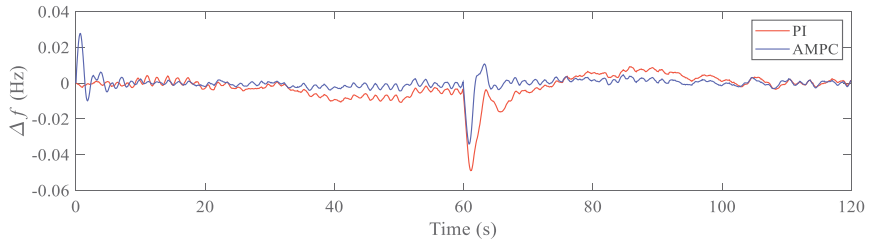

Fig 5.24 Comparison result.

Table 5.11 Comparative analysis

(Hz)	PI	AMPC
Min.	-0.0489	-0.0340
Max.	0.0088	0.0096
STD	0.0069	0.0040

Fig 5.24 shows a comparison result based on the frequency deviation of MG_1 with conventional PI control, whose comparison analysis is shown in Table 5.11.

The interconnected two MGs results also show that the proposed AMPC method can effectively solve the MG system frequency problem and performs better than the PI control. In addition, we have checked the proposed approach with more complex grids and various disturbances for evaluating robustness and adaptability in our previous work.

5.6 Conclusions

This work proposes a novel load frequency control method using AMPC for the MG system. The simulation results show that the proposed AMPC method can cope with the

MG system frequency problems. The proposed method can achieve the frequency control objectives in coordination with each other system, Even though the multiple MGs with different generator and load characteristics. Moreover, the proposed method has high response speed and robustness. The comparison data also show that the proposed method has a better performance than the PI controller. The proposed method does not need to require the experience to tune the parameters, which can achieve the automated optimal control compared to the PI controller. From the cost viewpoint, the proposed method can achieve low operating costs that could be a significant advantage for future MG construction.

Chapter 6: Conclusions and discussions

6.1 Novelties and conclusions of the dissertation

In this work, a novel AMPC-based robust load frequency control method is proposed for addressing the frequency issue. The simulation results show that the proposed AMPC method with high response speed and robustness can effectively address the power system frequency problems. The frequency fluctuation caused by the RESs and disturbances. The comparison data also exhibit that the proposed AMPC approach has a better ability to address the frequency problem than the PI controller.

As a result, the contributions and novelties of this work are summarized in the followings.

- The proposed methods are effective for power systems frequency control schemes.

- A simplified internal prediction model is applied to the proposed AMPC method, which can effectively approximate the system response. Therefore, it can decrease the computation burden comparing with the detailed high-order model.

- The proposed AMPC methods have fast response speed and high estimation accuracy, which can effectively address the power system frequency fluctuation caused by the uncertainty of the RESs

- The proposed methods can achieve low operating costs that could be a significant advantage for future MG development.

- From the MG operators' viewpoint, usually, MG operators must tune the parameters of the frequency controller based on their own experience. However, the proposed methods do not require the experience to tune the parameters, which can achieve automated optimal control for various types of the disturbances.

However, the proposed AMPC methods still spend considerable long time to estimate the state values. This issue is remaining as the future works. Although the simulation results show that the MG system can be represented by a simplified internal prediction model, there are some oscillations in the parameters estimation process. These oscillations should be reduced to achieve more effective method.

Social significance and business potential of research:

The effective LFC method developed in this thesis can solve the frequency problem in the power system more efficiently. As a result, the amount of renewable energy introduced in the power system can be significantly increased. In other words, this is a technology that will greatly contribute to the realization of carbon neutrality. In addition to the applications of the renewable energy, MGs are expected to improve the resilience of power supply against disasters, etc., and the developed technology is expected to contribute to the development of MGs in the future. Therefore, the social significance of this research is the realization of a carbon-neutral and disaster-resistant society. As a result of the above, if MGs gain recognition and their needs increase in the future, business development can be expected.

6.2 Future works

In future work, the inertia capacity inherent in the MG needs to be determined in advance since the system inertia is very low when 100% renewable energy is applied. Therefore, the proposed AMPC method must improve its performance to cope with the extremely low inertia system. In addition, it's essential to consider the highly accurate modeling, real-time system state estimation, and optimization of operating costs (redesign of objective function and constraints). Furthermore, the author will compare with other LFC methods to confirm the performance of the proposed AMPC approach. Meanwhile, the proposed method will be applied to connected multi-area MG system to identify the performance of it.

References

[1] W. Wang, N. Yorino, Y. Sasaki, Y. Zoka, A. Bedawy, S. Kawauchi, "Adaptive MPC-Based Cooperative Frequency Control for Community Microgrid," *Proc. of the 4th International Conference on Smart Power & Internet Energy Systems*, Beijing, China, Dec. 9-12, 2022.

[2] W. Wang, N. Yorino, Y. Sasaki, Y. Zoka, A. Bedawy, S. Kawauchi, "A Novel Adaptive Model Predictive Frequency Control using Unscented Kalman Filter," *Electric Power Systems Research*, Vol. 203, 2022.

[3] W. Wang, N. Yorino, Y. Sasaki, Y. Zoka, A. Bedawy, and S. Kawauchi, "Adaptive Model Predictive-Based Load Frequency Controller using Unscented Kalman Filter," *2021 IEEE PES Innovative Smart Grid Technologies (ISGT)*, 2021.

[4] W. Wang, N. Yorino, Y. Sasaki, Y. Zoka, A. Bedawy, and S. Kawauchi, "Adaptive MPC-Based Cooperative Frequency Control for Community Microgrid," *2022 4th International Conference on Smart Power & Internet Energy Systems (SPIES)*, (Online), Beijing, China, 9-12 December 2022.

[5] W. Wang, Y. Sasaki, N. Yorino, Y. Zoka, and A. Bedawy, "Adaptive Model Predictive Control Based Frequency Regulation for Low-inertia Microgrid," *The 5th International Conference on Power and Energy Technology (ICPET)*, Tianjin, July 27-30, 2023.

[6] W. Wang, Y. Sasaki, N. Yorino, Y. Zoka, A. Bedawy, and S. Kawauchi, "Adaptive MPC-Based Load Frequency Control for Microgrid with Renewable Energy," *The International Council Electrical Engineering (ICEE) Conference*, July 2-6, 2023.

[7] Y. Sasaki, D. Seikoba, J. Okihara, K. Kanaya, Y. Zoka, and N. Yorino, "A robust supply and demand controller against uncertainties of renewable energy sources," *2014 Power Systems Computation Conference*, 2014.

[8] N. Yorino, K. Amimoto, Y. Sasaki, Y. Zoka, H. Inami, and Shoya Ogawa, "Autonomous Distributed Frequency Control for the Management of Energy Storage Systems in Microgrid," *2022 IEEE Sustainable Power and Energy Conference (ISPEC)*, 2022.

[9] W. Wang, N. Yorino, Y. Sasaki, Y. Zoka, and S. Kawauchi:"Adaptive Model Predictive Load Frequency Controller Based on Unscented Kalman Filter," *2021 IEEE Sustainable Power and Energy Conference (ISPEC)*, 2021.

[10] G. Shahgholian, "A brief review on microgrids: Operation, applications, modeling, and control," *Int Trans Electrical Energy Systems*, Vol. 31. No. 6, 2021.

[11] S. Saha, M.I. Saleem, and T.K. Roy, "Impact of high penetration of renewable energy sources on grid frequency behavior," *International Journal of Electrical Power & Energy Systems, ELSEVIER*, Vol. 145, 2023.

[12] Y. Guler, and I. Kaya, "Load Frequency Control of Single-Area Power System with PI–PD Controller Design for Performance Improvement," *Journal of Electrical Engineering & Technology, Spring*, 2023.

[13] P. K. Pathak, A. K. Yadav, A. Shastri, and P.a. Alvi, "BWOA assisted PIDF-(1+I) controller for intelligent load frequency management of standalone micro-grid," *ISA Transactions, ELSEVIER*, Vol. 132, pp. 387-401, 2023.

[14] A. A. Hossam-Eldin, E. Negm, M. Ragab, and K. M. AboRas, "A maiden robust FPIDD2 regulator for frequency-voltage enhancement in a hybrid interconnected power system using Gradient-Based Optimizer," *Alexandria Engineering Journal, ELSEVIER*, Vol. 65, pp. 103-118, 2023.

[15] M. Kumar, "Resilient PIDA Control Design Based Frequency Regulation of Interconnected Time-Delayed Microgrid Under Cyber-Attacks," I*EEE Transactions on Industry Applications*, Vol. 59, No.1, pp. 492-502, 2023.

[16] D. H. Tungadio, and Y. Sun, "Load Frequency Controllers Considering Renewable Energy Integration in Power System," *Energy Reports*, Vol. 5, pp. 436-453, 2019.

[17] M. H. Khooban, and M. Gheisarnejad, "A Novel Deep Reinforcement Learning Controller Based Type-II Fuzzy System: Frequency Regulation in Microgrids," *IEEE*

Transactions on Emerging Topics in Computational Intelligence, Vol. 5, No. 4, pp. 689-699, 2021.

[18] A. Rai, and D. K. Das, "The Development of A Fuzzy Tilt Integral Derivative Controller Based on The Sailfish Optimizer to Solve Load Frequency Control in A Microgrid, Incorporating Energy Storage Systems," *Journal of Energy Storage*, Vol. 48, 2022.

[19] M. Adibi, and J. V. D. Woude, "Secondary Frequency Control of Microgrids: An Online Reinforcement Learning Approach," *IEEE Transactions on Automatic Control*, Vol. 67, No. 9, pp4824-4831, 2022.

[20] W. Dong, K. Liu, and C. Lv, "A Novel Frequency-changer Control Strategy Based on a Virtual Synchronous Motor," *CSEE Journal of Power and Energy Systems*, Vol. 5, No. 2, pp. 199-205, 2019.

[21] G. K. Suman, J. M. Guerrero, and O. P. Roy, "Robust Frequency Control in Interconnected Microgrids: An H2/H∞ Control Approach," *IEEE Systems Journal*, Vol. 16, No. 2, pp2044-2055, 2022.

[22] G. Zhang, J. Li, Y. Xing, D. Cai, and Q. Huang, "An H∞ Load Frequency Control Scheme for Multi-Area Power System Under Cyber-Attacks and Time-Varying Delays," *IEEE Transactions on Power Systems*, Vol. 38, No. 2, pp. 1336-1349, 2023.

[23] H. Shen, S. Jiao, J. H. Park, and V. Sreeram,"An Improved Result on H∞ Load Frequency Control for Power Systems With Time Delays," *IEEE Systems Journal*, Vol. 15, No. 3, pp. 3238-3248, 2021.

[24] H. H. Alhelou, N. Nagpal, N. Kassarwani, and P. Siano, "Decentralized Optimized Integral Sliding Mode-Based Load Frequency Control for Interconnected Multi-Area Power Systems," *IEEE Access*, Vol. 11, pp. 32296-32307, 2023.

[25] P. A. Gbadega, and A. K. Saha, "Load Frequency Control of a Two-Area Power System with a Stand-Alone Microgrid Based on Adaptive Model Predictive Control," *IEEE Journal of Emerging and Selected Topics in Power Electronics*, Vol. 9, No. 6, pp7253-7263, 2021.

[26] Y. Liu, Y. Chen, and M. Li, "Dynamic Event-Based Model Predictive Load Frequency Control for Power Systems Under Cyber Attacks," *IEEE Transactions on Smart Grid*, Vol. 12, No. 1, pp. 715-725, 2021.

[27] J. Liu, Q. Yao, and Y. Hu, "Model predictive control for load frequency of hybrid power system with wind power and thermal power," *Energy*, Vol.172, pp. 555-565, 2019.

[28] M. Negahban, M. V. Ardalani, M. Mollajafari, E. Akbari, M. Talebi, and E. Pouresmaeil, "A Novel Control Strategy Based on an Adaptive Fuzzy Model Predictive Control for Frequency Regulation of a Microgrid With Uncertain and Time-Varying Parameters," *IEEE Access*, Vol. 10, pp. 57514-57524, 2022.

[29] A. Kumar, N. Kumari, G. Shankar, R. M. Elavarasan, S. Kumar, A. K. Srivastava, and B. Khan, "Load Frequency Control of Distributed Generators Assisted Hybrid Power System Using QOHSA Tuned Model Predictive Control," *IEEE Access*, 2022.

[30] R. Kandepu, B. Foss, and L. Imsland, "Applying the unscented Kalman filter for nonlinear state estimation," *Journal of Process Control*, Vol. 18, No. 7-8, pp. 753-768, 2008.

[31] G. Valverde, and V. Terzija, "Unscented Kalman filter for power system dynamic state estimation," *IET Generation, Transmission & Distribution*, Vol. 5, No. 1, pp. 29-37, 2010.

[32] J. C. Sanchez, D. Erdogmus, J. C. Principe, J. Wessberg, and M. Nicolelis, "A Comparison between Nonlinear Mappings and Linear State Estimation to Model the Relation from Motor Cortical Neuronal Firing to Hand Movements," *SAB Workshop on Motor Control in Humans and Robots*, 2002.

[33] D. H. Tungadio, and Y. Sun, "Load frequency controllers considering renewable energy integration in power system," *Energy Reports*, Vol. 5, pp. 436-453, (2019).

[34] G. K. Suman, J. M. Guerrero, and O. P. Roy, "Robust Frequency Control in Interconnected Microgrids: An H2/H∞ Control Approach," *IEEE Systems Journal*, Vol. 16, No. 2, pp. 2044-2055, 2022.

[35] M.W. Siti, N.T. Mbungu, D.H. Tungadio, B.B. Banza, and L. Ngoma, “Application of load frequency control method to a multi-microgrid with energy storage system,” J*ournal of Energy Storage*, Vol. 52, 2022.
[36] M. Adibi, and J. Woude, “Secondary Frequency Control of Microgrids: An Online Reinforcement Learning Approach,” *IEEE Trans. on Automatic Control*, Vol. 67, No. 9, pp. 4824-4831, 2022.
[37] Z. Yi, Y. Xu, W. Gu, and Z. Fei, “Distributed Model Predictive Control Based Secondary Frequency Regulation for a Microgrid With Massive Distributed Resources,” *IEEE Trans. on Sustainable Energy*, Vol. 12, No. 2, pp. 1078-1089, 2021.
[38] Z. Zhao, J. Guo, X. Luo, and C. S. Lai, “Distributed Robust Model Predictive Control-Based Energy Management Strategy for Islanded Multi-Microgrids Considering Uncertainty,” *IEEE Trans. on Smart Grid*, Vol. 13, No. 3, pp. 2107-2120, 2022.
[39] L. Wang :「Model Predictive Control System Design and Implementation」, *Springer* 2009.
[40] S. Adachi and I. Marukawa:“Fundamentals of Kalman Filter”, T*okyo Denki University Press* (in Japanese), 2012.
[41] D. Zhang, H. Zhang, X. Zhang, “Research on AGC Performance During Wind Power Ramping Based on Deep Reinforcement Learning,” *IEEE Access*, Vol. 8, pp. 107409-107418, 2020.
[42] J. Li, T. Yu, “Multi-Agent Deep Reinforcement Learning for Sectional AGC Dispatch,” *IEEE Access*, Vol. 8, pp. 158067-158081, 2020.
[43] F. Zhang, Z. Hu, K. Meng, “HESS Sizing Methodology for an Existing Thermal Generator for the Promotion of AGC Response Ability,” *IEEE, Trans. on Sustainable Energy*, Vol. 11, No. 2, pp. 608-617, 2020.
[44] F. Beaufays, Y. Abdel-Magid, B. Widrow, “Application of Neural Networks to Load-frequency Control in Power Systems,” *Neural Networks*, Vol. 7, No. 1, pp. 183-194, 1994.
[45] D. K. Chaturvedi, P.S. Satsangi, P.K.Kalra, "Load frequency control: a generalized neural network approach", *Electr Power Energy Syst*, Vol. 21, No. 6, pp. 405-415, 1999.
[46] H. Bevrani, T. Hiyama, Y.Mitani, K. Tsuji, M. Teshnehlab, “Load Frequency Regulation under a Bilateral LFC Scheme using Flexible Neural Networks,” *Eng. Int. Syst.*, Vol. 14, No. 2, pp. 109-117, 2006.
[47] A. B. Rehiara, He Chongkai, Y. Sasaki, N. Yorino and Y. Zoka, “An Adaptive IMC-MPC Controller for Improving LFC Performance,” *2017 IEEE Innovative Smart Grid Technologies (Asia)*, Auckland, 2017.
[48] Z. Qiu, M. Santillo, J. Sun and M. Jankovic, “Enhanced Composite Adaptive IMC for Boost Pressure Control of a Turbocharged Gasoline Engine,” *2016 American Control Conference (ACC)*, Boston, MA, pp. 3286-3291, 2016.
[49] A. B. Rehiara, He Chongkai, Y. Sasaki, N. Yorino and Y. Zoka, “An Adaptive prediction Model for Load Frequency Control using Extreme Learning Machine,” *TELKOMNIKA Indonesian Journal of Electrical Engineering 16(6)*, Vol. 16, No. 6. pp.2879-2887, 2018.
[50] J. Guo, “Application of a Novel Adaptive Sliding Mode Control Method to the Load Frequency Control,” *European Journal of Control*, Vol. 57, pp. 172-178, 2021.
[51] J. Zhai, M. Zhou, S. Dong, “MPC-based Two-stage Rolling Power Dispatch Approach for Wind-integrated Power System,” *Journal of Electrical Engineering Technology*, Vol. 13, No. 2, pp. 648-658, 2018.
[52] A. E. Onyeka, Y. XingGang, Z. Mao, “Robust Decentralized Load Frequency Control for Interconnected Time Delay Power Systems using Sliding Mode Techniques,” *IET Control Theory & Applications*, Vol. 14, No. 3, pp. 470-480, 2020.
[53] C. F. Juang, C. F. Lu, “Load-frequency Control by Hybrid Evolutionary Fuzzy Pl controller,” *IEE Proc. Gener. Transm. Distrib*, Vol. 153, No. 2, pp. 196-204, 2006.
[54] C. S. Chang, W. Fu, “Area Load Frequency Control using Fuzzy Gain Scheduling of PI Controller,” *Electric Power Systems Research*, Vol. 42, No. 2, pp. 145-152, 1997.
[55] M. Han, X. Kong, "Distributed MPC of the standalone hybrid wind and solar generation system based on neural network modeling", *IEEE, WCICA*, 2016.

[56] H. Wang, Z. Lei, X. Zhang, "Multiobjective Reinforcement Learning-Based Intelligent Approach for Optimization of Activation Rules in Automatic Generation Control," *IEEE Access*, Vol. 7, pp. 17480-17492, 2019.
[57] Y. Qiu, J. Lin, F. Liu, "Explicit MPC Based on the Galerkin Method for AGC Considering Volatile Generations," *IEEE Trans. on Power Systems*, Vol. 35, No. 1, pp. 462-473, 2020.
[58] D. Rerkpreedapong, A. Hasanovic´, and A. Feliachi, "Robust Load Frequency Control Using Genetic Algorithms and Linear Matrix Inequalities," *IEEE Trans. on Power Systems*, Vol.18, No.2. 2003.
[59] L. Jiang, W. Yao, Q. H. Wu, J. Y. Wen, and S. J. Cheng, "Delay-Dependent Stability for Load Frequency Control with Constant and Time-Varying Delays," I*EEE Trans. on Power Systems*, Vol.27, No.2. 2012.
[60] K. A. Folly, N. Yorino, and H. Sasaki, "Improving the robustness of H∞-PSSs using the polynomial approach," *IEEE Trans. on Power Systems*, Vol.13, No.4. 1998.
[61] H. K. Sahoo, P. K. Dash, "Robust Estimation of Power Quality Disturbance using Unscented H∞ Filter," *Electrical Power and Energy System*, Vol. 73, pp. 438-447, 2015.
[62] Y. R. Rodrigues, M. Abdelaziz, L. Wang, I. Kamwa, "PMU Based Frequency Regulation Paradigm for Multi-Area Power Systems Reliability Improvement," *IEEE Trans. on Power System*, Vol. 36, No. 5, pp. 4387-4399, 2021.
[63] M. Liu, F. Bizzarri, A.M. Brambilla, "On the Impact of the Dead-Band of power System Stabilizers and Frequency regulation on Power System Stability," *IEEE Trans. on Power System*, Vol. 34, No. 5, pp. 3977-3979, 2019.
[64] J. Morsali, K. Zare, M. T Hagh, "AGC of Interconnected Multi-source Power System with Considering GDB and GRC Nonlinearity Effects," *IEEE Conference on Thermal Power Plants*, 2016.
[65] J. M. Maciejowski, "Predictive Control with Constraints," *Prentice Hall*, US, 2000.
[66] A. Mai Ersdal, K. Uhlen, "Model Predictive Load-Frequency Control," *IEEE Trans. on Power System*, Vol. 31, No. 1, pp. 777-785, 2016.
[67] A. M. Ersdal, L. Imsland, K. Uhlen, D. Fabozzi, N. F. Thornhill, "Model Predictive Load-frequency Control taking into account Imbalance Uncertainty," *ELSEVIER Control Engineering Practice*, Vol. 53, pp. 139-150, 2016.
[68] M. A. Mohamed, A. A. Zaki Diab, H. Rezk, T. Jin, "A Novel Adaptive Model Predictive Controller for Load Frequency Control of Power Systems Integrated with DFIG Wind Turbines," *Neural Comput. & Applic.*, Vol. 32, pp. 7171-7181, 2020.
[69] T. H. Mohamed, J. Morel, H. Bevrani, T. Hiyama, "Model Predictive based Load Frequency Control Design concerning Wind Turbines," *ELSEVIER Electrical Power and Energy System*, Vol. 43, pp. 859-867, 2012.
[70] R. Pasantha, L. Wang, "Automatic Generation Control of Multi-area Power System with Network Constraints and Communication Delays," *Journal of Modern Power System and Clean Energy*, Vol. 8, No. 3, pp. 454-463, 2020.
[71] E. A. Wan, R. Van Der Merwe, "The Unscented Kalman Filter for Nonlinear Estimation," *Proceedings of the IEEE 2000 Adaptive System for Signal Processing*, 2000.
[72] E. Ghahremani, I. Kamwa, "Online State Estimation of a Synchronous Generator Using Unscented Kalman Filter From Phasor Measurements Units," *IEEE Trans. on Energy Conversion*, Vol. 26, No. 4, pp. 1099-1108, 2011.
[73] J. Qi, Kai Sun, "Dynamic State Estimation for Multi-Machine Power System by Unscented Kalman Filer with Enhanced Numerical Stability," *IEEE Trans. on Smart Grid*, Vol. 9, No. 2, pp. 1184-1196, 2018.
[74] C. He, A. B. Rehiara, Y. Sasaki, N. Yorino, Y. Zoka, "Model Predictive Load Frequency Control using Unscented Kalman Filter," *International Workshop on Power Engineering in Remote Islands (IWPI2018)*, PE-18-206, pp. 1-6, 2018.
[75] P. Bhui, N. Senroy, A K. Singh, B. C. Pal, "Estimation of Inherent Governor Dead-Band and Regulation Using Unscented Kalman Filter," *IEEE Trans. on Power Systems*, Vol. 33, No. 4, pp. 3546-3558, 2018.

[76] N. Yorino, S. Sekizaki, K. Adachi, Y. Sasaki, Y. Zoka, A. Bedawy, T. Shimizu, "A Novel Design of Single-phase Microgrid based on Non-interference Core Synchronous Inverters for Power System Stabilization," *IET Gen., Trans & Dist.*, Mar. 2022.
[77] M. Kosaka, "Modern control and digital control," *Corona Press*, 2015.
[78] The Institute of Electrical Engineers of Japan, "Recommended Practice for Simulation Models for Automatic Generation Control," *Technical Report*, No.1386, 2016 (in Japanese).
[79] H. Bevrani, "Robust Power System Frequency Control," *Springer*, 2009.
[80] D. H. Tungadio, Y. Sun, "Load Frequency Controllers Considering Renewable Energy Integration in Power System, Energy Reports," Vol. 5, pp. 436-453, 2019.
[81] A. Rai, D. K. Das, "The Development of A Fuzzy Tilt Integral Derivative Controller Based on The Sailfish Optimizer to Solve Load Frequency Control in A Microgrid," *Incorporating Energy Storage Systems, Journal of Energy Storage*, Vol. 48, 2022.
[82] D. Zhao, S. Sun, A. Mohammadzadeh, A. Mosavi, "Adaptive Intelligent Model Predictive Control for Microgrid Load Frequency," *Sustainability*, Vol. 14, No. 18. 11772, 2022.
[83] P. A. Gbadega, A. K. Saha, "Load Frequency Control of a Two-Area Power System with a Stand-Alone Microgrid Based on Adaptive Model Predictive Control," I*EEE Journal of Emerging and Selected Topics in Power Electronics*, Vol. 9, No. 6, pp7253-7263, 2021.
[84] M. Adibi, J. V. D. Woude, "Secondary Frequency Control of Microgrids: An Online Reinforcement Learning Approach," *IEEE Transactions on Automatic Control*, Vol. 67, No. 9, pp4824-4831, 2022.
[85] G. K. Suman, J. M. Guerrero, O. P. Roy, " Robust Frequency Control in Interconnected Microgrids: An H2/H∞ Control Approach," *IEEE Systems Journal*, Vol. 16, No. 2, pp2044-2055, 2022.
[86] M. Ranjian, and R. Shankar, "A literature survey on load frequency control considering renewable energy integration in power system: Recent trends and future prospects," *Journal of Energy Storage, ELSEVIER*, Vol. 45, 2022.
[87] J. Heidary, M. Gheisarnejad, H. Rastegar, and M. H. Khooban, "Survey on microgrids frequency regulation: Modeling and control systems," *Electric Power Systems Research, ELSEVIER*, Vol. 213, 2022.
[88] N T. Mbungu, A A. Ismail, M. Aishabi, R C. Bansal, A. Elnady, and A K. Hamid, "Control and estimation techniques applied to smart microgrids: A review," *Renewable and Sustainable Energy Reviews, ELSEVIER*, Vol. 179, 2023.
[89] I. Moschos, and C. Parisses, "A novel optimal PIλDND2N2 controller using coyote optimization algorithm for an AVR system," *Engineering Science and Technology, an International Journal, ELSEVER*, Vol. 26, 2022.
[90] A. X. R. Irudayaraj, N. I. A. Wahab, M. Premkumar, M. A. M. Radzi, N. B. Sulaiman, V. Veerasamy, R. A. Farade, and M. Z. Islam, "Renewable sources-based automatic load frequency control of interconnected systems using chaotic atom search optimization," *Applied Soft Computing, ELSEVIER*, Vol. 119, 2022.
[91] W. Chen, N. Sun, Z. Ma, W. Liu, and H. Dong, "A Two-Layer Optimization Strategy for Battery Energy Storage Systems to Achieve Primary Frequency Regulation of Power Grid," *energies*, Vol. 16, No. 6, 2023.
[92] L. Xiong, X. Liu, H. Liu, and Yonghui Liu, "Performance Comparison of Typical Frequency Response Strategies for Power Systems With High Penetration of Renewable Energy Sources," *IEEE Journal on Emerging and Selected Topics in Circuits and Systems*, Vol. 12, pp. 41-47, 2022.
[93] W. Wang, B. Yuan, Q. Sun, and R. Wennersten, "Application of energy storage in integrated energy systems — A solution to fluctuation and uncertainty of renewable energy," *Journal of Energy Storage, ELSEVIER*, Vol. 52, 2022.
[94] H. H. Alhelou, N. Nagpal, N. Kassarwani, and Pierluigi Siano, "Decentralized Optimized Integral Sliding Mode-Based Load Frequency Control for Interconnected Multi-Area Power Systems," *IEEE Access*, Vol. 11, pp. 32296-32307, 2023.

[95] X. Zhang, C. Li, B. Xu, Z. Pan, and Tao Yu, "Dropout Deep Neural Network Assisted Transfer Learning for Bi-Objective Pareto AGC Dispatch," *IEEE Transactions on Power Systems*, Vol. 38, pp. 1432-1444, 2023.
[96] Z. Hu, S. Liu, W. Luo, and L. Wu, "Resilient Distributed Fuzzy Load Frequency Regulation for Power Systems Under Cross-Layer Random Denial-of-Service Attacks," *IEEE Transactions on Cybernetics*, Vol. 52, No. 4, pp. 2396-2406, 2022.
[97] M. Adibi, and J. v. d. Woude, "Secondary Frequency Control of Microgrids: An Online Reinforcement Learning Approach," *IEEE Transactions on Automatic Control*, Vol. 67, pp. 4824-4831, 2022.
[98] A. Cunillera, N. Bešinović, N v. Oort, and R M.P. Goverde, "Real-time train motion parameter estimation using an Unscented Kalman Filter," T*ransportation Research Part C: Emerging Technologies, ELSEVIER*, Vol. 143, 2022.
[99] S. Zhang, C. Zhang, S. Jiang, and X. Zhang, "A comparative study of different adaptive extended/unscented Kalman filters for lithium-ion battery state-of-charge estimation," *Energy, ELSEVIER*, Vol. 246, 2022.
[100] S. Mokhtari, and K K. Yen, "Dynamic state estimation with additive noise for load frequency control using bilateral fuzzy adaptive unscented Kalman filter," *Electric Power Systems Research, ELSEVIER*, Vol. 220, 2023.
[101] D. Zhang, H. Zhang, X. Zhang, "Research on AGC Performance During Wind Power Ramping Based on Deep Reinforcement Learning," *IEEE Access*, Vol.8, pp. 107409-107418, 2020.
[102] K. Sabahi, M. Teshammad, "Recurrent fuzzy neural network by using feedback error learning approaches for LFC in interconnected power system," *Energy conversion and Management*, Vol.50, No.4, pp. 938-946, 2009.
[103] D. K. Chaturvedi, P.S. Satsangi, P.K.Kalra. "Load frequency control: A generalized neural network approach," *Electr Power Energy Syst*, Vol.21, pp. 405-415, 1999.
[104] D. Qian, G. Fan, "Neural-Network-Based Terminal Sliding Mode Control for Frequency Stabilization of Renewable Power System," *IEEE/CAA*, Vol.5, No.3, pp. 706-717, 2018.
[105] A. Fathy, A. Kassem, "Optimal design of fuzzy PID controller for deregulated LFC of multi-area power system via mine blast algorithm," *Neural Computing and Applications*, Vol.32, No.9, pp. 4531-4551, 2020.
[106] C. S. Chang, W. Fu, "Area load frequency control using fuzzy gain scheduling of PI controller," *Electr. Power Syst*, pp. 145-152, 1997.
[107] Adelhard Beni Rehiara, Naoto Yorino, Yutaka Sasaki, Yoshifumi Zoka, "A Novel Adaptive LFC Based on MPC Method," *IEEJ Transactions on Electrical and Electronic Engineering*, Vol.14, No.8, pp.1145-1152, 2019.
[108] Z. Qiu, M. Santillo, J. Sun and M. Jankovic, "Enhanced composite adaptive IMC for boost pressure control of a turbocharged gasoline engine," *2016 American Control Conference (ACC)*, Boston, MA, pp. 3286-3291, 2016.
[109] H. Wang, Z. Lei, X. Zhang, "Multiobjective Reinforcement Learning-Based Intelligent Approach for Optimization of Activation Rules in Automatic Generation Control," *IEEE Access*, Vol.7, pp. 17480-17492, 2019.
[110] M. Liu, F. Bizzarri, A.M. Brambilla, "On the Impact of the Dead-Band of power System Stabilizers and Frequency regulation on Power System Stability," *IEEE, Transactions on Power System*, Vol. 34, pp. 3977-3979, 2019.
[111] J. Morsali, K. Zare, M.T. Hagh, "AGC of Interconnected Multi-source Power System with Considering GDB and GRC Nonlinearity Effects," *IEEE, Conference on Thermal Power Plants, CTPP*, 2016.
[112] R. Pasantha, L. Wang, "Automatic Generation Control of Multi-area Power System with Network Constraints and Communication Delays," *Journal of modern power system and clean energy*, Vol. 8, No.3, 2020.
[113] EricA. Wan and Rudolph, "The Unscented Kalman Filter for Nonlinear Estimation," *Merwe Oregon Graduate Institute of Science & Technology 20000 NW Walker Rd*, Beaverton, Oregon 97006.

[114] E. Ghahremani, "Online State Estimation of a Synchronous Generator Using Unscented Kalman Filter From Phasor Measurements Units," *IEEE Transactions on Energy Conversion*, Vol 26, pp. 1099-1108, 2011.
[115] J. Qi, Kai Sun, "Dynamic State Estimation for Multi-Machine Power System by Unscented Kalman Filer with Enhanced Numerical Stability," I*EEE Transactions on Smart Grid*, Vol 9, pp. 1184-1196, 2018.
[116] J. Qi, Kai Sun, "Dynamic State Estimation for Multi-Machine Power System by Unscented Kalman Filer with Enhanced Numerical Stability," *IEEE Transactions on Smart Grid*, Vol 9, pp. 1184-1196, 2018.
[117] L. Chaib, A. Choucha, " Optimal design and tuning of novel fractional order PID power system stabilizer using a new metaheuristic Bat algorithm," *ASEJ*, Vol.8, No.2, pp. 113-125, 2017.
[118] O. I. Elgerd, C. E. Fosha, JR, "Optimum Megawatt-Frequency Control of Multiarea Electric Energy Systems," *IEEE Trans*, Vol. Pas-89, No. 4, pp.556-563, 1970.
[119] R. P. Aggarwal, F. R. Bergseth, "Large Signal Dynamics of Load-Frequency control System and Their Optimization Using Nonlinear Programimg: I," *IEEE Trans*, Vol. Pas-87, No. 2, pp. 527-532, 1968.
[120] Ibraheem, P. Kumar, D. P. Kothari, "Recent Philosophies of Automatic Generation Control Strategies in Power Systems," *IEEE Trans*, Vol. 20. No. 1. pp. 346-357, 2005.
[121] S. Kayalvizhi, D. M. Vinod Kumar, "Load Frequency Control of an Isolated Micro Grid Using Fuzzy Adaptive Model Predictive Control," *IEEE Access*, Vol. 5, pp. 16241-16251, 2017.
[122] P. Anuoluwapo Gbadega, A. Kumar Saha, "Load Frequency Control of a Two-Area Power System with a Stand-Alone Micro-grid based on Adaptive Model Predictive Control," *IEEE Journal*, DoI. 10. 1109, pp. 1-1, 2020.
[123] I. Ernest Uyioghosa, A. Kumar Saha, "Adaptive Model Predictive Control for Two Area Interconnted Power System," *IEEE SAUPEC*, DoI 10.1109, 2021.
[124] J.Guo, "Application of a novel adaptive sliding mode control method to the load frequency control," *European Journal of Control*, pp. 172-178, 2021.
[125] A.E, Onyeka, Y.XingGang, Z. Mao, "Robust decentralized load frequency control for interconnected time delay power systems using sliding mode techniques," *IET Control Theory*, Vol.14 Iss.3, pp. 470-480, 2020.
[126] A. M. Ersdal, L. Imsland, K. Uhlen, "Model Predictive Load-Frequency Control," *IEEE Trans*, Vol. 31. No. 1. pp. 777-785, 2016.
[127] R. Kandepu, B. Foss, L. Imsland, "Applying the unscented Kalman filter for nonlinear state estimation," *Journal of Process Control*, Vol 18. pp. 753-768. 2008.
[128] C. Ionescu, D. Copot, "Hands-on MPC tuning for industrial applications," *Bulletin of the Polish Academy of Sciences*, Vol.67, No.5, pp. 925-945, 2019.
[129] L. Chaib, A. Choucha, " Optimal design and tuning of novel fractional order PID power system stabilizer using a new metaheuristic Bat algorithm," *ASEJ*, Vol.8, No.2, pp. 113-125, 2017.
[130] W. Gu, W. Liu, Z. Wu, B. Zhao and W. Chen, "Cooperative Control to Enhance the Frequency Stability of Islanded Microgrids with DFIG-SMES," *Energy*, Vol. 6, pp. 3951-3971, 2013.
[131] J. Pan, X. Lu, "Dynamic Performance Considered for Time Delayed Microgrid Load Frequency H∞ Robust Control via DE Algorithm," *International Core Journal of Engineering*, Vol. 5, pp. 163-173, 2020.
[132] J. Chen, X. Li, W. Xie,"Microgrid frequency control based on H∞ mixed sensitivity," *Power System Technology*, pp. 2399-2403, 2014.
[133] M. H. Khooban and M. Gheisarnejad, "A Novel Deep Reiforcement Learning Controller Based Type-II Fuzzy system: Frequency Regulation in Microgrids," *IEEE Transaction on Emerging Topics in Computational Intelligence*, Vol. 5, No. 4, pp. 689-699, 2021.
[134] A. Singh and S. Suhag, "Trends in Island Microgrid Frequency Regulation – A Review," *Smart Science*, Vol. 7, No. 2, pp. 91-115, 2019.

[135] Shichao. L, Xiaoyu. W, and Peter. L, "Impact of Communication Delays on Secondary Frequency Control in An Island Microgrid," *IEEE Transactions on Industrial Electronics*, Vol. 62, No. 4, pp. 2021-2031, April. 2015.
[136] T. Adefarati, R. C. Bansal, "Reliability, economic and environmental analysis of a microgrid system in the presence of renewable energy resources," *ELSEVIER Applied Energy*, Vol. 236, No. 15, pp. 1089-1114, Feb. 2019.
[137] Ali. R, Yazdan. B, Farahnaz. A, and Hassan. B, "Robust Load-Frequency Control in Islanded Microgrids: Virtual Synchronous Generator Concept and Quantitative Feedback Theory," *IEEE Transactions on Power Systems*, Vol. 36, No. 6, pp. 5408-5416, Nov. 2021.
[138] Junghyun. K, and Kyuman. L, "Unscented Kalman Filter-Aided Long Short-Term Memory Approach for Wind Nowcasting," *Aerospace MDPI*, 2021.
[139] J. Pahasa and I. Ngamroo, "Coordinated Control of Wind Turbine Blade Pitch Angle and PHEVs Using MPCs for Load Frequency Control of Microgrid," *IEEE System Journal*, Vol. 10, No. 1, pp. 97-105, 2016.
[140] L. Wang: "Model Predictive Control System Design and Implementation Using MATLAB", *Springer*, 2009.
[141] Bhuvnesh Khokhar, and K.P. Singh Parmar: "Utilizing diverse mix of energy storage for LFC performance enhancement of a microgrid: A novel MPC approach", *ELSEVIER, Applied Energy*, Vol. 333, 2023.
[142] J. Wu, and F. Yang: "A dual-driven predictive control for photovoltaic-diesel microgrid secondary frequency regulation", *ELSEVIER, Applied Energy*, Vol. 334, 2023.
[143] A. Naderipour, Z. Abdul-Malek, Iraj Faraji Davoodkhani, Hesam Kamyab, and Roshafima Rasit Ali: "Load-frequency control in an islanded microgrid PV/WT/FC/ESS using an optimal self-tuning fractional-order fuzzy controller", *Springer, Environmental Science and Pollution Research*, No. 30, pp. 71677-71688, 2023.
[144] G. Zhang, I. A. Khan, A. Daraz, A. l. Basit, and M. I. Khan: "Load Frequency Control of Marine Microgrid System Integrated with Renewable Energy Sources", *MDPI, The Development of Marine Renewable Energy*, Vol. 11, No. 4, 2023.
[145] J. Li, T. Yu, and X. Zhang: "Coordinated load frequency control of multi-area integrated energy system using multi-agent deep reinforcement learning", *ELSEVIER, Applied Energy*, Vol. 306, 2023.
[146] J. Li, and H. Cui: "Cloud-Edge Cooperative Load Frequency Control for Isolated Microgrid Using Emergent computation-based Large Scale Meta-Machine Learning", *IEEE Journal of Emerging and Selected Topics in Industrial Electronics*, pp. 1-13, 2023.
[147] Z. Tu, B. Fan, J. Khazaei, W. Zhang, and W. Liu: "Optimal Reset-Control-Based Load Frequency Regulation in Isolated Microgrids", *IEEE Transactions on Sustainable Energy*, Vol. 13, No. 4, pp. 2239-2249, 2022.
[148] K. S. Joshal, and N. Gupta: "Microgrids with Model Predictive Control: A Critical Review", *MDPI, Energies*, Vol. 16, No. 13, 2023.
[149] A. M. Taher, Hany M. Hasanien, Shady H.E A. Aleem, M. Tostado-Veliz, M. Calasan, R. A. Turky, and F. Jurado: "Optimal model predictive control of energy storage devices for frequency stability of modern power systems", *ELSEVIER, Journal of Energy Storage*, Vol. 57, 2023.
[150] A. Singh and S. Suhag: "Trends in Island Microgrid Frequency Regulation – A Review", *Smart Science*, Vol. 7, No. 2, pp. 91-115, 2019.
[151] J. Pahasa and I. Ngamroo: "Coordinated Control of Wind Turbine Blade Pitch Angle and PHEVs Using MPCs for Load Frequency Control of Microgrid", *IEEE System Jourbal*, Vol. 10, No. 1, pp. 97-105, 2016.
[152] T. Nguyen, H. Yoo, and H. Kim: "Analyzing the Impacts of System Parameters on MPC-Based Frequency Control for a Stand-Alone Microgrid", *Energies*, Vol. 10, No. 4, pp. 417, 2017.
[153] H. Javanmardi, M. Dehghani, M. Mohammadi, S. Siamak, and M. R. Hesamzadeh: "BMI-Based Load Frequency Control in Microgrids Under False Data Injection Attacks", *IEEE SYSTEMS JOURNAL*, Vol. 16, No. 1, pp. 1021-1031, 2022[154] X. Deng, R.

Mo, P. Wang, J. Chen, D. Nan, and M. Liu, “Review of RoCoF Estimation Techniques for Low-Inertia Power Systems,” *MDPI*, *Energies 2023*, Vol. 16, No. 9, 2023.

[154] X. Deng, R. Mo, P. Wang, J. Chen, D. Nan, and M. Liu, “Review of RoCoF Estimation Techniques for Low-Inertia Power Systems,” *MDPI*, *Energies 2023*, Vol. 16, No. 9, 2023.

[155] F. González, M. Hau, AndreasSumper, OriolGomis-Bellmunt, “Participation of wind power plants in system frequency control: Review of grid code requirements and control methods,” *Renewable and Sustainable Energy Reviews*, Vol. 34, pp. 551-564, 2014.

List of Publications by the Author

Title of Publications, Oral Presentations, Reports or Patents	Date of Publications or Presentations	Name of Journals or Conferences	Authors
[1] A Novel Adaptive Model Predictive Frequency Control using Unscented Kalman Filter	2022-8-23	Elsevier, Electric Power Systems Research	Weichao Wang, Naoto Yorino, Yutaka Sasaki, Yoshifumi Zoka, Ahmed Bedawy, Seiji Kawauchi
[2] Frequency Regulation of High-Penetration Renewable Energy Microgrids Using Adaptive Model Predictive Control	2023-10-9	CSEE Journal of Power and Energy Systems	Weichao Wang, Yutaka Sasaki, Naoto Yorino, Yoshifumi Zoka Ahmed Bedawy
[3] Adaptive Model Predictive Control Based Frequency Regulation for Low-inertia Microgrid	2023-7-29	The 5th International Conference on Power and Energy Technology (ICPET)	Weichao Wang, Yutaka Sasaki, Naoto Yorino, Yoshifumi Zoka, Ahmed Bedawy
[4] Adaptive MPC-Based Load Frequency Control for Microgrid with Renewable Energy	2023-7-4	The International Council Electrical Engineering (ICEE) Conference	Weichao Wang, Yutaka Sasaki, Naoto Yorino, Yoshifumi Zoka, Ahmed Bedawy, Seiji Kawauchi
[5] Adaptive MPC-Based Load Frequency Control for Microgrids Considering High Penetration of Renewable Energy	2023-3-24	IEEJ PES-IEEE PES Thailand Joint Symposium on Advanced Technology in Power Systems 2023	Weichao Wang, Yutaka Sasaki, Yoshifumi Zoka, Naoto Yorino, Ahmed Bedawy
[6] Adaptive MPC-Based Cooperative Frequency Control for Community Microgrid	2022-12-12	2022 4th International Conference on Smart Power & Internet Energy Systems (SPIES)	Weichao Wang, Naoto Yorino, Yutaka Sasaki, Yoshifumi Zoka, Ahmed Bedawy, Seiji Kawauchi
[7] Adaptive Model Predictive-Based Load Frequency Controller using Unscented Kalman Filter	2021-12-6	10th IEEE PES Innovative Smart Grid Technology (ISGT-Asia 2021)	Weichao Wang, Naoto Yorino, Yutaka Sasaki, Yoshifumi Zoka, Ahmed Bedawy, Seiji Kawauchi
[8] Adaptive Model Predictive Load Frequency Controller Based on Unscented Kalman Filter	2021-12-24	2021 IEEE Sustainable Power and Energy Conference (ISPEC)	Weichao Wang, Naoto Yorino, Yutaka Sasaki, Yoshifumi Zoka, Ahmed Bedawy, Seiji Kawauchi
[9] 再エネ・蓄電池を含むマイクログリッドにおける適応型モデル予測周波数制御	2023-9-25	2023 年電気学会電力技術/電力系統技術合同研究会	王 偉朝, 佐々木 豊, 餘利野 直人, 造賀 芳文

[10] 自立マイクログリッドにおける適応型モデル予測制御を用いた負荷周波数制御に関する検討	2023-3-15	2023 年電気学会全国大会	王 偉朝, 佐々木 豊, 餘利野 直人, 造賀 芳文
[11] 適応型モデル予測制御を用いた再エネ・蓄電池を含むマイクログリッドの周波数制御	2022-8-24	2022 年電気学会電力技術/電力系統技術合同研究会	王 偉朝, 佐々木 豊, 餘利野 直人, 造賀 芳文
[12] A Novel Adaptive MPC-based Frequency Control for A Microgrid	2022-9-5	2022 年 電気学会 電子・情報・システム部門大会	Weichao Wang, Naoto Yorino, Yutaka Sasaki, Yoshifumi Zoka
[13] A Comparison Study on Prediction Modelling using Unscented Kalman Filter for Load Frequency Control	2021-10-23	2021 年度(第 72 回)電気・情報関連学会中国支部連合大会	Weichao Wang, Naoto Yorino, Yutaka Sasaki, Yoshifumi Zoka
[14] UKF を用いたモデル予測形負荷周波数制御に関する研究	2021-3-9	2021 年電気学会全国大会	王 偉朝, 餘利野 直人, 造賀 芳文, 佐々木 豊
[15] A Novel Adaptive Model Predictive Frequency Control Using Unscented Kalman Filter	2021-9-21	2021 年電気学会電力技術/電力系統技術合同研究会	Weichao Wang, Naoto Yorino, Yutaka Sasaki, Yoshifumi Zoka
[16] 再生可能エネルギー電源の不確定性を考慮したマイクログリッド内の電力需給調整に関する基礎的研究	2019-9-19	2019 年電気学会電力技術/電力系統技術合同研究会	漆崎 裕介, 王 偉朝, 上島 李樹, 今西 一就, 阪井 柊弥, 佐々木 豊, 造賀 芳文, 餘利野 直人

Appendix

Appendix 1 for power system

The state space matrices of power systems in (4.3) are given in the following.

$$A_i = \begin{bmatrix} -\frac{1}{T_{g,i}} & 0 & -\frac{1}{R_i T_{g,i}} & 0 \\ \frac{1}{T_{t,i}} & -\frac{1}{T_{t,i}} & 0 & 0 \\ 0 & \frac{1}{M_i} & -\frac{D_i}{M_i} & -\frac{1}{M_i} \\ 0 & 0 & 2\pi \sum_{\substack{j=1 \\ j \neq i}}^{n} T_{ij} & 0 \end{bmatrix} \tag{A1}$$

$$B_i = \begin{bmatrix} \frac{1}{T_{g,i}} & 0 & 0 & 0 \end{bmatrix}^T \tag{A2}$$

$$C_i = \begin{bmatrix} 0 & 0 & \beta_i & 1 \end{bmatrix} \tag{A3}$$

The frequency response characteristic (β) is expressed by governor speed droop (R) and the MG system damping constant (D) as follows.

$$\beta_i = D_i + \frac{1}{R_i} \tag{A4}$$

The constraints of the proposed AMPC controller are set as follows.

Max frequency deviation ($\Delta f_i^{\max}$) =0.2Hz,

Min frequency deviation ($\Delta f_i^{\min}$) =-0.2Hz,

Max control output ($u_i^{\max}$) =0.2pu,

Min control output ($u_i^{\min}$) =-0.2pu,

Max control output ($y_i^{\max}$) =0.25pu,

Min control output ($y_i^{\min}$) =-0.25pu,

Dead band (DB) is used in this work, which to increase the steady-state speed regulation of the governor and avoid the hunting phenomenon (a momentary fluctuation) of the signal. The generation rate constraint (GRC) of 10%/min is set for the thermal unit turbine and the constant of DB is set to ± 0.001pu (Hz).

The PI controllers (Integral controller) with the optimally tuned parameters for the 2-area and the 3-area power system are adopted, which also agree with the optimal setting for the robustness against uncertainty of the system and against communication delay of control signal.

Area1: K_P=0 and K_I=-0.3

Area2: K_P=0 and K_I=-0.2

Area3: K_P=0 and K_I=-0.4

The integral error equations are used for comparative data analysis, which are given as follows.

$$IAE = \int_0^T \left\{ \left| \Delta f_i \right| + \left| \Delta P_{tie,ij} \right| \right\} dt \tag{A5}$$

$$ISE = \int_0^T \left\{ \Delta f_i^2 + \Delta P_{tie,ij}^2 \right\} dt \tag{A6}$$

$$ITAE = \int_0^T t \left\{ \left| \Delta f_i \right| + \left| \Delta P_{tie,ij} \right| \right\} dt \tag{A7}$$

$$ITSE = \int_0^T t \left\{ \Delta f_i^2 + \Delta P_{tie,ij}^2 \right\} dt \tag{A8}$$

Where T is simulation time, t=2s is sample time.

Appendix 2 for MG systems

The state space matrices of MG systems in (5.1) are given in the following.

$$\boldsymbol{A}_i = \begin{bmatrix} -\dfrac{1}{T_{g,i}} & 0 & -\dfrac{1}{R_i T_{g,i}} \\ \dfrac{1}{T_{t,i}} & -\dfrac{1}{T_{t,i}} & 0 \\ 0 & \dfrac{1}{M_i} & -\dfrac{D_i}{M_i} \end{bmatrix} \tag{A9}$$

$$\boldsymbol{B}_i = \begin{bmatrix} \dfrac{1}{T_{g,i}} & 0 & 0 \end{bmatrix}^T \tag{A10}$$

$$\boldsymbol{C}_i = \begin{bmatrix} 0 & 0 & \beta_i \end{bmatrix} \tag{A11}$$

$$\boldsymbol{E}_i = \begin{bmatrix} 0 & 0 & -\dfrac{1}{M_i} \end{bmatrix} \tag{A12}$$

$$A = \begin{bmatrix} -\frac{1}{T_{g1}} & 0 & 0 & 0 & 0 & 0 & -\frac{1}{R_1 \cdot T_{g1}} & 0 & 0 & 0 \\ 0 & -\frac{1}{T_{g2}} & 0 & 0 & 0 & 0 & -\frac{1}{R_2 \cdot T_{g2}} & 0 & 0 & 0 \\ 0 & 0 & -\frac{1}{T_{g3}} & 0 & 0 & 0 & -\frac{1}{R_3 \cdot T_{g3}} & 0 & 0 & 0 \\ \frac{1}{T_{t1}} & 0 & 0 & -\frac{1}{T_{t1}} & 0 & 0 & 0 & 0 & 0 & 0 \\ 0 & \frac{1}{T_{t2}} & 0 & 0 & -\frac{1}{T_{t2}} & 0 & 0 & 0 & 0 & 0 \\ 0 & 0 & \frac{1}{T_{t3}} & 0 & 0 & -\frac{1}{T_{t3}} & 0 & 0 & 0 & 0 \\ 0 & 0 & 0 & \frac{1}{M} & \frac{1}{M} & \frac{1}{M} & -\frac{D}{M} & \frac{1}{T_{BESS1}} & \frac{1}{T_{BESS2}} & \frac{1}{T_{BESS3}} \\ 0 & 0 & 0 & 0 & 0 & 0 & \frac{1}{T_{BESS1}} & -\frac{1}{T_{BESS1}} & 0 & 0 \\ 0 & 0 & 0 & 0 & 0 & 0 & \frac{1}{T_{BESS2}} & 0 & -\frac{1}{T_{BESS2}} & 0 \\ 0 & 0 & 0 & 0 & 0 & 0 & \frac{1}{T_{BESS3}} & 0 & 0 & -\frac{1}{T_{BESS3}} \end{bmatrix} \tag{A13}$$

$$B = \begin{bmatrix} \frac{1}{T_{g1}} & 0 & 0 & 0 & 0 & 0 & 0 & 0 & 0 & 0 \\ 0 & \frac{1}{T_{g2}} & 0 & 0 & 0 & 0 & 0 & 0 & 0 & 0 \\ 0 & 0 & \frac{1}{T_{g3}} & 0 & 0 & 0 & 0 & 0 & 0 & 0 \end{bmatrix}^T \tag{A14}$$

$$C = \begin{bmatrix} 0 & 0 & 0 & 0 & 0 & 0 & \beta & 0 & 0 & 0 \end{bmatrix} \tag{A15}$$

$$E = \begin{bmatrix} 0 & 0 & 0 & 0 & 0 & 0 & -\frac{1}{M} & 0 & 0 & 0 \end{bmatrix}^T \tag{A16}$$

Optimal parameters of the PI controller are set for comparison by checking the frequency response of the system.

Where, K_P=0.02, K_I=-0.1

The constraints of the proposed AMPC controller are set as follows.

Max frequency deviation (Δf^{max}) =0.2Hz,

Min frequency deviation (Δf^{min}) =-0.2Hz,

Max control output (u^{max}) =0.2pu,

Min control output (u^{min}) =-0.2pu,

The renewable energy sources (RESs), WT and PV are used to MG system, whose structure is shown in the followings. The simulation environment is built using MATLAB/Simulink R2021b. In the WT power model, the average wind speed is set to 10.1m/s, pitch angle is set to constant value of 20deg. In the PV model, a ramp function is considered to construct the PV output variation.

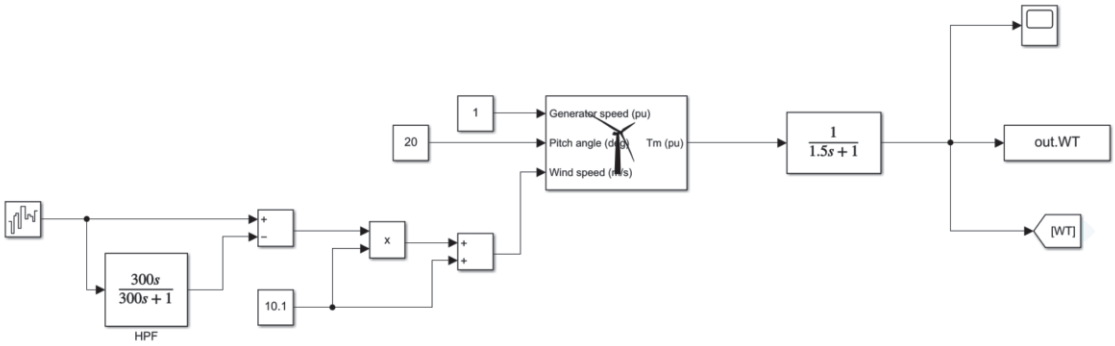

Fig A.1 WT power.

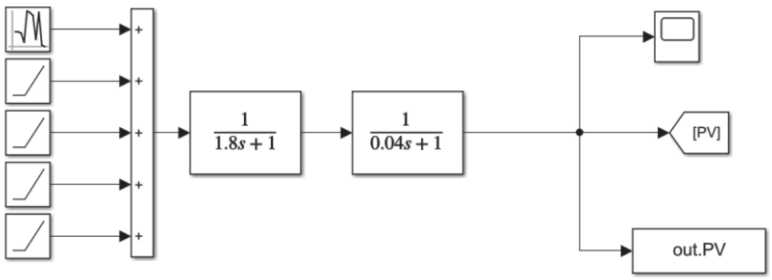

Fig A.2 PV power.